In This Issue:

Articles

Technical News Briefs

Journal of Research of the National Bureau of Standards

A Wavelength Standard for the Near Infrared Based on the Reflectance Of Rare-Earth Oxides

Volume 91 Number 5 September–October 1986

Victor R. Weidner, Patricia Y. Barnes, and Kenneth L. Eckerle

National Bureau of Standards
Gaithersburg, MD 20899

This work describes the techniques used to prepare and analyze a reflectance wavelength standard composed of three rare-earth oxides. A mixture of dysprosium oxide (Dy_2O_3), erbium oxide (Er_2O_3), and holmium oxide (Ho_2O_3) provides a pressed powder specimen exhibiting a near infrared reflectance spectrum characterized by many discrete absorption minima in the wavelength range 700 to 2000 nm. The object of this activity was to develop a wavelength standard for improving the accuracy of reflectance measurements in the near infrared. The reflectance minima of the rare-earth oxide mixture was analyzed for the effects of varying spectral resolution and temperature. The uncertainties associated with the various parameters affecting the measurements and the determination of the location of the reflectance minima have been analyzed. The overall uncertainty in the location of these reflectance minima is believed not to exceed ±1 nm.

Key words: dysprosium oxide; erbium oxide; holmium oxide; near infrared reflectance; rare-earth oxides; spectral bandwidths; wavelength calibration; wavelength standard.

Accepted: February 28, 1985

1. Introduction

This work describes the techniques used to prepare and characterize a reflectance wavelength standard composed of three rare-earth oxides. A mixture of dysprosium oxide (Dy_2O_3), erbium oxide (Er_2O_3), and holmium oxide (Ho_2O_3) provides a pressed powder specimen exhibiting a near infrared reflectance spectrum characterized by many discrete reflectance minima in the wavelength range 700 to 2000 nm. This wavelength standard is primarily intended for checking the wavelength accuracy of spectrophotometric instrumentation designed for measuring diffuse reflectance in the near infrared.

About the Authors: Victor R. Weidner, Patricia Y. Barnes, and Kenneth L. Eckerle are with the Radiometric Physics Division in NBS' National Measurement Laboratory.

2. Experimental

2.1 Instrumentation

Measurements of spectral reflectance of the rare-earth oxide mixture were made by means of a Varian-Cary Model 2390 recording spectrophotometer [1][1]. The optical system of this double beam instrument consists of a filter predisperser and a double-pass monochromator with UV-VIS and near IR gratings. A deuterium lamp is used as a source for the ultraviolet spectral range. The visible and near infrared source is a tungsten-halogen lamp. The deuterium lamp also serves as a wavelength scale calibration source when the instrument is operated in a single beam mode, providing emission lines at 486.0 and 656.1 nm in the visible spec-

---

[1] Figures in brackets indicate literature references.

trum and 2nd, 3rd, and 4th order lines of the 656.1 nm line with the near infrared grating.

The spectrophotometer is equipped with an integrating sphere diffuse reflectance reflectometer. This device is capable of measuring total hemispherical reflectance over the wavelength range 200 to 2500 nm, using a photomultiplier detector for the ultraviolet and visible spectral range, and a lead sulfide detector for the near infrared. When operating with the lead sulfide detector, the reference mode (which determines the method used to control the reference signal level) operates at constant gain. The constant gain is maintained by varying the spectral bandwidth as a function of wavelength. The available range of spectral bandwidth settings is approximately 1 to 14 nm when using the diffuse reflectance attachment. The noise associated with the recording of a spectrum increases as the spectral bandwidth is narrowed and the spectral resolution must be sacrificed in order to maintain reasonable noise levels when recording spectra near the extreme short and long wavelength range of the lead sulfide detector. In order to record a spectrum over the full near infrared spectral range at approximately constant resolution, the gain must be reset every 25 to 50 nm. When constant resolution is not important, a complete scan of the near infrared range can be made at a fixed gain setting. For the measurements described in this work, the control of spectral resolution was of primary importance and gain settings were varied to provide a number of fixed spectral bandwidths for analysis of the effects of resolution on the location of the wavelengths of minimum reflectance of the rare-earth oxide mixture.

2.2 Materials

2.2.1 Rare-Earth Oxides. The rare-earth oxides of dysprosium, erbium, and holmium were selected for preparation of the reflectance wavelength studies after extensive measurements of the near infrared reflectance spectra of numerous rare-earth oxides. None of the single component rare-earth specimens analyzed exhibited enough absorption bands to serve as a wavelength standard for the full

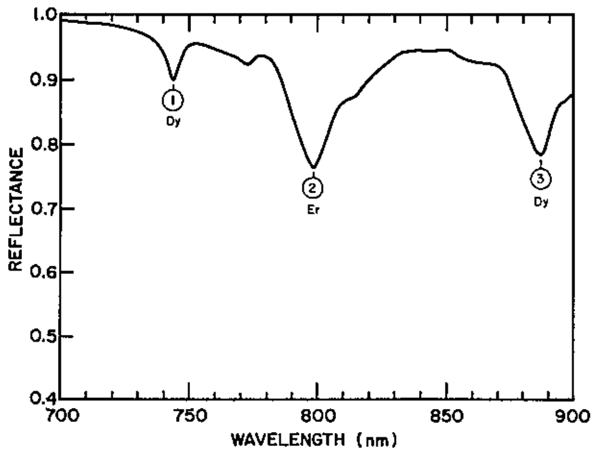

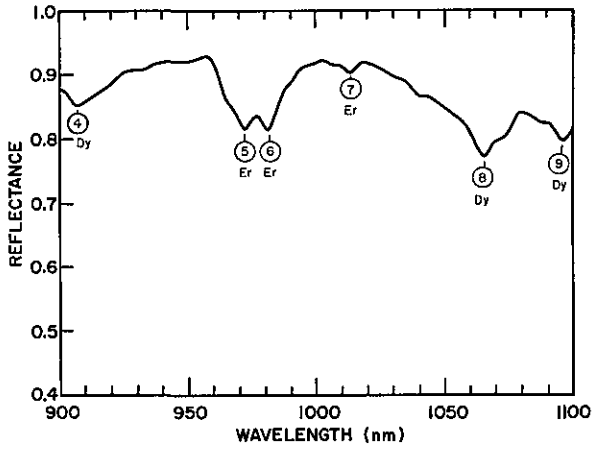

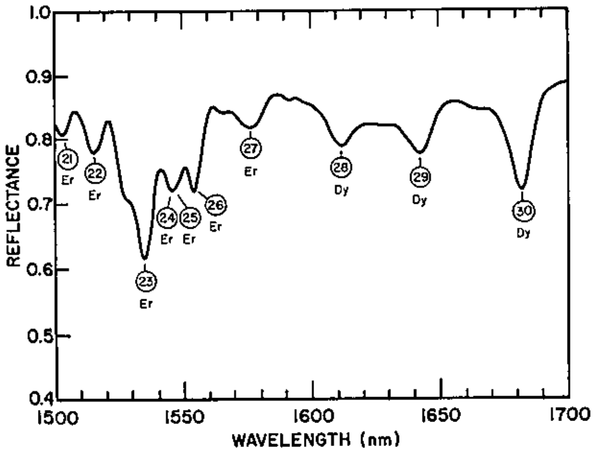

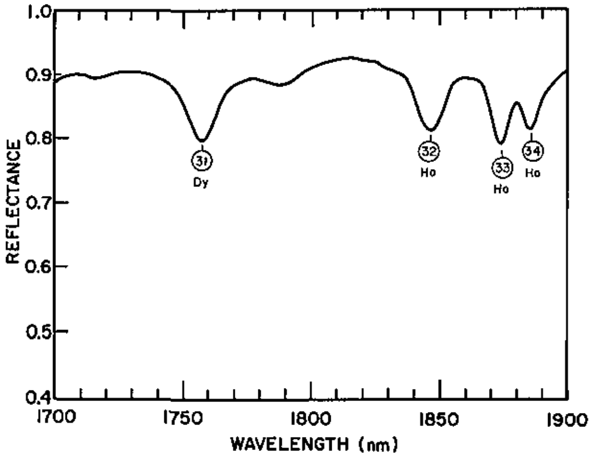

700 to 2500 nm spectral range and none showed any promise at wavelengths much beyond 2000 nm. The oxides of dysprosium, erbium, and holmium were selected because their infrared absorption bands occurred at various wavelengths throughout the 700 to 2000 nm spectral range with a minimum of overlapping of the bands attributed to each oxide. The disadvantage of mixing the three component rare-earth oxides was the loss of some intensity of depth of the individual absorption bands. The reflectance spectra of the three component rare-earth oxide mixture is illustrated in figures 1-1 through 1-7 for a nominal spectral bandwidth of 4 nm. The absorption features selected for analysis are numbered 1–37 and the rare-earth oxide attributed to each of these absorption features is identified by the elemental symbols Dy, Er, and Ho appearing with each band number.

The three rare-earth oxides were mixed in equal parts by weight. The purity of each rare-earth oxide was indicated by the manufacturer [2] to be 99.99 percent. The specimens are identified by lot numbers; (Dy: lot no. Dy-0-4-018), (Er: lot no. Er-0-4-028), and (Ho: lot no. Ho-0-4-007). Each rare-earth oxide was weighed in portions of 2 g ±0.01g. These were combined to form a total weight of 6 g. After throughly mixing the three components, the mixture was pressed into an aluminum cavity having a depth of 0.5 cm and diameter of 2.85 cm. This produced a specimen with a powder density of approximately 2 g/cm^3. The powder specimen was provided with a sapphire window of 1.5 mm thickness. This window retained the powder and protected it against damage and contamination. Sapphire was selected as a window material because it is essentially free of absorption features in the near infrared.

2.3 Measurement Techniques

2.3.1 Calibration of the Spectrophotometer Wavelength Scale. The spectrophotometer wavelength scale error was evaluated by measuring the emission lines of the following elements: neon at 703.24 nm, xenon at 881.94 and 979.97 nm, mercury at 1013.97 and 1529.58 nm, and krypton at 1816.73

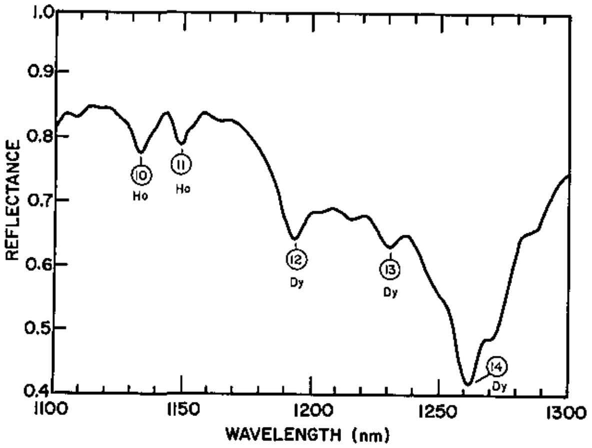

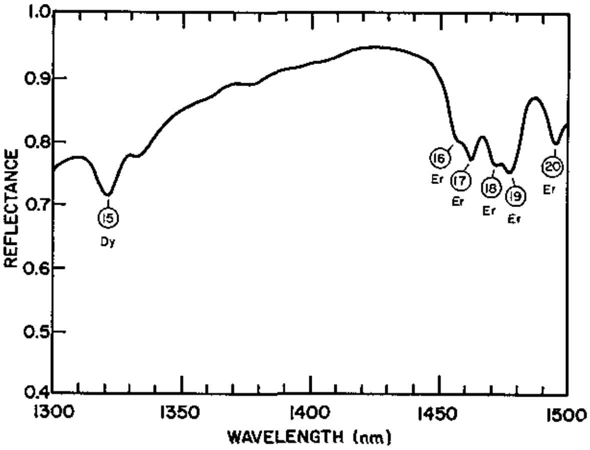

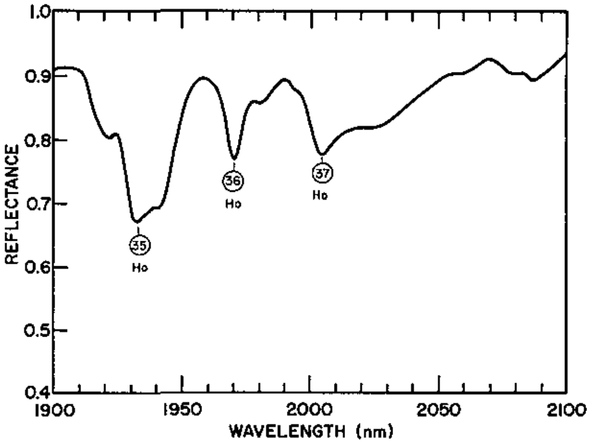

Figures 1-1 through 1-7–Beginning upper left at a wavelength 700 nm the near infrared spectral reflectance of a rare-earth oxide mixture composed of Dy_2O_3, Er_2O_3, and Ho_2O_3 in equal portions by weight compressed to a density of 1g/cm^3.

nm. [3] In addition to these, the absorption band of 1-2-4 trichlorobenzene at 2152.60 nm [4] was also measured.

The wavelength scale of the spectrophotometer was calibrated at the beginning of the study and again after completion of the spectral analysis of the rare-earth oxide spectra. The day-to-day stability of the instrument wavelength scale was monitored by recording the 2nd order emission of the 656.1 nm deuterium line at 1312.2 nm after a nominal warm-up time of 1 hour. The record of this day-to-day stability check is illustrated in figure 2 for the time period of November 13 to December 24. The data in figure 2 show that the wavelength scale was stable to ±0.2 nm during this time interval.

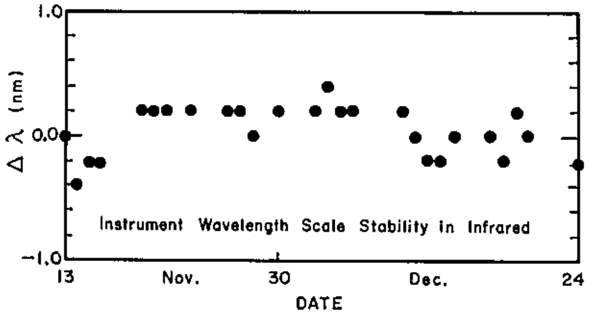

Figure 2–The day-to-day record of the stability of the spectrophotometer wavelength scale in the near-infrared.

The wavelength error was evaluated by scanning the emission lines at a rate of 0.01 nm/sec. and recording the resulting spectrum on a scale of 0.2 nm/cm. The recorded emission peaks were bisected, using a proportional divider, to determine the wavelengths at the center of the recorded triangular lines. Using this technique, the wavelength scale was read to the nearest 0.01 nm.

The wavelength errors were evaluated for spectral bandwidths of 2, 3, 4, 5, and 10 nm. The differences between the published or "true" wavelengths of the emission lines as determined from the measurements on the spectrophotometer, are plotted in figures 3-1 and 3-2 for analysis of the instrument wavelength error. The data points were found to be closely grouped for the measurements at spectral bandwidths of 2, 3, 4, and 5 nm. The data points for the 10 nm spectral bandwidth measurements were somewhat separated from the others. For this reason the analysis of the 2, 3, 4, and 5 nm bandwidth data are illustrated in figure 3-1 and the 10 nm bandwidth data in figure 3-2. Since the day-to-day wavelength scale stability check indicates a possible point spread of 0.4 nm, this grouping of the bandwidth data into one group for the 2, 3, 4, and 5 nm measurements seemed reasonable.

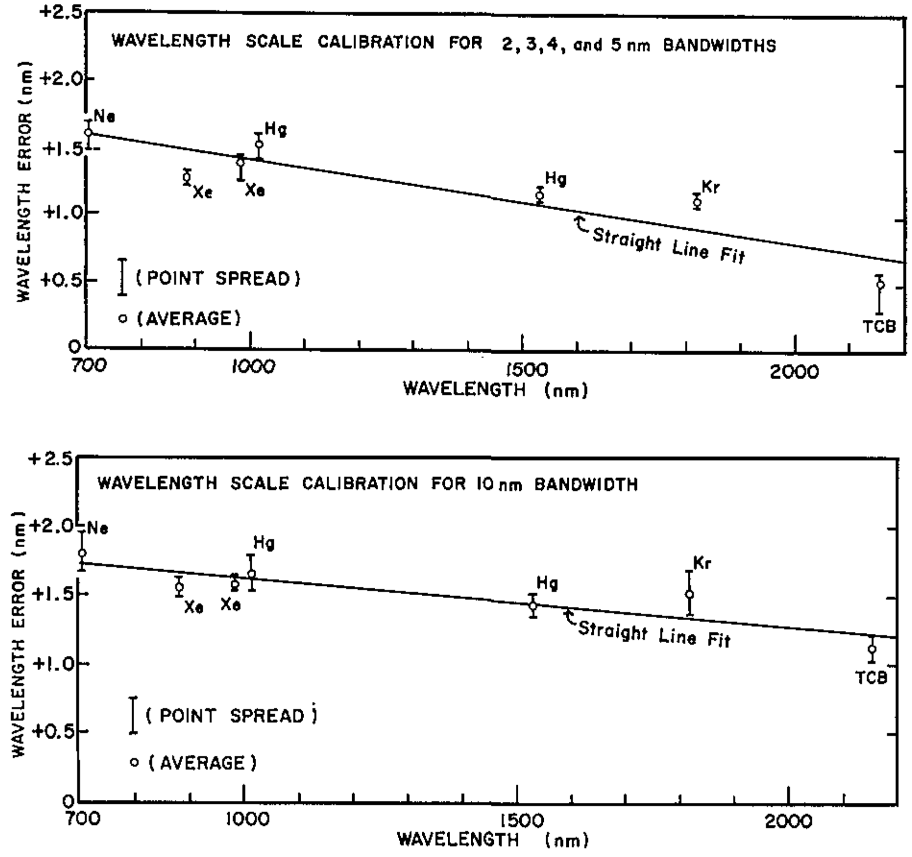

Figure 3-1 (upper) and **Figure 3-2**–The wavelength scale calibration results for the selected spectral bandwidths showing the data point spread (vertical bars), data point averages (open circles on the vertical bars), the linear least-squares fit to the data point averages (sloping solid straight line).

The spread of data points in figures 3-1 and 3-2 is indicated by the vertical bars. The average of the data points within the vertical bar is indicated by the open circle on the bar. A linear least-squares fit of the the average data points, (represented by the open circles), is shown as a straight line across the graph. This line was taken as a indication of the wavelength scale error of the spectrophotometer for these spectral bandwidths over the near infrared spectral range 700 to 2150 nm. This linear least-squares fit represents a nominal wavelength correction. The data spread bars shown in figures 3-1 and 3-2 are sometimes completely above or below the least-squares fit. Repeated measurements probably would not improve the fit because of hidden factors that influence where a particular emission line will appear.

A mathematical estimation of the uncertainty in the calibration of the instrument wavelength scale can be derived from the sum of the following observed uncertainties:

The wavelength scale uncertainty (a) is:

$$a = 2d + r + v$$

where:

$2d$ = twice the standard deviation of the linear least-squares fit for the emission line wavelengths,

$r = 1/2$ the range of the data point spread for the worst case for location of an emission line,

v = the day-to-day stability of the wavelength scale.

For the 2, 3, 4, and 5 nm spectral bandwidths:

$$a = \pm 0.57 \text{ nm}$$

For a 10 nm spectral bandwidth:

$$a = \pm 0.66 \text{ nm}.$$

Other uncertainties associated with the overall determination of the wavelengths of minimum reflectance of the rare-earth oxide mixture will add to these uncertainties. These uncertainties will be discussed in section 2.3.4.

2.3.2 Spectral Bandwidths. The spectral bandwidth settings used in the analysis of the rare-earth oxide mixture were selected to provide data on the effect of changing resolution on the location of the reflectance minima that are characteristic of this material in the near infrared. The spectral bandwidths in the near infrared are controlled by adjusting the reference signal gain. This adjustment involves the monochromator slit width mechanism which in effect controls the spectral bandwidth or resolution. The bandwidth is displayed on the instrument control panel. In order to check the validity of the spectral bandwidth readout on the display panel, a series of measurements were made of the half-band widths of the mercury emission line at 1014 nm for nominal bandwidth settings of 2, 3, 4, 5, and 10 nm. In the single beam mode of operation the gain can be adjusted without changing the selected bandwidth. The half-band width is determined by scanning the emission line with the gain adjusted until the peak of the emission is approximately 100 percent. The measured width of the recorded emission spectra at half the peak height is an indication of the spectral bandwidth. A comparison of the nominal spectral bandwidth, as indicated on the instrument display panel, and the measured half-band width of the mercury emission spectra is given in table 1. The comparison shows that the actual bandwidths are less than the nominal bandwidths for the 2, 3, 4, and 5 nm settings and the same for the 10 nm setting.

2.3.3 Determination of the Wavelength of Minimum Reflectance. The spectral reflectance of the rare-earth oxide mixture is shown in figures 1-1 through 1-7 for a nominal spectral bandwidth of 4 nm. The number of observed absorption bands varies as a function of the spectral bandwidth setting selected for recording the spectrum. There are 37 reflectance minima identified in the figures. Most can be observed at bandwidths less than 4 nm. Only a few can be observed at 10 nm spectral bandwidth.

The reflectance spectra of the mixture of rare-earth oxides was recorded on a chart with a wavelength display of 0.5 nm/cm and a wavelength scan range of 0.05 nm/sec. This speed is a relatively slow scan rate for these absorption bands so that the effect of recorder inertia error is essentially eliminated as a source of wavelength scale error.

The reflectance was measured with a sapphire window between the rare-earth oxide mixture and the sample port of the integrating sphere of the reflectometer. The 100 percent (baseline) calibration was set with a pressed powder Halon (polytetrafluoroethylene) specimen, also covered by a sapphire window. The near infrared spectral reflectance of a sapphire window covered Halon

Table 1. Comparison of the spectral bandwidths as indicated by the instrument readout (A) with the spectral bandwidths as derived from the half-height bandwidth measurements of the 1014 nm Hg emission line (B).

Spectral Bandwidths	
(A)	*(B)*
2 nm	1.4 nm
3	2.6
4	3.6
5	4.6
10	10.0

specimen versus an uncovered Halon Specimen (100 percent) is shown in figure 4. The spectral transmittance of the sapphire window is also shown in figure 4.

The determination of the wavelengths of minimum reflectance of the rare-earth mixture was accomplished through an analysis of the recorded spectral curves. The location of the wavelengths of minimum reflectance for a given absorption band was graphically determined by bisecting the absorption band. The technique is illustrated in figure 5. The horizontal grid lines of the chart paper that intersect the two slopes of the absorption band are bisected by means of a proportional divider. The points of bisection locate a line between the two slopes that intersects the minimum reflectance point, (usually at the lowest point of the curve). The wavelength at this point of intersection was taken as the measured wavelength of minimum reflectance for the absorption feature. The true wavelength of the minimum was determined by applying a wavelength correction to this measured value. This correction was discussed in section 2.3.1. Various uncertainties are associated with these assigned true wavelengths. These will be discussed in section 2.3.4.

2.3.4 Accuracy of the Wavelengths of Minimum Reflectance. The overall uncertainty in the location of the wavelengths of minimum reflectance is believed to be no greater than ±1 nm. This conclusion is based on the reproducibility of the following calibration parameters:

a) The uncertainty of the calibration of the spectrophotometer wavelength scale using the emission lines of Ne, Xe, Hg, and Kr, and the absorption band of 1-2-4 trichlorobenzene, and the day-to-day instabilities of the instrument; (±0.57 nm and ±0.66 nm depending on the spectral bandwidth).

b) The imprecision of the graphical technique for deriving the measured wavelengths of minimum reflectance; (±0.41 nm), (twice the largest standard deviation), (see table 2).

c) The maximum observed temperature effect; (±0.15 nm).

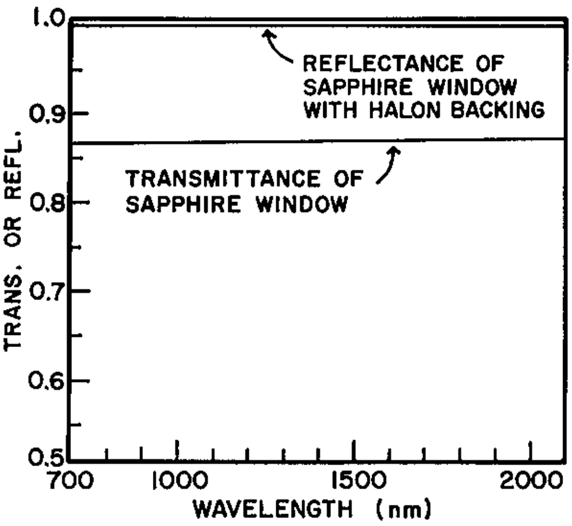

Figure 4–The spectral transmittance of the sapphire window used to cover the rare-earth oxide pressed powder specimen, and the spectral reflectance of a sapphire window covering the Halon diffuse reflectance standard.

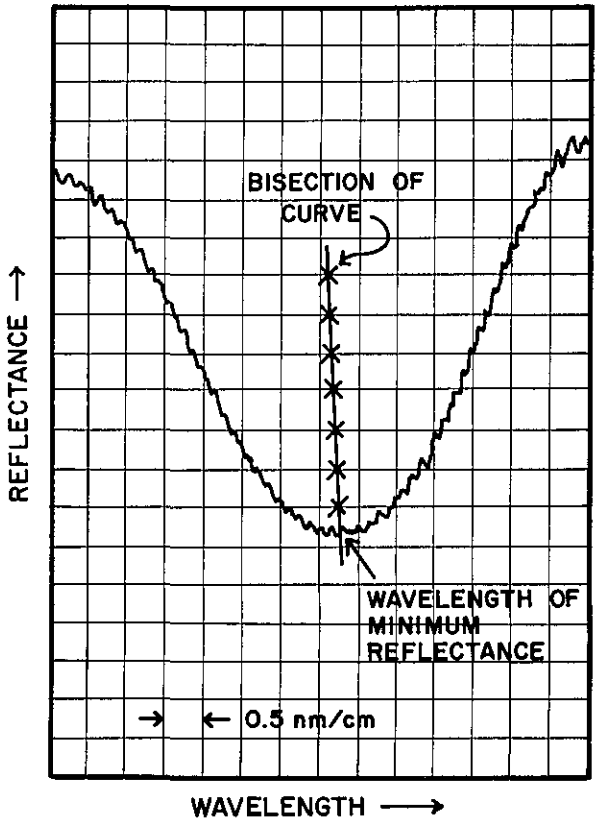

Figure 5–The wavelengths of minimum reflectance are determined by bisecting the recorded absorption feature as illustrated in this example.

A mathematical estimation of the overall uncertainty (T) in the location of the wavelengths of minimum reflectance can be derived from the square root of the sum of the independent errors squared:

$$T=\sqrt{a^2+b^2+c^2}$$

where:

a = uncertainty in the instrument wavelength scale,

Table 2. Ten measurements of the reflectance minima for each of three absorption bands at a spectral bandwidth of 4 nm, showing the spread of values obtained by the graphical location of the minima. The average, standard deviation, and standard error for the ten values are also given. These measurements are for 25 °C.

Measurement No.	Band No. 14 (Dy_2O_3)	Band No. 23 (Er_2O_3)	Band No. 32 (Ho_2O_3)
1	1261.00	1535.68	1847.09
2	1260.93	1535.65	1847.00
3	1261.15	1535.70	1846.77
4	1261.00	1535.70	1847.00
5	1261.03	1535.60	1846.73
6	1261.20	1535.65	1846.78
7	1261.08	1535.63	1846.50
8	1260.93	1535.60	1846.70
9	1260.93	1535.69	1846.73
10	1261.00	1535.70	1846.43
Average	1261.03	1535.66	1846.77
Standard Deviation	0.09	0.04	0.21
Standard Error	0.03	0.01	0.07

Note: The data in this table have not been corrected for the wavelength scale error of the spectrophotometer.

b = twice the standard deviation for the graphical determination of the minima,
c = the largest observed temperature effect.

For spectral bandwidths of 2, 3, 4, and 5 nm:
$T = \pm 0.72$ nm
For a spectral bandwidth of 10 nm:
$T = \pm 0.79$ nm.

These uncertainties are for a 95 percent confidence level. Some other possible uncertainties are discussed in the conclusion.

3. Measurements

3.1 Influence of the Sapphire Window and the Baseline Calibration

In measuring diffuse spectral reflectance, some reference must be used to establish a 100 percent level (baseline). In this double beam spectrophotometer, the reference beam enters the integrating sphere and is incident on a Halon target. The sample beam enters through another port and is incident on the sample. In order to establish a 100 percent level calibration curve, a sample of pressed Halon is placed at the sample port. The 100 percent level is established by the ratio of the sample (Halon) reflectance to the reference beam signal (also Halon). The instrument records this baseline in a computer memory. When the Halon sample is replaced by a test specimen, the reflectance of the specimen is recorded relative to this stored baseline or 100 percent level. This method is called the substitution method. The reflectance of the test specimen is a relative measurement. Halon is used to establish the 100 percent level because its absolute reflectance is very high and it has no significant absorption features that would introduce a distortion in the recorded spectra. The absolute reflectance of the test specimen can be obtained by adjusting the relative measurement to the absolute reflectance of the Halon [5].

In this study a sapphire window is placed over the rare-earth oxide test specimen. This window is 1.5 mm thick. A similar window is placed over the Halon sample during the recording of the 100 percent level. By using a sapphire window on both the Halon and the rare-earth oxide specimens, the effects of the window reflectance and absorbance are cancelled out in the baseline calibration.

The sapphire window has no absorption bands in the near infrared that would influence the determination of the wavelength of minima reflectance of the rare-earth oxide mixture. The absolute reflectance data for Halon [5] also show that it can be used as a baseline standard for purposes of this investigation.

3.2 Influence of Spectral Bandwidth

The effects of spectral bandwidth on the location of the rare-earth oxide reflectance minima are shown in table 3. The absorption bands are numbered from 1 at approximately 742 nm to 37 at approximately 2005 nm. Measurements were made at nominal spectral bandwidths based on the instrument display readout of this parameter. However, the data listed in table 1 indicate that the spectral bandwidths were less than the nominal values for all but the 10 nm setting.

The blank spaces in table 3 are blank for the following reasons: (1) The noise level was too large to make reliable measurements. This was the case for bands 1, 2, 36, and 37 at the 2 nm spectral bandwidth setting. (2) Two adjacent bands merged together because the selected spectral bandwidths did not resolve the two bands. This was the case for bands 24 and 25 at 3 nm spectral bandwidth. (3) The band became too shallow due to the large spectral bandwidth. This case occurs for many of the bands at 5 and 10 nm spectral bandwidths.

Table 3 does not give a clear picture of the exact effects of changing spectral bandwidth on the location of the the wavelengths of minimum reflec-

Table 3. The adopted wavelengths of minimum reflectance for the rare-earth oxide mixture at 25 °C and for spectral bandwidths (SBW) of 2, 3, 4, 5, and 10 nm.

Rare-earth oxide	Band No.	SBW 2 nm	SBW 3 nm	SBW 4 nm	SBW 5 nm	SBW 10 nm
Dy_2O_3	1	-----	743.0	743.4	743.4	-----
"	2*	-----	799.0	799.0	798.6	798.0
"	3*	887.2	886.9	886.7	886.7	886.5
"	4	906.3	906.8	907.5	907.3	-----
Er_2O_3	5	970.6	971.3	971.6	971.6	-----
"	6	979.6	980.8	980.8	980.8	-----
"	7	1012.9	1013.2	1012.9	1012.8	-----
Dy_2O_3	8	1064.7	1065.0	1065.0	1064.9	-----
"	9	1095.6	1096.0	1096.2	1096.4	-----
Ho_2O_3	10*	1132.2	1132.3	1132.4	1132.9	1132.9
"	11*	1148.1	1148.4	1148.5	1148.7	1148.6
Dy_2O_3	12	1192.9	1192.7	1192.9	1192.9	-----
"	13	1230.2	1230.2	1230.2	1230.3	-----
"	14*	1261.0	1260.9	1260.8	1260.8	1261.8
"	15	1320.7	1320.7	1320.8	1320.7	1320.2
Er_2O_3	16	1456.2	1456.4	1456.7	-----	-----
"	17	1461.7	1461.9	1462.2	-----	-----
"	18	1471.2	1471.6	1471.6	-----	-----
"	19	1477.4	1477.6	1477.5	-----	-----
"	20	1494.8	1494.9	1495.0	1495.0	-----
"	21	1503.4	1503.5	1503.5	-----	-----
"	22	1516.0	1516.0	1515.9	1515.7	-----
"	23*	1535.5	1535.6	1535.6	1535.4	1534.6
"	24	1544.7	-----	-----	-----	-----
"	25	1548.1	-----	-----	-----	-----
"	26	1555.1	1555.0	1554.8	-----	-----
"	27	1577.1	1577.2	1577.2	-----	-----
Dy_2O_3	28	1611.8	1611.7	1611.7	1611.9	-----
"	29	1642.7	1642.7	1642.5	1642.5	-----
"	30*	1682.6	1682.3	1682.2	1682.2	1681.4
"	31*	1757.6	1757.8	1757.9	1757.8	1757.6
Ho_2O_3	32*	1847.5	1847.3	1846.9	1847.0	1847.3
"	33	1874.3	1874.0	1873.8	1874.0	-----
"	34	1885.0	1885.3	1885.7	1885.5	-----
"	35*	1930.9	1931.6	1932.2	1932.5	1935.5
"	36*	-----	1970.6	1970.7	1970.8	1970.8
"	37	-----	2004.5	2005.9	2005.8	2006.3

The uncertainty in the wavelengths of minimum reflectance are believed to be no greater than ±1 nm.

---

* (preferential bands)

tance for the rare-earth oxide absorption bands because some of the uncertainties discussed in section 2.3.4 are large enough to mask the bandwidth effects. However, the apparent shift in the wavelengths of the minima are sometimes larger than the overall uncertainty. Therefore, all the results are listed in the table.

For purposes of checking the wavelength scale of a reflectance spectrophotometer there are many reflectance minima listed in table 3. A few of the minima might be considered as being preferable because the absorption bands are observed at bandwidths as large as 10 nm. These bands are marked with an asterisk after the band number in the table.

3.3 Influence of Temperature

All the data listed in table 3 was obtained at a temperature of 25 °C ±0.5 °C. The effects of temperature on the location of the wavelengths of minimum reflectance of the rare-earth oxide mixture were studied by analyzing one absorption band for each of the three rare-earth components. The results are shown in table 4 for bands 14, 23, and 32, at 20 °C, 25 °C, and 30 °C. These measurements were made with a spectral bandwidth of 4 nm. Because these measurements did not prove or disprove the effects of temperature, and effect was as-

Table 4. The observed effects of temperature on the wave lengths of minimum reflectance for 20 °C, 25 °C, and 30 °C. The temperature effects are not revealed by the observed differences because of larger uncertainties discussed in section 2.3.4.

(spectral bandwidth = 4 nm)

Temperature	Band No. 14 (Dy_2O_3)	Band No. 23 (Er_2O_3)	Band No. 32 (Ho_2O_3)
20 °C	1260.8 nm	1535.7 nm	1847.0 nm
25 °C	1260.8	1535.6	1846.9
30 °C	1261.0	1535.5	1846.7

sumed based on the largest differences observed for the data in table 4 for purposes of estimating the overall uncertainty (see sec. 2.3.4).

3.4 Influence of Instrument Sensitivity Function

The instrument function is the relative sensitivity of the instrument as a function of wavelength as observed in the single beam mode of operation with no sample in the beam. The instrument sensitivity is influenced by a number of parameters such as the energy output of the source as a function of wavelength, grating efficiency, reflection of mirrors, transmission of windows, and spectral response of the detector. The near infrared instrument sensitivity of the Varian-Cary 2390 spectrophotometer, increases from 700 nm to approximately 1150 nm, then decreases with increasing wavelength. There are some local variations in this sensitivity curve due to absorption features associated with optics and atmospheric conditions. The effect of the instrument sensitivity function on the wavelengths at which absorption features appear for a specimen being scanned is to shift the scale to longer wavelength when the instrument sensitivity is increasing from shorter wavelength to longer wavelength (positive slope) and to shift the scale to shorter wavelength when the instrument sensitivity is decreasing from shorter wavelength to longer wavelength (negative slope). The amount of wavelength shift increases as the slope becomes steeper with changing wavelength.

The shift in wavelength due to the influence of the instrument sensitivity can be determined to a close approximation, using the following equation:

$$d\lambda = \frac{a\, w^2}{6}$$

where:

$d\lambda$ = the wavelength displacement,

a = the slope of the sensitivity curve normalized at the center of a triangle,

w = the width at the half-height of the geometrical passband.

The wavelength shift is greater for very wide spectral bandwidths and almost negligible for very narrow spectral bandwidths. The effect of instrument sensitivity function is not cancelled by operating the instrument in a double-beam mode. The measured location of emission lines such as those described in section 2.3.1 is not influenced by the instrument sensitivity function because the emission lines are relatively narrow with respect to the spectral bandwidth.

The data for the reflectance minima listed in table 3 and 1 have been adjusted for the influence of the instrument sensitivity function. The amount of adjustment varied from zero where the sensitivity slope was essentially flat to as much as 0.26 nm where the slope was steep and the spectral bandwidth was 10 nm. For all but 10 of the values listed in these tables, the wavelength shift due to the influence of the instrument sensitivity function was less than 0.1 nm.

4. Results

4.1 Reflectance of the Rare-Earth Oxide Mixture

The general reflectance spectrum of the rare-earth oxide mixture is illustrated in figures 1-1 through 1-7 for a nominal spectral bandwidth of 4 mm. The absorption bands are numbered in order to associate the data listed in the tables with the spectral features illustrated in the figures.

4.2 Numerical Results

Most of the absorption bands appearing in figures 1-1 through 1-7 were analyzed and the recommended values for the wavelengths of minimum reflectance are listed in table 3 for the indicated spectral bandwidths. Preferred bands are identified by asterisks after the band numbers in the table.

5. Other Measurements

A check of the reflectance of the Er_2O_3 absorption bands at approximately 1012 nm (Band No. 7) and 1535 nm (Band No. 23), and Dy_2O_3 band at approximately 1260 nm (Band No. 14) was made on the NBS Reference spectrophotometer for diffuse reflectance [6]. This spectrophotometer uses a 1-meter monochromator equipped with a prism predisperser. The spectral bandwidth was set at 5 nm or 10 nm. The reflectometer is a 30 cm diameter integrating sphere with a lead-sulfide detector. Measurements are recorded with the wavelength drive set at fixed wavelengths. At each wavelength setting the signal is processed by a current-to-frequency converter and integrated over a 4 second time interval. The reflectance of the sample is measured relative to the sphere wall which is coated with a spectrally neutral white diffuser [5].

The wavelength correction for the reference spectrophotometer was determined by measuring the emission lines of a Hg lamp at 1013.97 nm and 1529.58 nm. These measurements indicate that the reference instrument wavelength scale was reading too high by +0.82 nm at 1014 nm and +0.35 nm at 1530 nm for a 5 nm spectral bandwidth. The reflectance minima of the Er_2O_3 bands at approximately 1012 nm and 1535 nm are close to the Hg emission wavelengths. The sample reflectance was measured at 0.2 nm intervals. From these data, the reflectance minima for band numbers 7, 14, and 23 were determined to be 1012.9 nm, 1260.7 nm and 1535.5 nm respectively for a spectral bandwidth of 5 nm after correcting for the wavelength scale error. Band No. 23 was determined to be at 1534.5 nm for a 10 nm spectral bandwidth.

A comparison of reflectance minima results for bands 7, 14, and 23 as determined on the Varian-Cary and Reference spectrophotometers, indicates that a wavelength bias of approximately 1 nm exists between the two instruments after the wavelength scale has been corrected for all known sources of error (see table 5). Measurements of the reflectance minima made by the Instrumental Research Laboratory [7], of the U.S. Department of Agriculture (USDA) indicate a similar wavelength bias between their spectrophotometers and the Varian-Cary instrument used in this work. Repeated measurements on the Varian-Cary instrument after 1.5 years indicate that the bias remains constant. Because of the strong evidence for this wavelength bias and confidence in the wavelength accuracy of the NBS Reference spectrophotometer, and the supporting evidence from the USDA, the data in table 3 has been adjusted to correct for the Varian-Cary near infrared wavelength scale bias. The over-all uncertainty of ±1 nm given in section 2.3.4 remains the same for these adjusted reflectance minima.

Table 5. A comparison of the data for reflectance minima numbers 7, 14, and 23 as determined on the Varian-Cary spectrophotometer and the NBS Reference spectrophotometer.

Band No.	SBW (nm)	Reflectance Minima Varian-Cary Instrument (1)	Reference Instrument (2)	Difference (2)-(1)
7	5	1011.8	1012.9	−1.1
14	5	1259.8	1260.7	−0.9
23	5	1534.4	1535.5	−1.1
23	10	1533.6	1534.5	−0.9

6. Conclusion

In addition to those uncertainties discussed above there are also other factors that might introduce uncertainties affecting the results of this study. Although these have not been quantitatively investigated, they include: 1) purity of the rare-earth oxides. 2) variation in the ratios of the three rare-earths that are mixed to form the specimen, and 3) variation in the density of the pressed powder. All three of these factors can be controlled to a high degree of precision in the preparation of the three-component rare-earth mixture used in this study. The purity of the individual constituents is sufficiently high (99.99%) so that it is not likely that slight variations in this parameter will affect the location of the wavelengths of minimum reflectance. The ratios of the three rare-earth components was established by careful weighing. For a weighing of 2 g, an uncertainty of ±0.01 g is too small to have much effect on the location of the wavelengths of minimum reflectance. Mixing of the three components must be thorough, however, to avoid inhomogeneities.

Figures 1-1 through 1-7 should only be used as a key to the appearance of the reflectance spectra. Refer to table 3 for the numerical values. The reflectance data shown in the figures should not be used for purposes of a reflectance standard. The absolute reflectance of pressed Halon [5] has been established for this type of calibration.

A wavelength standard based on the diffuse reflectance of a mixture of three rare-earth oxides has been analyzed and calibrated for the near infrared spectral range 700 to 2000 nm. The reflectance minima obtained from a mixture of Dy_2O_3, Er_2O_3, and Ho_2O_3 have been determined for nominal spectral bandwidths of 2, 3, 4, 5, and 10 nm. The principal sources of error influencing the accuracy of the assigned wavelengths of the reflectance minima are the calibration of the spectrophotometer wavelength scale and the imprecision in the techniques used to record and estimate these minima.

This proposed wavelength standard should provide a useful means for checking the accuracy of the near infrared wavelength scale of spectrophotometers equipped with suitable accessories for measuring diffuse reflectance if the required wavelength accuracy does not have to be better than ±1 nm.

An uncertainty of ±1 nm for this near infrared wavelength standard is less accurate than current wavelength standards for the ultraviolet and visible spectral ranges. A wavelength standard based on a solution of Ho_2O_3 in perchloric acid [8] provides 14 transmittance minima for wavelength scale calibration in the ultraviolet and visible spectrum. The overall uncertainty for this wavelength standard is ±0.1 nm for the location of the transmittance minima.

References

[1] Certain commercial equipment or products are metioned in this paper in order to adequately document the work. In no case does this imply that the equipment or product is being endorsed by the National Bureau of Standards or that it is necessarily the best equipment or product for the application.

[2] The rare-earth oxides were obtained from Research Chemicals, a division of Nucor Corp., Phoenix, Arizona.

[3] CRC Handbook of Chemistry and Physics, 63rd Edition, CRC Press Inc., (1982–1983).

[4] Acquista, N., and E. K. Plyler, Calibrating Wavelengths in the Region from 0.6 to 2.6 Microns, J. Res. Natl. Bur. Stand., Vol. 49, 13–16 (July 1952).

[5] Weidner, V. R., and J. J. Hsia, Reflection Properties of Pressed Polytetrafluoroethylene Powder, J. Opt. Soc. Am., Vol. 71, 856–861, (July 1981).

[6] Venable, W. H. Jr., J. J. Hsia, and V.R. Weidner, Development of an NBS Reference Spectrophotometer for Diffuse Transmittance and Reflectance, Natl. Bur. Stand., Tech. Note 594–11, October 1976.

[7] Memorandum from: Dr. Karl H. Norris and William R. Hruschka, Instrumentation Research Laboratory, USDA, BARC-W, Beltsville, MD 20912.

[8] Weidner, V. R.; R. Mavrodineanu, K. D. Mielenz, R. A. Velapoldi, K. L. Eckerle, and B. Adams, Spectral Transmittance Characteristics of Holmium Oxide in Perchloric Acid Solution, J. Res. Natl. Bur. Stand., **90–2** (1985).

Journal of Research of the National Bureau of Standards

The Triple Point of Oxygen In Sealed Transportable Cells

Volume 91 Number 5 September–October 1986

George T. Furukawa

National Bureau of Standards
Gaithersburg, MD 20899

The triple points of oxygen samples sealed in miniature pressure cells were investigated by means of adiabatic calorimetry. The triple point of a 99.999 percent pure commercial oxygen sample was found to be 0.94_0 mK higher than that of an "ultra-pure" sample prepared by thermal decomposition of potassium permanganate ($KMnO_4$). The higher value is attributed principally to argon impurity in the commercial oxygen. The results of eight sets of observations using six thermometers, calibrated on the International Practical Temperature Scale of 1968 as maintained at the National Bureau of Standards, and two sealed cells of the ultra-pure oxygen show a range of 0.17_8 mK. The capsule-type platinum resistance thermometers that have been used are shown to have outstanding stability and the multiple calibrations made on them at the National Bureau of Standards extending over six years are shown to be consistent to within 0.15 mK at 54.361 K. The results of measurements on an internationally circulated sealed cell of commercial oxygen show its temperature to be 0.58_1 mK higher than those of the ultra-pure oxygen.

Key words: adiabatic calorimeter; International Practical Temperature Scale of 1968; melting point; miniature oxygen cell; oxygen preparation; oxygen triple point; platinum resistance thermometer; temperature fixed point; triple point.

Accepted: March 19, 1986

1. Introduction

The triple point of oxygen (54.361 K) is one of the defining fixed points of the International Practical Temperature Scale of 1968 (IPTS-68) [1][1]. In a report on the international comparison of triple point temperatures of pure gases sealed in miniature pressure cells [2], the results on oxygen showed a range of values of about 2 mK while the results on argon, neon, and hydrogen showed a range of about 0.4 to 0.5 mK. With oxygen, the lower temperatures that were realized were considered to be representative of purer samples and the higher temperatures to be due to the presence of argon which raises the apparent triple point [3,4]. The amount of argon that was known to be present in some of the oxygen samples could not completely account for the higher values. This paper describes, as part of the continuing research at the National Bureau of Standards (NBS) on the reproducibility of the triple points of pure substance sealed in cells, the measurements of the triple points of three oxygen samples. One of the measurements was on the oxygen cell (designated IMGC-80_2) that was used in the international comparison of fixed points; it was prepared at the Istituto di Metrologia "G. Colonnetti" (IMGC, Italy) using commercially available high-purity oxygen

About the Author: George T. Furukawa is with the Temperature and Pressure Division in the NBS Center for Basic Standards.

---

[1] Figures in brackets indicate literature references.

[5]. One of the other two samples was also from a commercial source. The third sample was prepared by thermal decomposition of potassium permanganate ($KMnO_4$) under meticulous conditions to yield a sample of ultra-high purity. Measurements were obtained on two cells of this prepared oxygen. The measurements on each of the samples show reproducibility of about ±0.02 to ±0.03 mK, but the range of the triple points of the three samples is about 1 mK.

As an integral part of the investigation, the results of the measurements using six capsule-type standard platinum resistance thermometers were compared to determine the stability of these thermometers and the consistency of their calibrations at NBS. (Henceforth, for convenience, the capsule-type platinum resistance thermometers that meet the specifications of the IPTS-68 [1] will be referred to by the abbreviation SPRT's.) As shown previously in the work on the triple point of argon [6], the present measurements will also show that these six SPRT's have outstanding stability and that the NBS calibrations on them over a number of years are highly reproducible.

2. Method and Experimental Procedure

2.1 Method

The technique for determining the triple points of pure gases sealed in miniature pressure cells involves the measurement of equilibrium temperatures at various known ratios of liquid-to-solid phases of the sample under adiabatic conditions. (Under the conditions of the experiment, the vapor volume is larger than 10 times the sum of the volumes of the two condensed phases. Hence, the change in the vapor volume over the range of various fractions melted was considered negligible and the amount of impurities in the vapor to be constant.) Similar techniques have been used for many years in the calorimetric determination of chemical purity and the triple-point (or the melting point) of a variety of substances [7].

For an "ideal" system (where Raoult's law is valid and the impurities remain segregated in liquid solution), the equilibrium at temperature T between a liquid mixture and a pure solid of the major component can be represented by

$$\ln\frac{\lambda_1^0(T)}{\lambda_1(T)}=\frac{\Delta H}{R}\left(\frac{1}{T}-\frac{1}{T_0}\right) \tag{1}$$

where $\lambda_1^0(T)$ is the absolute activity of the pure liquid at temperature T and similarly $\lambda_1(T)$ is the absolute activity of the same substance in the particular liquid mixture [8]. T_0 is the melting (or freezing) point of the pure solid, R is the molar gas constant, and ΔH is, in order to simplify the equilibrium relation to (1), the average molar heat of fusion over the temperature interval T to T_0 (see reference [9] for an extended relation). Since $\lambda_1^0(T)/\lambda_1(T)$ is greater than unity, T is less than T_0. From the Gibbs-Duhem relation, for an ideal mixture

$$\lambda_1=(1-x_2)\lambda_1^0, \tag{2}$$

where

$$x_2=N_2/(N_1+N_2) \tag{3}$$

and N_1 is the number of moles of the major component (oxygen) and N_2 the number of moles of the minor component (impurities). By combining eqs (1) and (2), there is obtained

$$-\ln(1-x_2)=\frac{\Delta H}{RTT_0}(T_0-T). \tag{4}$$

When x_2 is small (i.e., when the oxygen sample is highly pure), $-\ln(1-x_2)$ is approximately equal to x_2 and TT_0 and T_0^2 are nearly equal. Then eq (4) is approximately

$$x_2=\frac{\Delta H}{RT_0^2}(T_0-T). \tag{5}$$

For oxygen, $\Delta H=443.5$ J mol^{-1} [10]; therefore, $\Delta H/RT_0^2$ evaluates to 0.01805 K^{-1} and eq (5) simplifies to

$$x_2=0.01805\,(T_0-T). \tag{6}$$

Equation (6) indicates that in order for the temperature depression (T_0-T) due to impurities to be less than 0.1 mK, x_2 must be less than 2×10^{-6} mol fraction. (It is to be noted that compared to metals, the value of $\Delta H/RT_0^2$ for oxygen, as well as for most molecular substances, is relatively large. In the case of zinc, $\Delta H/RT_0^2=0.0019$ K^{-1}, which indicates that the total impurity concentration must be one-tenth of that for oxygen or less than 0.2 ppm in order for the temperature depression to be less than 0.1 mK.)

If the assumption that the impurities remain segregated in the liquid phase holds, then at equilibrium the impurity concentration in the liquid would vary inversely with the fraction F of oxygen melted. Thus,

$$x_2=x_2^*/F, \tag{7}$$

where x_2^* is the overall impurity concentration or the impurity concentration of the liquid when the oxygen is completely melted. When eqs (6) and (7) are combined, there is obtained

$$x_2^*/F=0.01805\,(T_0-T) \tag{8}$$

or

$$(T_0-T)=55.40\,x_2^*/F. \tag{9}$$

Equation (9) shows that the impurity concentration x_2^* can be obtained from the "slope" ($55.40\,x_2^*$) of the linear relation of the observed equilibrium temperature T versus $1/F$. At $1/F=0$, $T=T_0$, the triple point of pure oxygen. The temperature at $1/F=1$ is that value when vanishingly small amount of solid oxygen is present in equilibrium. As mentioned earlier, the method [i.e., eq (9)] has been employed for many years in the determination of impurity concentration as part of the heat-capacity measurements because the fraction F melted can be accurately determined and the difference in the equilibrium temperatures (T_0-T) caused by the impurities can be amplified in accordance with the reciprocal of fraction melted [7]. The practice has been to observe a number of equilibrium temperatures at different fractions melted and obtain the "best values" of x_2^* and T_0.

In experimental situations, the results deviate more or less from the idealized equations given above due to many factors. First of all, in the case of oxygen, the commercially available high-purity material is obtained principally by separation from air and, hence, other components of air are expected to be present as impurities, e.g., nitrogen, argon, and other noble gases. Neon, krypton, and xenon have been reported to lower the freezing (liquidus) point of oxygen [3]. Both nitrogen and argon are known to form solid solutions with oxygen [11,12]. Most likely, in high-purity oxygen, the former three noble gases would also form solid solutions. Furthermore, oxygen and argon mixtures form a peritectic in the oxygen-rich region. The rather sparse experimental data suggest that the peritectic point composition is in the region of 80 to 85 mol percent oxygen [12,13]; the peritectic temperature is around 55.8 K; and the "peritectic break" occurs at about 88 mol percent oxygen. In this oxygen-rich region of the system, the liquidus and solidus curves are very closely spaced. The samples for oxygen triple point measurements are expected to have small enough argon concentrations that they would behave as binary isomorphous systems [14] and that no peritectic reaction would be observed (i.e., there will be a "melting range"). The solid solution would be richer in argon than the liquid solution, making the equilibrium temperature T greater than T_0, in contrast with the premise upon which eqs (1) to (9) were derived.

There are other considerations in the real experimental situations. Whenever the compositions of the liquid and solid phases are the same and remain the same, although the ratios of the amounts of the two phases are changed by melting, the equilibrium temperatures remain unchanged. This is the case with a 100-percent pure sample and with eutectic mixtures. The outstanding example of an eutectic is that of the tin-iron system with its eutectic composition at 0.001 mol-percent of Fe and the eutectic temperature only 8 mK lower than the freezing point of pure tin [15]. Also, if the compositions of the liquid phase and of the solid phase in equilibrium remain unchanged, even though the ratios of the amounts of the two phases are changed, the equilibrium temperature will remain the same. The outstanding case of this is the ice bath, where there is an infinite amount of air present to maintain the water saturated with air as the pure ice melts. This situation would be expected at low temperatures where an impurity, e.g., water in normal heptane, is frozen but is sufficiently soluble in the major component to affect its freezing point (182 K); the liquid is saturated with the impurity over the entire range of fraction melted. [Experimental data seem to be non-existent, but the system oxygen-carbon dioxide could possibly be another example of such a system.]

The peritectic point of a binary system is an invariant point with four phases (including the vapor) in equilibrium; the equilibrium temperature remains unchanged as the amounts of the two solid phases and the liquid solution are changed on heating. In such systems or solids with more than one component (solid solutions), the self-diffusion rate is so slow compared with that in the liquid, that it is unlikely during the experimental period that there would be a true phase equilibrium [16,17]. In the extreme case where a frozen solid is uniform in composition and there is no diffusion in the solid, equilibrium temperature would remain unchanged at different fractions melted because the liquid composition would remain the same as that of the solid. In the real experimental case, there would be expected some segregation of impurities on freezing but very little diffusion in the solid.

Considering the above possibilities that would affect the triple point of oxygen, on most of which there is no direct quantitative information, it was decided to prepare as pure an oxygen sample as possible and to use extreme care in filling cells with the sample for triple point measurements. A small amount of impurity would have a relatively large effect on the small sample that was to be used. In the application of the method to obtain triple points for temperature standards, the sample should be sufficiently pure that the difference (T_0-T) would be negligible. Although the oxygen samples were not expected to "behave ideally," the ideal solution theory was used as a guide in correlating the results.

2.2 Calorimetric Cryostat

The equilibrium temperatures were measured, at various known melted fractions of the oxygen samples, in an adiabatic cryostat that had been used previously for determination of heat capacities [18]. The miniature pressure cell of the oxygen sample was installed in place of the vessel that would contain the substance for heat-capacity measurements. Figure 1 shows schematically the general arrangement of the apparatus. The calorimetric apparatus was designed to provide as nearly adiabatic conditions as possible so that the observed equilibrium temperatures could be accurately correlated with the measured amounts of electrical energy that were introduced into the pressure-cell system. Briefly, the apparatus was designed as follows. The electrical leads (insulated 0.16 mm diameter copper wires) that entered the vacuum space of the apparatus through the hard-wax, "hermetic" lead seal of the terminal box were brought to the refrigerant temperature on the copper tempering ring. All tempering of electrical leads was done either by cementing them into close-fitting machined grooves (see fig. 1, "tempering ring," "ring lead control," and "thermometer-heater lead control") or by soldering them to the ends of copper strips cemented on "temperature-station" surfaces ("auxiliary isothermal shell" and pressure cell). To achieve adiabatic conditions, the leads were first heated on the floating copper ring lead-control close to the temperature of the thermometer-heater lead control. The leads that went to the pressure-cell system were tempered next on the thermometer-heater lead control to the temperature of the auxiliary isothermal copper shell around the pressure cell. Before the leads went to the SPRT's, they were tempered on the auxiliary isothermal copper shell and then on the pressure cell. The insulation resistances between all leads and between the leads and their tempering surfaces were regularly checked to be 10^9 ohms or larger. The temperatures of the adiabatic shield, thermometer-heater lead control, and ring lead control were controlled by automatic adjustment of electrical power in the heaters wound on their surfaces, using appropriately placed differential thermocouples of constantan and Chromel-P wires. The heaters on the adiabatic shield were wound and cemented into close-fitting grooves machined into the shield. As mentioned above, the temperature of the floating ring lead-control was controlled relative to the temperature of the thermometer-heater lead control which was in turn controlled relative to the temperature of the auxiliary isothermal shell. The temperature of the adiabatic shield, that enclosed the pressure-cell system, was also controlled relative to the temperature of the auxiliary isothermal shell. The adiabatic shield, the thermometer-heater lead control, and the auxiliary isothermal shell were gold plated to reduce radiative heat transfer. During operation, the vacuum space was maintained at 10^{-3} Pa or less. With the double-dewar cooling system shown, temperatures of about 48 K to 49 K were reached by pumping on nitrogen in the inner dewar while liquid nitrogen at atmospheric pressure was in the outer dewar. (Hereafter, an oxygen sample, its pressure cell, auxiliary isothermal shell, tempering strips and the installed SPRT or SPRT's will be referred to as an oxygen sample system.)

2.3 Energy Measurements

The source of electrical energy for the heaters (100 Ω) wound on the oxygen cells consisted of two 12 V lead storage batteries connected in parallel. The heater wire was an alloy (principally nickel and chromium) of low-temperature coefficient of resistance [19] so that the voltage readings across the heater would be nearly constant during current flow. All voltages [across the heater and across the reference resistor of known value (about 1 Ω) in series with the heater] were determined using a digital voltmeter with seven-digit readout. The range change feature of the digital voltmeter readily accommodated the 100-fold voltage change across the heater and reference resistor. The time interval of heating, which was never less than 120 s, was determined to within ±0.01 s with a precision analog clock operated using the NBS 60 Hz frequency standard. The clock was operated synchronously with a switch that turned the current from a "dummy load" to the oxygen cell heater. (For details of the circuitry, see reference [20].) The voltages across the heater and the reference resistor were read alternately every 15 s; the

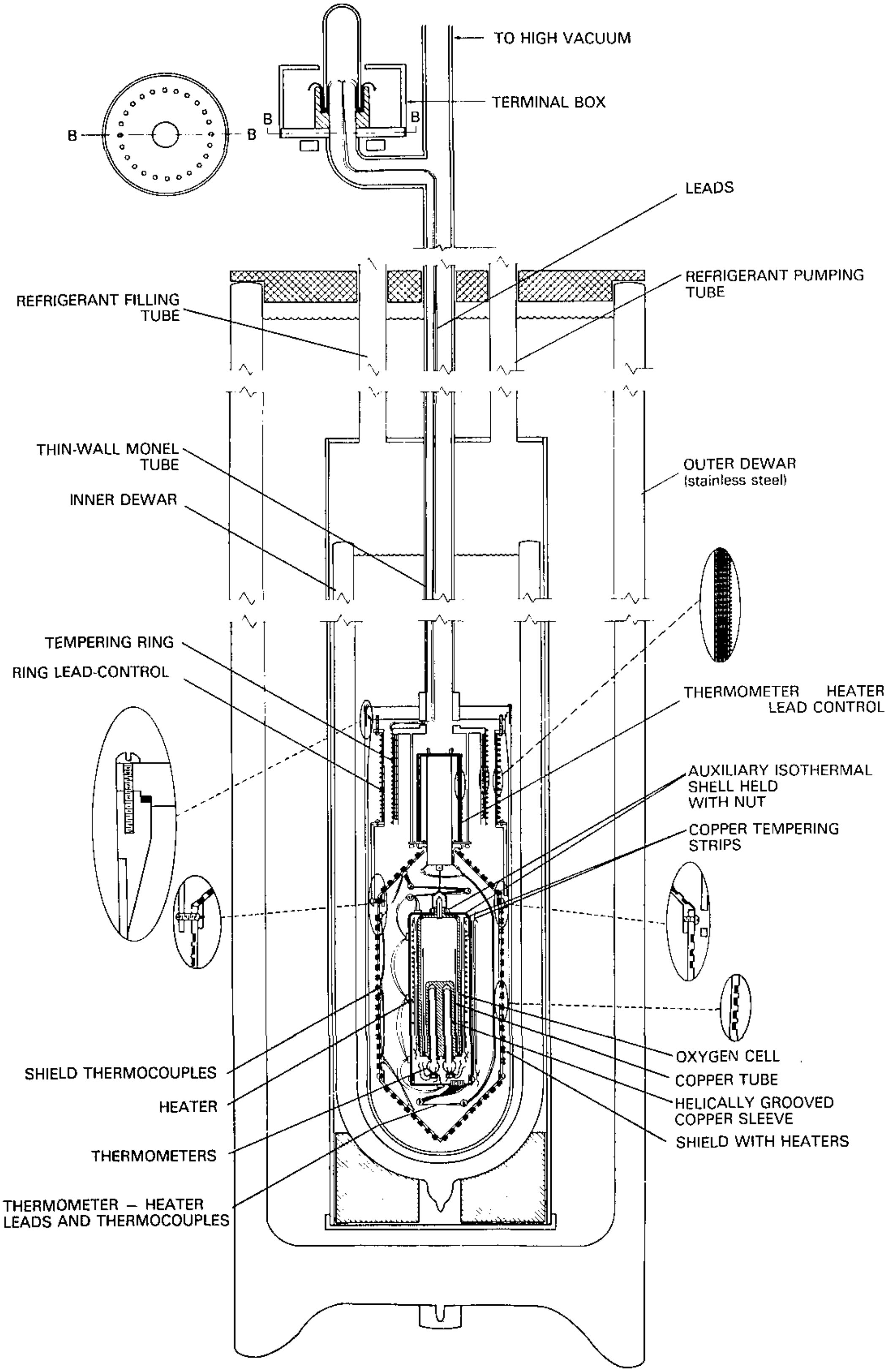

Figure 1—Schematic of adiabatic calorimetric apparatus shown with oxygen cell system PO-3 installed.

readings were averaged to obtain the electric power that was introduced. The energy increments that were introduced were relatively large (30 to 300 J) for the determination of the heat of fusion of the oxygen sample or the heat capacity of the oxygen-sample system, but only 3 to 20 J during measurements of the equilibrium temperatures at various small amounts of sample melted. The estimated accuracy of the electrical energy measurements was about ±0.01 percent.

2.4 Experimental Procedure

The experimental procedure was very similar to that described for the investigation of argon triple point cells [6]. Briefly, with helium gas for heat exchange in the vacuum space of the cryostat, the inner and outer dewars were filled with liquid nitrogen. When the oxygen cell cooled to about 80 K, the inner dewar was refilled with liquid nitrogen and pumped overnight using a high-capacity vacuum pump. During cooling, the liquid oxygen sample was found to supercool about 1 K before recalescence was observed. By morning, the oxygen sample had cooled to about 48 or 49 K. The helium exchange gas was then removed and the vacuum space pumped out to a high vacuum (less than 10^{-3} Pa), automatic temperature controls were switched on, and the temperatures of the adiabatic shield, of the floating ring lead-control, and of the themometer-heater lead control were controlled at the temperature of the auxiliary isothermal shell of the sample cell. Under these experimental conditions, a single filling of nitrogen in the inner dewar provided enough refrigeration to control the cryostat near the triple point of oxygen for about 80 hours.

After temperature equilibrium was established, the first series of measurements involved the determination of the heat capacity below the triple point, of the total heat of fusion, and of the heat capacity above the triple point. The procedure was as follows. Three heat-capacity "points" were obtained at successively increasing temperature below the triple point. The final temperature of the third heat-capacity point was arranged so that it would not be more than 1 K below the triple point. The first two values of heat capacity were used to estimate the amount of electrical energy required to heat within 1 K of the triple point. Electrical energy was then introduced continuously from the equilibrium temperature just below the triple point to just above it. The amount of energy to be introduced was estimated from the heat capacity and the approximate heat of fusion. After the equilibrium temperature was established just above the triple point, three heat-capacity points were obtained at successively increasing temperatures in the liquid phase of oxygen. The plot of these two sets of three heat-capacity points was used to determine the total heat of fusion and later the fraction of sample melted during the melting-point experiments.

The heat of fusion L of the sample was calculated from the total heat Q introduced from the temperature T_i just below the triple point to the temperature T_j just above it and the heat capacities in the two regions below and above the triple point according to the relation:

$$L = Q - C_s(T_{tp} - T_i) - C_l(T_j - T_{tp}), \tag{10}$$

where C_s is the heat capacity in the region of solid oxygen at temperature $(T_i + T_{tp})/2$, C_l is the heat capacity in the region of liquid oxygen at temperature $(T_{tp} + T_j)/2$, and T_{tp} is the triple point temperature of oxygen. To determine the amount of electrical energy required to melt known amounts of oxygen, the sample was first cooled to a temperature about 1 K below the triple point and the equilibrium temperature was established under adiabatic conditions as previously described. After determining the equilibrium temperature T_1, the amount of heat Q_1 required to melt the desired initial fraction F_1 was calculated according to

$$Q_1 = F_1 \times L + C_s(T_{tp} - T_1), \tag{11}$$

where C_s is the heat capacity in the region of solid oxygen at temperature $(T_1 + T_{tp})/2$. After the equilibrium temperature was determined at fraction F_1 melted, energy Q_2 was added to obtain the equilibrium temperature at fraction F_2 melted according to

$$Q_2 = (F_2 - F_1)\, L. \tag{12}$$

The energies for other fractions melted were determined in the same manner.

Depending upon the impurity concentration, a small fraction of sample may be already melted at the initial temperature T_i or T_1 below the triple point. This "premelting" was calculated, and the adjustments were made wherever applicable, on the assumption that all of the impurities were in liquid solution (no solid solution) and the liquid solution to be ideal. The relation used was

$$F_p = 55.40\, x_2^*/(T_{tp} - T_i), \tag{13}$$

where F_p is the fraction premelted, x_2^* is the mole fraction impurity in the oxygen sample, 55.40 is $RT_0^2/\Delta H$ given in eq (9), and T_i or T_1 is the initial temperature just below the triple point [20]. (Note: The symbols T_{tp} and T_0 for the triple point of pure oxygen will be used interchangeably.)

3. Oxygen Samples

Measurements were made on three oxygen samples in four sealed pressure cells. One sample was a commercially available "scientific-grade" oxygen stated by the supplier to be 99.999 percent pure with less than the following amounts of impurities in volume parts per million (vppm): 5 of argon, 3 of nitrogen, 0.5 of water, and 1 of carbon dioxide. Since the cost of chemical analysis was prohibitively high and since the material was unlikely to be used as our temperature standard, no further chemical analysis was made. This oxygen sample will be referred to as "commercial oxygen." The second oxygen sample was provided by the IMGC sealed in a pressure cell, as part of the Comitè Consultatif de Thermométrie (CCT) sponsored program on the comparison of fixed points by means of sealed cells. This sample was also from a commercial source; its purity was stated to be 99.998 percent with impurities in vppm: 1.8 of nitrogen, 3.0 of argon, and 0.7 of methane [5]. The third oxygen sample was prepared by thermally decomposing potassium permanganate ($KMnO_4$). Extreme precautions were taken during the preparation to obtain a sample of the highest purity. This oxygen sample will be referred to as "prepared oxygen." The details of the procedure used in the preparation are given in the following section.

3.1 Prepared Oxygen Sample

In the preparation of oxygen by thermal decomposition of $KMnO_4$, according to the process: $2KMnO_4 + \text{heat} \rightarrow MnO_2 + K_2MnO_4 + O_2$, copious amounts of fine powder are known to be produced that can be readily carried along with the stream of oxygen gas that is generated [21]. Figure 2 shows schematically the arrangement that was used to prepare the oxygen sample. The heating mantle around the $KMnO_4$ sample flask contained an iron-constantan thermocouple which was used to monitor the heating temperature. Except for the valves, the valve manifold, and the high-pressure collection cylinder (1000 cm^3), the entire system was constructed of borosilicate glass. The fine powder that was produced was confined in the generator by means of a column of tightly-packed, borosilicate glass-wool filter.

The $KMnO_4$ sample (about 1500 g of "reagent-grade" material) was heated first to about 125 °C and pumped at high vacuum for seven days. At the same time, the glass-wool filter and the glass parts were heated to about 100 to 150 °C and pumped together with the $KMnO_4$ sample. Earlier, the stainless-steel collection cylinder had been heated to 300 °C, pumped at high vacuum, filled with a small amount of the commercial scientific-grade oxygen, and evacuated repeatedly seven times over a period of one week. The high-vacuum line always included two liquid nitrogen traps in series to

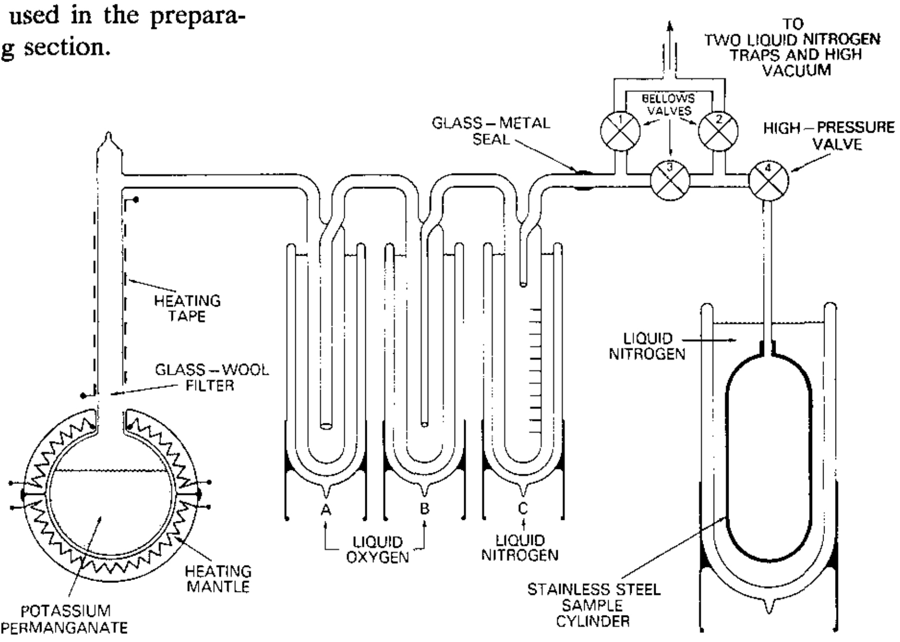

Figure 2—Arrangement used for preparing oxygen by thermal decomposition of potassium permangante $KMnO_4$.

minimize any back diffusion of oil from the oil-diffusion vacuum pump. After the heating and pumping to remove as much of the moisture and air as possible from the oxygen-preparation system, dewars of liquid oxygen were placed around the drying traps A and B and a dewar of liquid nitrogen was placed around the graduated collection tube C which was used to measure the amount of liquid oxygen that would be transferred to the stainless-steel cylinder. The $KMnO_4$ sample was heated to about 210 °C, at which temperature liquid oxygen began to collect in the liquid-nitrogen cooled collection tube. When about 15 cm^3 of liquid oxygen were collected, the heat in the mantle was turned off and the liquid oxygen that was collected was discarded by pumping. When the liquid oxygen was completely removed, the glass-wool filter and all glass parts were heated again to about 100 to 150 °C and pumped. In the meantime, the $KMnO_4$ oxygen generator had cooled sufficiently to cease generating oxygen. The system was kept at about 100 to 150 °C and was pumped overnight.

In the morning the generation of oxygen was resumed with liquid oxygen around the two drying traps (A and B) and liquid nitrogen around the collection tube (C). It was noted that, because of the insulating properties of the fine powder that was first formed adjacent to the heating mantle, the generation of oxygen started only after the thermocouple in the heating mantle indicated about 350 °C. After the oxygen began to collect the power in the heating mantle was reduced and a temperature of about 300 °C was maintained. (Although the discarded liquid oxygen was "decidedly blue," the newly collected liquid oxygen appeared to be less blue. If small amounts of ozone had been collected in the discarded sample, the higher temperatures that were used during the second time would decompose further any ozone, if present [22].)

After about 110 cm^3 of liquid sample were collected, the stainless steel cylinder was cooled in liquid nitrogen. The sample in the collection tube was then transferred to the cylinder by placing a dewar of liquid oxygen around the tube. Dewars of liquid oxygen were kept around the two drying traps during this transfer. Later, the pressure of oxygen sample (78.5 atm) in the stainless steel cylinder at ambient temperature indicated that about 3.5 moles were collected (about 75 percent yield based on the amount of $KMnO_4$ used). No chemical analysis of the prepared oxygen was made but the very small range of the melting points of samples from the cylinder indicate that it is highly pure (see section 6). Two cells were later filled from the cylinder.

4. Sealed Oxygen Cells

The measurements of the triple point of oxygen were made in four miniature pressure cells of different designs. Three were designed and fabricated at NBS. These cells were hydraulically pressure tested with distilled water to 250 atm before filling with oxygen. The fourth cell was fabricated and filled with oxygen at IMGC. One of the NBS cells, which was filled with the commercially obtained oxygen sample, was fabricated from type 316 stainless steel pipe of 48.3 mm O.D. and 3.7 mm wall thickness. It was identical in construction to one of the cells designated as AR-NBS-7 which was used in the study of the triple point of argon (see figure 2 of reference [6]). The cell accommodated one thermometer and the sample volume was about 50 cm^3. The extra large diameter was selected to determine whether future cells of the same diameter could be used with as many as seven SPRT's for calibration at the triple point of pure gases. The care that was exercised in its fabrication and in its filling with the oxygen sample was similar to that to be described for the following two NBS cells.

Two of the NBS cells, which were to contain the oxygen sample prepared from $KMnO_4$, were smaller than the cell used to contain the commercial oxygen, particularly since there was only a limited amount of the prepared pure sample. These cells were fabricated from commercial type 304 stainless steel of 25.4 mm o.d. and 2.1 mm wall thickness. One of these two cells accommodated one thermometer and the sample volume was 20 cm^3; the other cell accommodated three thermometers and its sample volume was 16 cm^3. The shapes of these two cells were about the same as shown for the three-thermometer cell in figure 1 and for the one-thermometer cell in figure 3. Copper tubes were installed inside the cells to enhance thermal equilibrium. The wall thicknesses of the copper tubes were adjusted so that the condensed oxygen would completely surround the thermometer. Since the diameters of the structures containing the re-entrant wells for the one-thermometer cells (including the cell for the commercial oxygen) were smaller, the wall thicknesses of the copper tubes for the cells were greater than for the three-thermometer cell. Before these copper tubes were assembled inside the cells, they were heated in a vacuum furnace (about 10^{-4} Pa) at 800 °C for about 24 hours to remove any hydrogen or other gases that may be dissolved in the copper. The stainless steel joints were "heliarc" welded.

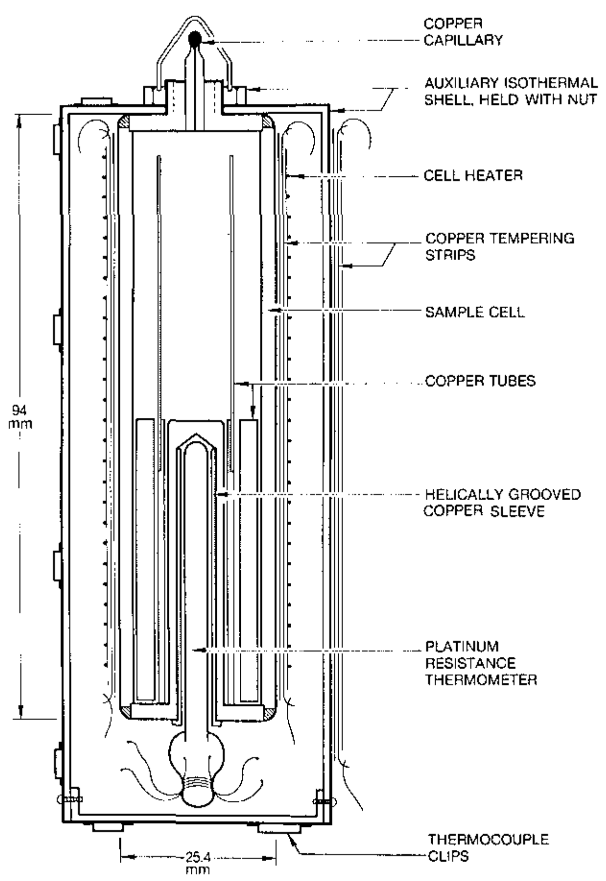

Figure 3—Oxygen cell system PO-1, shown for clearer view of construction. The cell PO-1 is similar to cell PO-3 shown in figure 1.

Extreme care and precautions were taken in cleaning and then filling the cells with the oxygen samples, since the design of the cells required these processes to be done through a copper or stainless steel capillary tube (3.2 mm o.d. and 0.6 mm i.d.). The copper capillary was silver brazed first to the top lid of the stainless steel cell and thoroughly cleaned before welding the lid. The cell used with the commercial oxygen had a stainless steel capillary which was welded to the lid [6]. The cells were filled individually with sample at different times. Since the cells were first pressure-tested with distilled water before filling with oxygen, they were thoroughly dried by baking first at about 120 °C inside a vacuum chamber for one week. During the week, the heated vacuum chamber containing the cell was filled several times with high-purity commercial oxygen and evacuated to displace any water vapor inside the cell. Care was taken to remove all of the water at the lower temperatures to avoid any possible reaction of water with the metal at the higher temperatures, forming the oxide and dissolving the hydrogen. After baking for an additional two weeks at 300 °C in vacuum, the cell was cooled under vacuum and back-filled with the high-purity commercial oxygen. Finally, the capillary filling tube of the cell was attached to a high-pressure manifold containing a stainless steel Bourdon-tube pressure gauge and an appropriate number (four) of valves for cleaning and filling the cell with sample. To the same manifold was attached the sample source with its separate high-pressure valve. The manifold, the Bourdon-tube gauge, and the cell were thoroughly evacuated (less than 10^{-4} Pa) for several days with two liquid-nitrogen traps in series in the vacuum line. During this time, the cell was heated to about 400 °C with a small tube-furnace. To avoid excessive oxidation of the cell, in particular the copper capillary tube, a gentle flow of argon or nitrogen was maintained inside the tube-furnace during the baking period. The manifold was occasionally heated using a "hot-air gun." After closing the valve to the vacuum system and after cooling the cell to ambient temperature, a small amount of the sample gas was introduced into the system and allowed to remain for several hours, after which the system was continuously evacuated overnight with the cell heated again to 400 °C. This process was repeated five times. After the fifth time, the valve to the vacuum line was closed and a small amount of the sample gas was introduced into the manifold system while the cell was at about 300 °C. It is expected that the copper surface and, to a lesser extent, the stainless steel surface were oxidized in the process. The purpose for oxidizing the surface was that the oxidized surface should be a barrier that would reduce the rate of future loss of sample oxygen through gradual oxidation of the metal surfaces. Following the oxidizing treatment, the cell was evacuated overnight and allowed to cool to the ambient temperature. Then, over a period of the next 10 days, the cell was purged 10 times by repeated filling with a small amount of the sample gas, allowing the gas to remain in the cell for a few hours, and then evacuating overnight. Finally, after the 10th purging operation, the cell was filled with sample to the desired pressure as read on the Bourdon-tube gauge and sealed by pinching the copper (or stainless steel) capillary tube flat over a length of about 2 cm. The tube was cut at about the middle of the "flat" with a pair of pliers and tested immediately for gas leakage by immersing the cell in water. The flat of the stainless steel capillary tube was cut with a heliarc torch. The cut flats of the three cells, which were sealed at widely separated occasions, did not exhibit any gas leakage, nor did the adjacent cut flats attached to the manifold. The cut edge of the flats and also the flats were covered with "soft solder" for added sealing and strength.

The cells were filled to sufficiently high pressures so that the heat of fusion of the sample in the cell would be comparable to or larger in magnitude than the heat capacity of the sample cell system (cell, sample, thermometer, auxiliary isothermal shell, copper tempering strips, and wires) and, therefore, the error contributed by the heat capacity in determining the amounts of sample melted would be negligible. The oxygen pressure in the cylinder of commercially obtained sample was 150 atm; hence, the 50 cm^3 cell was filled directly to 113 atm at ambient temperature from the cylinder by controlling the valve to the manifold and observing the Bourdon-tube gauge. The heat of fusion of the sealed sample was 102 J and the heat capacity of this sample cell system was approximately 128 J/K at 54.5 K. The oxygen sample and this cell will be referred to as CO-7.

The desired filling pressures for the cells that would contain the oxygen sample prepared from $KMnO_4$ were higher than the 78.5 atm pressure of the sample in the storage cylinder. The one-thermometer cell was filled to 100 atm at ambient temperature by first cooling the cell nearly to the temperature of a Dry Ice-ethyl alcohol mixture and then introducing the sample from the storage cylinder. The heat of fusion of the sealed sample was 35 J and the heat capacity of this sample cell system was approximately 38 J/K at 54.5 K. This specimen of prepared oxygen and the cell will be referred to as PO-1.

The three-thermometer cell was filled to 163 atm at ambient temperature by first cooling the cell to the temperature of liquid nitrogen and then introducing the oxygen sample from the storage cylinder for a measured period of a few minutes through a flow control valve. After closing the control valve, the sample cell was allowed to warm to the ambient temperature and the pressure read on the Bourdon-tube gauge. On the basis of this pressure reading and the period of time the flow control valve was open, an estimate was made of the time that would be needed for the second filling, at the same flow condition, to fill the cell to the desired pressure. The heat of fusion of the sealed sample was 53 J and the heat capacity of this sample cell system was approximately 35 J/K at 54.5 K. This specimen of oxygen and the cell will be referred to as PO-3.

The thermometer wells of the three pressure cells that were made at NBS were designed to be about 1 mm larger in diameter than the typical outer diameter of capsule-type SPRT's to accommodate copper sleeves that closely fitted the well and the capsule SPRT. Widely spaced helical grooves were machined into the outer surface of the sleeves to vent air, so that the SPRT could be easily installed or removed from the well without-causing possible harm to the SPRT. To enhance heat transfer between the parts, a thin film of stopcock grease was used on surfaces that were in contact.

The cells were designed to accommodate the auxiliary isothermal shells which were held in place at the top by nuts (see figs. 1 and 3). The auxiliary isothermal shell, made of copper, served to protect the SPRT from stray thermal radiation and also temper the electrical leads before they were tempered on the cell itself. During the measurement process, the shell provided an isothermal surface for adiabatic control and thus reduced thermal gradients in the cell. A thin film of stopcock grease was applied to the screw threads and the surfaces in contact to enhance heat transfer. The auxiliary isothermal shell had clips for differential thermocouples for controlling the temperature of the adiabatic shield. The shell for the oxygen cell CO-7 with one SPRT, as well as the cell itself, had six copper strips (four for the SPRT's leads and two for the heater leads) for tempering the electrical leads. Lens paper was used for electrically insulating the copper strips from the surface on which they were cemented for thermal contact. Similarly, the oxygen cell PO-1 and its auxiliary isothermal shell had six copper strips each for tempering the electrical leads. The electrical insulation in this case was Mylar film that was about 0.01 mm thick. The oxygen cell PO-3 with wells for three SPRT's had 10 copper tempering strips cemented on it and on its auxiliary isothermal shell. Mylar film was used for electrical insulation.

The fourth cell was constructed and filled with oxygen at IMGC [5]. As previously mentioned, this cell is one of the reference cells that is being circulated among different national laboratories as part of the program on International Intercomparison of Fixed Points by Means of Sealed Cells sponsored by the CCT. The cell design is indicated as Model C by IMGC [5]. It has a re-entrant well that can accommodate a tapered copper plug which is large enough for installing three SPRT's. The heat of fusion of the sample was 47 J and the heat capacity of the assembled sample cell system was 40 J/K at 54.5 K. This cell with its oxygen sample will be referred to as IMGC-8$0_2$.

In order to accommodate three SPRT's in the IMGC-80_2 cell, a small groove was first machined along the taper on the plug in which the three SPRT's were to be installed. The groove vented air so that the three SPRT's could be safely handled with the cell. A special auxiliary isothermal shell was constructed for the cell and 10 copper tempering strips were attached for measurements with three SPRT's, similar to cell PO-3.

The heater for introducing known amounts of electrical energy into the oxygen sample system was wound directly over the copper tempering strips on the cylindrical surface of all four cells using glass fiber insulated heater wire. In the earlier tests with sealed argon cells [6], the location of the heater did not seem to affect the measurement; however, the heater was wound mostly on the upper half of CO-7, and PO-3 cells to drive any condensate to the bottom of the cell. On cells PO-1 and IMGC-80_2, the heater was evenly distributed over the cylindrical surface in order to determine whether more even distribution of heating would reduce the equilibrium time. No significant difference in equilibrium time or in the measurements was observed among the cells.

5. Thermometry

5.1 Thermometers and Temperature Scales

A total of six capsule SPRT's with NBS-IPTS-68 calibrations [23] was used. Three of the SPRT's (1812279, 1812282, and 1812284) were those furnished to the National Physical Laboratory (NPL, U.K.) for the international comparison of temperature scales below 0 °C [24]. As a result of that comparison, these three SPRT's have calibrations also on the NPL-IPTS-68 [24]. These SPRT's were calibrated three times before shipping to the NPL and twice after they were returned. These three SPRT's will be referred to as the international SPRT's. In addition, the "standard thermometer" 1728839 that was employed for comparison of the temperature scales at the NPL had also been calibrated on August 22, 1969 in terms of the NBS-IPTS-68. The other three SPRT's (1774092, 1774095, and 1842382) have been calibrated twice; they have been used only at NBS.

The history of calibrations of the six SPRT's at 54.361 K is summarized in table 1 by comparing their resistance ratios for the temperature, relative to that of the latest calibration, and converting the differences to corresponding temperature values. A similar comparison of calibration for 83.8 K of the same SPRT's was described previously in the measurements of the argon triple point [6]. To be consistent with the comparison of calibrations presented in the earlier argon work [6], wherever the value of the resistance ratio W at 54.361 K was smaller than the value for the latest calibration, the corresponding value of temperature difference is given in the table with a minus sign. However, in using such calibrations, the value of temperaturethat is calculated for a given observed value of W would actually be larger.

The relatively large differences for 8/29/74 and earlier calibration for SPRT's 1812279, 1812282, and 1812284, which among themselves agree closely, suggest possibly that a small change occurred in the calibration between the times these SPRT's were shipped to the NPL and returned. Therefore, there is an uncertainly of about 0.1 mK in the comparison of the IPTS-68 maintained at the NBS [23] and that at NPL [24]. As mentioned earlier, the other three SPRT's 1774092, 1774095, and 1842382 have been used only at the NBS. The agreement in the calibrations for SPRT 1774092 and 1774095, although performed six years apart, approach the precision of single calibrations around 54.361 K. The difference in the calibrations for SPRT 1842382 is larger than that which would be expected for normal calibrations. Nevertheless, table 1 shows that the calibrations on all six SPRT's are highly consistent and reproducible over a number of years and that capsule SPRT's when used with care, can retain their calibration over many years. This outstanding stability is further supported by the consistency of values of triple points of argon obtained earlier [6] with the same six SPRT's and by the consistency of values of triple points of oxygen to be presented later in this paper. This indicates also that the SPRT reference standards that maintain the NBS-IPTS-68 [23] are stable, unless, of course, all SPRT's that are involved in this comparison drift at the same rate, which is unlikely.

The outstanding stability of SPRT's and the consistency of calibrations of SPRT's that can be realized are demonstrated additionally by the results obtained at the NPL on the oxygen triple point using SPRT 1728839 with NBS-IPTS-68 calibration [4]. The SPRT 1728839 represented also the NPL-IPTS-68 for the international comparison of SPRT calibrations [24]. The value (54.3615 K) obtained on the NBS-IPTS-68 for the oxygen triple point at the NPL using SPRT 1728839 [4] is in perfect agreement with the differences found by comparing SPRT's between the NPL-IPTS-68 (represented by SPRT 1728839) and the NBS-

Table 1. Calibration history of thermometers (calibration in terms of the NBS-IPTS-68)[a].

Thermometer	Calibration Date and Deviation at 54.361 K from the Latest Calibration					Deviation from the NPL-IPTS-68[c]
	mK					mK
	2/2/77[b]	2/1/71				
1774092	0	+0.032				
1774095	0	−0.016				
	6/22/76[b]	3/18/76	8/29/74[d]	8/9/74[d]	7/18/74	
1812279	0	−0.051	−0.116	−0.126	−0.076	+0.6[e]
1812282	0	−0.043	−0.110	−0.100	−0.083	+0.5[e]
1812284	0	−0.055	−0.149	−0.154	−0.074	+0.6[e]
	7/22/81[b]	1/10/78				
1842382	0	−0.080				

[a] NBS-IPTS-68 is a "wire scale"; see reference [23].

[b] Latest calibration; hence, zero deviation is shown.

[c] From reference [24].

[d] These calibrations were submitted to the NPL for the international comparison of temperature scales [24]. The average of these two calibrations was compared with NPL-IPTS-68.

[e] The positive figures indicate that the triple point of oxygen as realized at the NPL is "hotter" than the value 54.361 K on the NBS-IPTS-68. Based on W(54.361 K) of the NPL-IPTS-68 and average NBS-IPTS-68 indicated as d above, the average deviation for the three SPRT's corresponds to +0.588 mK.

IPTS-68 [23] (represented by SPRT's 1812279, 1812282, and 1812284); see table 1 for the differences of the latter three SPRT's. The NBS calibration date and the date of NPL measurement of the oxygen triple point with SPRT 1728839 are almost five years apart [4]. (Note: the SPRT 1728839 was calibrated originally in terms of the NBS-1955 scale. Later, the scale was converted to NBS-IPTS-68 in accordance with the published differences [25,26].)

For measurements in the oxygen triple-point cells, the capsule SPRT's were installed as shown in figures 1 and 3. To obtain the resistance ratio W (i.e., the resistance at the oxygen triple point to that at 0 °C), the capsule SPRT's were installed in special holders [26] for resistance measurements at the triple point of water (TP). (For the description of the procedure for converting the observed resistance at the TP to that at 0 °C, see reference [27].) All analyses of measurements were made in terms of the resistance ratio W with zero thermometer current. The conversion to values of temperature (NBS-IPTS-68) was made only at the end of the analysis for presentation of the results.

5.2 Measurement of Thermometer Resistance

A Guildline Model 9975 current comparator bridge [28] was used for measuring the resistance of the SPRT's. In conjunction with the bridge, a 10 Ω Rosa-type reference resistor [29] and a strip-chart recorder were used. The reference resistor was thermostated at about 30 °C, near the maximum of its resistance versus temperature curve. On the basis of the indications of an industrial-type 100 Ω platinum resistance thermometer installed in the thermometer well of the reference resistor, the variations in the temperature of the reference resistor were not greater than ±1 mK. The amplifiers of both the bridge and the recorder were adjusted so that 1 mm on the recorder chart corresponded to about 3×10^{-7} Ω. The recorder tracings were estimated to about 0.3 mm so that the readings of the measurement system would correspond closely to 1×10^{-7} Ω. During measurements, the bridge and the strip-chart recorder provided a continuous record of the temperature of the oxygen cell. The strip-chart recorder was run always at the relatively slow speed of 5 cm per hour so that the observed "equilibrium tracings" would indeed be equilibrium temperature tracings. The chart recorder was operated continuously so that it would also serve as a clock for regulating the measurement process.

In using the current comparator bridge, there was some concern regarding the manner in which the reference resistor might change in resistance with current. For the determination of the resistance ratio W, measurements at the triple points of water and oxygen are required which involve nearly 11-fold current variation in the reference resistor (from about 3.6 to 0.33 mA, respectively, with $\sqrt{2}$ mA through the SPRT). However, since the temperature of the reference resistor was controlled near the maximum of its resistance versus temperature curve, and since the resistor was immersed directly in oil, the effect of small power variations on its resistance at the low power that was used was considered negligible.

To minimize the effect on the resistance ratio caused by the slow drift in the resistance of the reference resistor, the resistances of the SPRT's at the triple point of water, R(TP), were determined just prior to or very soon after the measurements at the triple point of oxygen. The values of R(TP) were plotted as a function of the date for each SPRT. Usually the observed value of R(TP) was used for calculating the resistance ratio; but, whenever there was a significant difference in the successive values of R(TP), the value of R(TP) was selected from the plot at the date that corresponded to the date at which the observations at the triple point of oxygen were made.

To make negligible the error that would arise from variations in self-heating in the SPRT's, measurements were made at two currents (1 and $\sqrt{2}$ mA) and the value at zero power (zero current) was obtained by linear extrapolation of the power dissipated in the SPRT. The validity of this linear extrapolation was checked with every new installation of the oxygen triple-point cell in the calorimetric cryostat by measurements at three currents (1, $\sqrt{2}$, and $0.3\sqrt{2}$ or 3 mA). The self-heating values of the SPRT's, obtained from the measurements at 1 and $\sqrt{2}$ mA, served as a check during measurements and in the analysis of the measurement data, since the values for a given SPRT should not show large differences from one measurement to another.

The procedure for measuring thermometer resistance was to determine the zero of the measurement system on the strip-chart recorder during the period the sample was being heated and the subsequent 10 to 20 minutes after the heating while the sample system was reaching temperature equilibrium. Actually, the zero was determined by simply switching the bridge current off, following the completion of the measurement of the equilibrium temperature. Hence, during this period, the thermometer connections and the settings on the amplifier switches of the bridge (galvanometer sensitivity switch for the bridge) and the strip-chart recorder were undisturbed and at the same positions at which the equilibrium readings were obtained, so that any "offset" would be included as part of the zero. After the zero of the measurement system was satisfactorily determined, the thermometer resistance at the new equilibrium temperature was then measured. The equilibrium temperatures were observed for 30 minutes to an hour or longer for each SPRT, depending upon the position in the measurement sequence in a particular "run." (A run represents a freezing of the oxygen samples and the series of equilibrium temperature measurements at different fractions melted.) Except where the sample was less than about 15 percent or between about 85 and 100 percent melted, the oxygen sample system reached temperature equilibrium after heating within about 15 to 20 minutes. The usual practice was to record for at least 12 to 18 minutes (1 to 1.5 cm of chart record) of readings that were essentially constant near the zero of the measurement system at 1 mA and then at $\sqrt{2}$ mA, plus the determination of the sensitivity at these two currents. The sensitivity was determined by reducing the bridge dial reading 50 units (least significant units) which corresponded to a change of about 15 cm in the recorder pen position or about 50 $\mu\Omega$. (Note: The recorder chart width was 25 cm. For convenience, the zero tracing was located toward the right of the chart around the 20-cm position and the recorder was connected to the bridge so that when the bridge readings were reduced the recorder pen would deflect to the left. With this arrangement, the recorder tracing gives the "temperature versus time curve" which can be copied directly.) The recorder tracings for determining the sensitivity corresponded usually to 5 to 10 minutes in length. Since the sensitivity should be nearly constant and also the zero should be at approximately the same location on the strip chart, they served as checks on the proper performance of the measurement system.

After the completion of the equilibrium readings on an SPRT, the thermometer current was switched off before introducing electrical energy into the oxygen sample system for the next fraction melted. If the oxygen sample system contained three SPRT's, equilibrium measurements on the other SPRT's were successively made. Since the complete measurements with three SPRT's required two to three hours or longer, occasionally the measurements on the first of the three SPRT's were repeated to check the state of equilibrium of the oxygen sample system. Any differences were usually within 0.01 mK; however, differences as large as 0.03 mK occurred below about 15 percent and between about 85 and 100 percent melted. Often it was convenient to allow the system to reach equilibrium overnight after heating. Unless the adiabatic control conditions changed drastically overnight, tests showed that the readings of the next morning were within 0.01 or 0.02 mK of thoseof the previous day. Again, larger changes, as much as 0.05 mK, were observed below about 15 percent and between about 85 and 100 percent melted.

6. Results and Discussions

A total of 12 sets of equilibrium temperature measurements was made at different ratios of liquid to solid oxygen with six SPRT's using the four oxygen cells and two cryostats. (A set of measurements with an SPRT is the observations of all runs with the SPRT and cell for a given installation in the cryostat. If the cell were remounted in the cryostat, the new measurements with the SPRT were counted in another set. A cell with three SPRT's can yield three sets of equilibrium temperature measurements for the same installation.) SPRT 1774095 was used with oxygen cell CO-7 containing the commercial oxygen; this SPRT was also used with oxygen cell PO-1 containing the prepared oxygen. In addition, SPRT 1774095 was used together with SPRT's 1774092 and 1842382 with oxygen cell PO-3 containing the prepared oxygen. SPRT 1812282 was used with oxygen cell PO-1 and also used together with SPRT's 1812279 and 1812284 with oxygen cell PO-3. The three international SPRT's 1812279, 1812282, and 1812284 were also used together in oxygen cell IMGC-80$_2$. The measurements of SPRT 1774095 with oxygen cell CO-7 was made in cryostat "S"; the other measurements were all made in cryostat "T." For economy of space, representative sets of measurements are shown for each of the oxygen cells in figures 4, 5, 6, and 7 by plotting $W(T)$ versus the fraction melted F and $W(T)$ versus the reciprocal of fraction melted $1/F$ for the measurements of SPRT 1774095 with cells CO-7, PO-1, and PO-3 and measurements of SPRT 1812282 with cell IMGC-80$_2$. Since SPRT 1774095 was not used with cell IMGC-80$_2$, the results with SPRT 1812282 were selected because the SPRT was also used with cells PO-1 and PO-3. Some of the observations given for the $W(T)$ versus $1/F$ plot are not shown for the $W(T)$ versus F plot. One vertical division in $W(T)$, which corresponds to $\Delta W=0.000001$, is equivalent to 0.256 mK. [Note: the results obtained in this investigation will be expressed to the nearest 0.001 mK. For a given assemblage of equilibrium temperature tracings for two currents (see section 5.2), the SPRT resistance at zero current that was calculated was estimated to be precise to ±0.001 to ±0.002 mK.]

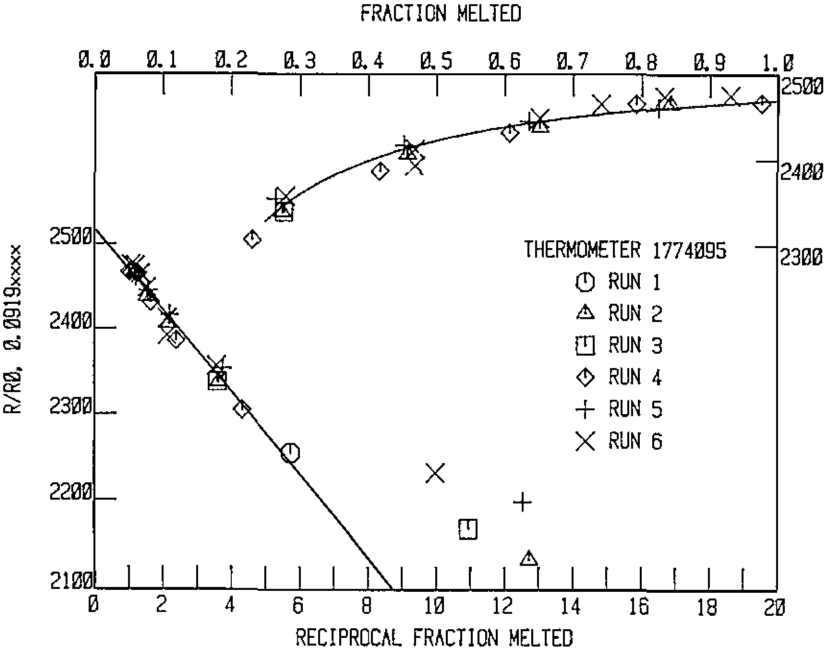

Figure 4—Values of resistance ratios (W) at equilibrium temperatures of various amounts of the commercial oxygen sample melted; for thermometer 1774095, cell CO-7, cryostat "S." The upper part of the figure shows values of W (scale on the right) at various fractions of the sample melted. The lower part shows the same values of W (scale on the left) plotted in terms of the reciprocals of the fractions melted. The solid curves represent the results of least-squares fitting of eq (9) to the data.

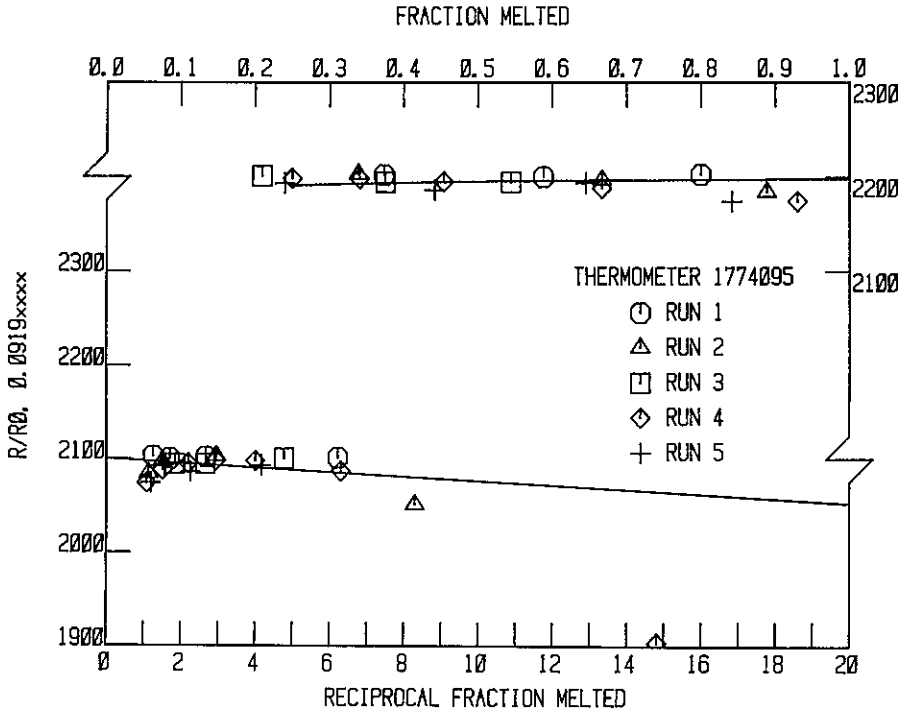

Figure 5—Values of resistance ratios (W) at equilibrium temperatures of various amounts of the prepared oxygen sample melted; for thermometer 1774095, cell PO-1, cryostat "T." (See fig. 4 for explanation of the plot.)

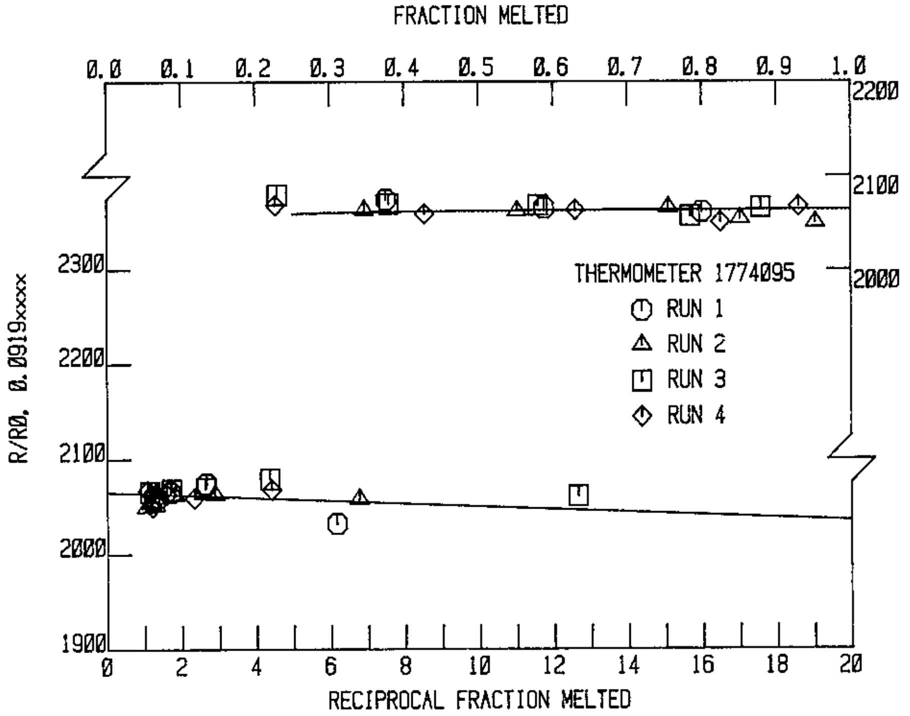

Figure 6—Values of resistance ratios (W) at equilibrium temperatures of various amounts of the prepared oxygen sample melted; for thermometer 1774095, cell PO-3, cryostat "T." (See fig. 4 for explanation of the plot.)

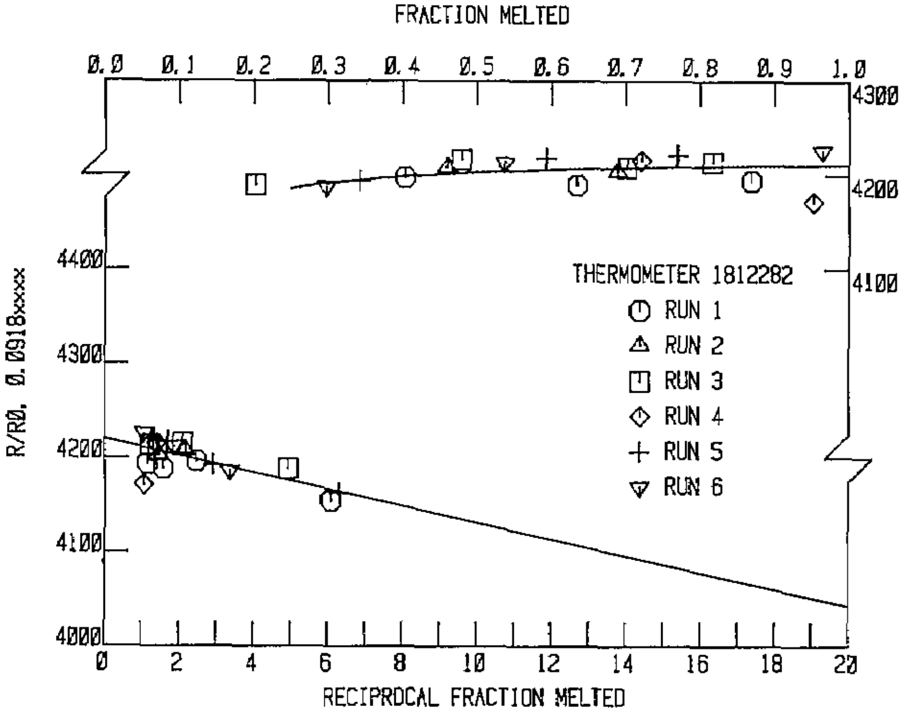

Figure 7—Values of resistance ratios (W) at equilibrium temperatures of various amounts of the commercial oxygen sample melted; thermometer 1812282, cell IMGC-802, cryostat "T." (See fig. 4 for explanation of the plot.)

In the figures, the straight line associated with the $W(T)$ versus $1/F$ plot was obtained by fitting the observations by the least-squares method to the linear relation given by eq (9). The curve associated with the $W(T)$ versus F plot was calculated by employing with eq (9) the values for the slope ($55.40\ x_2^*$) and $W(T_0)$ ("triple point of pure oxygen") obtained by the least-squares method for the set of measurements on the sample. The results are apparently in good agreement with the idealized eq (9). The deviations that are shown most likely originate from the experimental process, where thermal equilibrium for the system was not awaited long enough or from lack of complete adiabatic condition. The least-squares values of the slopes give for the mole-fraction impurity x_2^* of eq (9) 1.2×10^{-6}, 8.2×10^{-8}, 7.0×10^{-8}, and 4.1×10^{-7} for cells CO-7, PO-1, PO-3, and IMGC-80$_2$, respectively. [Note: The slopes of the figures correspond to $\Delta W/\Delta(1/F)$. For eq (9), the conversion $\Delta T/\Delta(1/F)=256\times\Delta W/\Delta(1/F)$ was made at 54.4 K.] Compared with the stated amounts of impurities, the values seem to give rather high purity for the commercial samples, by a factor of 10 or more, possibly because of the deviation from true phase equilibrium or of the narrow separation of the liquidus and solidus curves in the case of the oxygen-argon system. The purity of the prepared oxygen sample is at present unknown except that it was prepared with extreme care.

Some of the equilibrium temperatures above about 0.8 fraction melted are shown to be relatively low. Also, the observed equilibrium temperatures at low fraction melted (less than about 0.1) show large deviations in terms of the high degree of agreement in the range 0.1 to 0.8 fraction melted. A plausible explanation for part of this is attributed to the lack of complete adiabatic condition. In the region above about 0.8 fraction melted, the equilibrium temperature can be made relatively higher or lower depending upon the direction of heat transfer relative to the oxygen cell system. Where the fraction melted is small or large, the amount of liquid to solid interface is relatively small. The adjustment to temperature gradients can occur more rapidly when there is a well-distributed large liquid to solid interface; small heat loss or gain of the oxygen cell system can be accommodated by melting or freezing. However, at small amounts of liquid to solid interface the accommodation becomes less and the thermometer begins to indicate more temperature gradients and more of what is happening to the oxygen cell system, because the sample, as well as the cell, have relatively low thermal conductivity. The degree of deviation from the true equilibrium temperature depends upon the quality of adiabatic condition and the location of the thermometer where temperature gradients exist. However, the observed deviations shown are small in terms of the final mean value for the oxygen triple point.

Table 2 summarizes all of the sets of oxygen triple point measurements with the six SPRT's. The values of $W(T)$ tabulated are those at $1/F=1$ obtained by the method of least squares mentioned above. The values of temperatures on the NBS-IPTS-68 scale are based on the latest calibration (see table 1). The values of temperatures on the NPL-IPTS-68 for the international SPRT's are based on the calibrations obtained at the time of the international comparison of temperature scales [24]. The values of temperatures on the NPL-IPTS-68 for SPRT's 1774092, 1774095, and

Table 2. Measurements at the triple point of oxygen.

Oxygen Cells: CO-7, commercial oxygen, sealed April 1980
PO-1, prepared oxygen, sealed February 1983
PO-3, prepared oxygen, sealed July 1983
IMGC-80$_2$, commercial oxygen, sealed November 1978

SPRT	Oxygen Triple Point Cell			
	CO-7 W, $1/F=1.00$[a] K, NBS-IPTS-68 K, NPL-IPTS-68	**PO-1** W, $1/F=1.00$[a] K, NBS-IPTS-68 K, NPL-IPTS-68	**PO-3** W, $1/F=1.00$[a] K, NBS-IPTS-68 K, NPL-IPTS-68	**IMGC-80$_2$** W, $1/F=1.00$[a] K, NBS-IPTS-68 K, NPL-IPTS-68
1774092			0.09173132[c] 54.361342 54.360880[f]	
1774095	0.09192447 54.362366 54.361904[f]	0.09192095[b] 54.361465 54.361003[f]	0.09192064[c] 54.361386 54.360924[f]	
1812279			0.09180512[d] 54.361304 54.360827[e]	0.09180740[d] 54.361887 54.361410[e]
1812282		0.09183956[b] 54.361311 54.360839[e]	0.09183948[d] 54.361290 54.360818[e]	0.09184211[d] 54.361963 54.361491[e]
1812284			0.09182449[d] 54.361358 54.360921[e]	0.09182644[d] 54.361857 54.361420[e]
1842382			0.09171159[c] 54.361468 54.361006[f]	
Mean (NBS-IPTS-68)		54.361388 K	54.361358 K	
Mean (NBS-IPTS-68) (NPL-IPTS-68)		54.361373 K 54.360911 K[f]		54.361902 K 54.361440 K[f]
Range of observed values		0.000178 K		0.000106 K

[a] From linear least-squares fit of W versus $1/F$.

[b] The SPRT's 1774095 and 1812282 were at different times in PO-1 oxygen triple point cell.

[c] The SPRT's 1774092, 1774095, and 1842382 were together in PO-3 oxygen triple point cell.

[d] The SPRT's 1812279, 1812282, and 1812284 were together in PO-3 and in IMGC-80$_2$ oxygen triple point cells.

[e] Directly from NPL-IPTS-68 calibrations on these SPRT's at the time of the international comparisons [24].

[f] From the average differences in the NPL and NBS versions of the IPTS-68 found for SPRT's 1812279, 1812282, and 1812284. (The latest NBS calibrations are used.)

1842382 are based on the average difference (0.462 mK) between the latest calibration of the three international SPRT's on the NBS-IPTS-68 and on the NPL-IPTS-68 at the triple point of oxygen (54.361 K). The mean NBS-IPTS-68 temperature value given for the two oxygen cells PO-1 and PO-3 using the six SPRT's was also converted to the NPL-IPTS-68 temperature value using the above average difference. The ranges of observed values given for cells PO-1 and PO-3 and for cell IMGC-80$_2$ are based on the NBS-IPTS-68 values. [To convert the NPL-IPTS-68 temperature values to those on the NBS-IPTS-68 calibration at the time of the NPL-IPTS-68 comparison, use +0.588 mK (see footnote e, table 1).]

The values of the triple point of oxygen obtained with cells PO-1 and PO-3 are essentially the same. Their means using different SPRT's differ by only 0.030 mK. This indicates that these two cells were filled consistently at different times (February and July of 1983, respectively) from the storage cylinder of prepared oxygen. The high degree of "flatness" of the equilibrium temperatures over a broad range of liquid to solid ratios (or the low impurity content obtained from the "slope," which was mentioned earlier) indicates that the prepared oxygen is purer (see figures 5 and 6) than the commercial oxygen samples.

The SPRT's 1774092 and 1774095 were calibrated together, as were the three international SPRT's, but the SPRT 1842382 was not calibrated together with any of the other five SPRT's (see table 1). The SPRT's 1774092, 1774095, and 1842382 were measured together in the oxygen triple point cell PO-3; also the three international SPRT's were used together in cell PO-3. The mean triple point value 54.361364 K (S.D.=0.031 mK) for SPRT's 1774092 and 1774095 is only 0.047 mK higher than the mean value 54.361317 K (S.D. =0.036 mK) for the three international SPRT's. On the other hand, the value 54.361468 K for SPRT 1842382 is 0.151 mK higher than the mean for the international SPRT's. The figure 0.151 mK is probably the combined inconsistency (spread) of the averages of calibrations and oxygen triple point measurements with the six SPRT's. [This figure turns out fortuitously to be the same as the maximum change in the calibration of the international set of SPRT's (see table 1).]

The following discussions, unless stated otherwise, are in terms of the NBS-IPTS-68. The mean of the observations (range: 0.079 mK) with cells PO-1 and PO-3 using SPRT 1774095 is 54.361426 K. The triple point of cell CO-7 using the same SPRT is 0.940 mK higher than the above mean of cells PO-1 and PO-3. The amount of argon impurity (5 ppm, quoted by the supplier) is not enough to cause this increase in terms of the increase of about 10 μK per ppm of argon found by Ancsin [3] or about 15 μK per ppm found by Compton and Ward [4] by introducing known amounts of argon impurity. The nitrogen impurity (3 ppm) is expected to lower the triple point of oxygen. The mean of the observations (S.D.=0.055 mK) with the IMGC-80$_2$ cell using the three international SPRT's is 54.361902 K and the mean of the four observations (S.D.=0.030 mK) with PO-1 and PO-3 cells using the same SPRT's is 54.361321 K. These results indicate that the triple point of the IMGC-80$_2$ cell is 0.581 mK higher than the mean triple point of cells PO-1 and PO-3. This difference is in close agreement with the comparisons of other laboratories of this cell with other oxygen cells [5]. Again the argon impurity (3 ppm) known to be present in the commercial oxygen that was used in IMGC-80$_2$ cell cannot account for this higher triple point. Further investigation is required to determine the source of this discrepancy.

Ward and Compton [24] reported as part of the international comparison of the temperature scales the values of *W* at the oxygen triple point for the international SPRT's 1812279, 1812282, and 1812284. These values are compared in table 3 with the values obtained at the NBS with the same SPRT's for cells PO-1, PO-3, and IMGC-80$_2$. The average value for SPRT 1812282 obtained with cells PO-1 and PO-3 is given. These observed values of *W* for the SPRT's suggest that the oxygen triple point realized at NPL by Compton and Ward [4] is on the average 0.142 mK hotter than the NBS cells PO-1 and PO-3.

Unfortunately, there are only a few SPRT's which were used in both the international comparison of temperature scales [24] and the more recent international comparison of sealed fixed-point cells [5,24]. The results of the international comparison of the temperature scales reported by Ward and Compton [24] show that the NPL realization of the oxygen triple point as represented by SPRT 1728839 is 0.1 mK hotter than that realized at the National Measurement Laboratoy (NML, Australia) as represented by SPRT's 1705628 and 1731676. The temperature value reported by NPL using SPRT 1728839 is 0.14 mK smaller than the value reported by NML using SPRT 1731676 on the same oxygen cell in the international comparison of sealed fixed-point cells [5]. These observations are entirely consistent with the difference +0.142 mK for the realization of the oxygen triple point between NPL and NBS given in table 3; i.e.,

Table 3. Comparison of the values of the resistance ratio W at the triple point of oxygen.

	Capsule Platinum Resistance Thermometer		
	1812279	**1812282**	**1812284**
NPL, W	0.0918058	0.0918402	0.0918248
NBS, W	0.09180512[a]	0.09183952[b]	0.09182449[a]
NBS-NPL, ΔW	−0.00000068	−0.00000068	−0.00000031
NPL-NBS, ΔT	+0.174 mK	+0.174 mK	+0.079 mK
		Mean = +0.142 mK (S.D. = 0.055 mK)[c]	
IMGC-80$_2$, W	0.09180740	0.09184211	0.09182644
IMGC-80$_2$-NPL, ΔW	+0.00000160	+0.00000191	+0.00000164
NPL-IMGC-80$_2$, ΔT	−0.410 mK	−0.489 mK	−0.420 mK
		Mean = −0.440 mK (S.D. = 0.043 mK)[c]	

[a] From measurements with NBS oxygen cell PO-3.

[b] From the average of the measurements with NBS oxygen cells PO-1 and PO-3, taking the two cells to be the "same."

[c] S.D. = standard deviation of a single observation.

the NML realization of the oxygen triple point and the NBS realization of the oxygen triple point with cells PO-9 and PO-3 are very nearly the same, while the NPL realization may be about 0.1 mK hotter.

Ward and Compton [4] used a commercial oxygen containing nitrogen, argon, and krypton impurities. They carefully chemically analyzed their oxygen samples with a sensitivity of 1 ppm for the above impurities [31] and also experimentally determined the effect of these gases on the triple point of oxygen and corrected for their effects [4]. Their corrected oxygen triple point is apparently only 0.142 mK hotter than that of the prepared oxygen of the present investigations. Ancsin [32] reported triple point measurements on "homemade" pure oxygen and commercial oxygen with the supplier analysis in vppm: 15 of argon, 13 of nitrogen, and 10 of krypton. The triple point of the commercial oxygen was shown to be about 0.76 mK lower than that of the homemade oxygen. Ancsin [32] states that this lowering is much more than could be accounted for by the measured effect of the impurities. Considering the close agreement of the oxygen triple point of cells PO-1 and PO-3 with that of the NPL cell [4] and, in contrast, the deviations found by Ancsin [32] and found in the present work on cells CO-7 and IMGC-80$_2$ using commercial oxygen with only supplier analysis, it seems that the analysis of commercial oxygen samples must be improved or there are effects of impurities that have not been accounted.

The results of some of the measurements on the sealed oxygen cells given in the final report on the International Intercomparison of Fixed Points by Means of Sealed Cells [5,30] do not seem to be in complete accord with the above conclusion on the use of commercial oxygen. Table 4 lists, along with the NBS cells, the oxygen triple point cells that were used as part of the above international comparison program. The general statement on the chemical analyses is that they are "nominal" as given by the supplier of the oxygen gas. A few of the analyses may have been obtained by the laboratory that prepared the cell. The report is not explicit on the source of individual analysis. For some of the SPRT's that were used in the measurement, calibrations both of individual laboratories and of the NPL are given (see Appendix II of reference [5]). The calibrations of the NPL had been obtained as part of an earlier investigation on the international comparison of temperature scales represented by SPRT's [24] or were obtained later, either by calibration at the NPL or indirectly by calibration through SPRT's that were so calibrated. In the report the final analysis of the measurements is given in terms of the NPL-IPTS-68. After normalizing to common measurements since there would be variations in the calibrations on the scale, the realized temperatures of the cells of table

Table 4. Stated chemical analysis of oxygen samples used in sealed cells for international comparison of fixed points (from Reference [5]).

Oxygen Cells[a]	Impurities, Volume Parts per Million (VPPM)							
	H_2	N_2	A	Kr	Xe	N_2O	H–C[b]	CO_2
IMGC, 1 (99.998%)[c]		8	<10	Kr+Xe =	<1			
IMGC, 8 (99.998%)[c]		1.8	3				0.7	
INM, 8 (99.998%)[c]		5	12	3				
INM, BCM4[c]	<0.1	5	12	Kr+Xe =	3		<0.2	0.2
NIM, PP07[c]		3.1	0.15				0.15	<0.5
NIM, PP11 (99.999%)[c]		4.2	0.8				0.83	0.5
NRC, 15 (99.99%)[d]		20	20	15	5	5	10	5
NRLM, 7801 (99.99%)[c]								
PRM, $KMnO_4$)[e]								
NBS, CO-7 (99.999%)[f]		<3	<5					<1
NBS, PO-1 ($KMnO_4$)[e]								
NBS, PO-3 ($KMnO_4$)[e]								

[a] IMGC, Istituto di Metrologia "G. Colonnetti," Torino, Italy.
INM, Institut National de Metrologie, Paris, France.
NIM, National Institute of Metrology, Beijing, China.
NRC, National Research Council, Ottawa, Canada.
NRLM, National Research Laboratory of Metrology, Tsukuba, Japan.
PRMI, Physico-technical and Radio-technical Measurements Institute, Moscow, U.S.S.R.
NBS, National Bureau of Standards, Gaithersburg, MD, U.S.A.

[b] Hydrocarbon as CH4.

[c] Stated analysis of oxygen sample from reference [5].

[d] Stated in reference [5] as Matheson Research Grade. Analysis was obtained from Matheson Catalog 81 for "typical sample."

[e] Sample from thermal decomposition of $KMnO_4$.

[f] Not compared in reference [5].

4 (except for cells IMGC-$8O_2$ and NRLM-7801) are found to be within about ±0.1 or ±0.2 mK of the IMGC-1 and NRC oxygen cells (see table VI.3b of reference [5]), which are given as 54.36072 K and 54.36088 K, respectively, on the NPL-IPTS-68. (There are not enough measurements on the PRM1 cell to make any conclusion.) The range of measurements on some of the cells by ASMW (SPRT 217997) is 0.17 mK, by INM (SPRT 1812283) is 0.04 mK, by NIM (SPRT 7709) is 0.14 mK, by NML (SPRT 1731676) is 0.10 mK, by NPL (SPRT 1728839) is 0.16 mK, and by NRC (SPRT 1158062) is 0.11 mK. Using the difference 0.142 mK given earlier for the realization of the oxygen triple point between NPL and NBS, the triple point of IMGC-1 cell becomes 0.14 mK colder than the mean of NBS cells PO-1 and PO-3; the NRC-15 cell comes within 0.02 mK of the NBS cells. This suggests that in spite of the relatively high impurity content of some of the oxygen samples in the cells of table 4, the realized triple points are fairly close to that of the prepared oxygen. It is to be noted, however, that in all of the cells, excluding those indicated earlier as exceptions, the nitrogen impurity content is relatively high. Ancsin [32,3] found the effect on the oxygen triple point by adding 100 vppm of impurities to be : N_2, −2 mK; Ar, +1 mK, Kr, −0.4 mK; and Xe, −0.4 mK. The effect of the impurities may have closely balanced each other. In the cases of the oxygen cells IMGC-8, NRLM-7801 (chemical analysis not given), and NBS-CO-7, the results indicate that the effect of argon was greater than those of other impurities.

7. Conclusions

The results show that oxygen samples purer than the highest quality commercial grade can be prepared by thermal decomposition of $KMnO_4$ and that oxygen triple points can be obtained reproducibly within ±0.1 mK in sealed miniature pressure cells. When carefully handled, capsule-type platinum resistance thermometers can have stability of ±0.1 mK or better. The NBS calibrations of the six NBS SPRT's and the NPL SPRT 1728839 obtained at different times are consistent within about ±0.1 mK. When commercial oxygen is used in sealed cells, accurate chemical analysis should be obtained on the sample. The triple points of oxygen samples containing a combination of impurities should be investigated since commercial oxygen is expected to have a variety of air components.

The author is grateful to M. L. Reilly for help in the computer analysis of the data.

References

[1] The International Practical Temperature Scale of 1968. Amended Edition of 1975, Metrologia **12** 7 (1976).

[2] Pavese, F., Temperature, Its Measurement and Control in Science and Industry (American Institute of Physics, New York, 1982), Vol. 5, Part 1, p. 209.

[3] Ancsin, J., Metrologia **6** 53 (1970).

[4] Compton, J. P., and S. D. Ward, Metrologia **12** 101 (1976).

[5] Pavese, F., Final Report of the International Intercomparison of Fixed Points by Means of Sealed Cells: 1978–1984, Bureau International des Poids et Mesures, Monograph 84/4 (1984).

[6] Furukawa, G. T., Temperature, Its Measurement and Control in Science and Industry (American Institute of Physics, New York, 1982), Vol. 5, Part 1, p. 239.

[7] McCullough, J. P., and G. Waddington, Anal. Chim. Acta **17** 80 (1957).

[8] Guggenheim, E. A., Thermodynamics, An Advanced Treatment for Chemists and Physicists (Interscience Publishers, Inc., New York, 1949), Chap. V.

[9] Hildebrand, J. H., and Scott, R. L., The Solubility of Nonelectrolytes, Third Edition (Dover Publications, Inc., New York, 1964), Chap. 1.

[10] American Institute of Physics Handbook (McGraw-Hill Book Company, Inc., New York, 1972), p. 4–238.

[11] Ruhemann, M., and B. Ruhemann, Low Temperature Physics (Cambridge University Press, London, 1937), Chap. VI.

[12] Veith, H., and E. Schroder, Zeit. phys. Chem. **A179** 126 (1937).

[13] Din, F.; K. Goldman, and A. G. Monroe, Proceedings Commission I, Ninth International Congress of Refrigeration, Paris, 1955, p. 1.003.

[14] Rhines, F. N., Phase Diagrams in Metallurgy, Their Development and Application (McGraw-Hill Book Company, Inc., New York, 1956), Chap. 3.

[15] Connolly, J. J., and J. V. McAllan, Acta Met. **23** 1209 (1975).

[16] Yen, W. M., and R. E. Norberg, Phys. Rev. **131** 269 (1963).

[17] Hood, G. M., and J. N. Sherwood, Mol. Cryst. **1** 97 (1966).

[18] Furukawa, G. T., and M. L. Reilly, J. Res. Nat. Bur. Stand. (U.S.) **74A** 617 (1970).

[19] Furukawa, G. T.; M. L. Reilly and W. G. Saba, Rev. Sci. Instr. **35** 113 (1964).

[20] Westrum, E. F.; G. T. Furukawa and J. P. McCullough, in Experimental Thermodynamics, Vol. I, Calorimetry of Non-Reacting Systems, Ed. McCullough, J. P., and D. W. Scott, (Plenum Press, New York, 1968), Chap. 5.

[21] Hoge, H. J., J. Res. Natl. Bur. Stand. (U.S.) **44** 321 (1950).

[22] Sidgwick, N. V., The Chemical Elements and Their Compounds (Oxford University Press, London, 1950), Vol. II, Chap. VI.

[23] Furukawa, G. T.; J. L. Riddle and W. R. Bigge, J. Res. Natl. Bur. Stand. (U.S.) **77A** 309 (1973).

[24] Ward, S. D., and J. P. Compton, Metrologia **15** 31 (1979).

[25] Bedford, R. E.; M. Durieux, R. Muijlwijk, and C. R. Barber, Metrologia **5**, 47 (1969).

[26] Riddle, J. L.; G. T. Furukawa and H. H. Plumb, Platinum Resistance Thermometry, Natl. Bur. Stand. (U.S.), Monograph No. 126, 1973, 129 pages.

[27] Furukawa, G. T.; J. L. Riddle and W. R. Bigge, J. Res. Natl. Bur. Stand. (U.S.) **80A** 477 (1976).

[28] Kusters, N. L.; M. P. MacMartin and R. J. Berry, Temperature, Its Measurement and Control in Science and Industry (Instrument Society of America, Pittsburgh, PA, 1972), Vol. 4, Part 2, p. 1477.

[29] Rosa, E. B., Bull. Bur. Stds. (U.S.) **5** 413 (1908–1909).

[30] Pavese, F.; J. Ancsin, D. N. Astrov, J. Bonhoure, G. Bonnier, G. T. Furukawa, R. C. Kemp, H. Maas, R. L. Rusby, H. Sakurai, and Ling Shan-Kang, Metrologia **20** 127–144 (1984).

[31] Compton, J. P., and S. D. Ward, Analyst **99** 214 (1974).

[32] Ancsin, J., Metrologia **9** 26 (1973).

Journal of Research of the National Bureau of Standards

A Multi-kilogram Capacity Calorimeter For Heterogeneous Materials

Volume 91 Number 5 September–October 1986

K. L. Churney, A. E. Ledford, M. L. Reilly, and E. S. Domalski

National Bureau of Standards
Gaithersburg, MD 20899

A large capacity calorimeter was designed and constructed in order to determine the enthalpies of combustion of kilogram-size samples of municipal solid waste (MSW) in flowing oxygen near atmospheric pressure. The combustion of the organic fraction of the samples was complete to greater than 99.9+%. The percent coefficient of variation (100 × standard deviation/average), *% CV*, of calibration measurements using microcrystalline cellulose was 0.2%. The *% CV* of the measurements of the enthalpy of combustion of a processed MSW sample was 0.4%. The combined systematic errors due to departure from usual design standards and conventional operating procedures is estimated to be less than 0.4% of the calorific value.

Key words: calorific value; combustion; flow calorimeter; kilogram capacity calorimeter; municipal solid waste.

Accepted: April 24, 1986

1. Introduction

Proof that small test samples are representative of a large parent material is essential to the credibilitity of test methods used to characterize the material. The importance and cost of this proof increases as the heterogeneity of the parent material becomes greater. The calorimeter described in this paper was built to determine if the calorific values of kilogram-size parent and gram-size test samples are the same within 1% for an extremely heterogeneous material—municipal solid waste (MSW).

A description of the industrial problem concerning the calorific value of MSW and the response to solve this problem by the National Bureau of Standards (NBS), U.S. Department of Energy (DoE), and the U.S. Environmental Protection Agency (EPA) are summarized in section 2. The calorimeter and its auxiliary measurement systems for determining the calorific value of MSW are described in section 3. The main features of a typical experiment, the methods of data reduction, and typical results are given in section 4. With this background, the design basis and the performance characteristics of the calorimeter are discussed in section 5.

The combustion flow calorimeter designed for the measurements is novel in three respects: 1) It can accommodate a large solid sample. Thus, it

About the Authors: K. L. Churney, A. E. Ledford, and E. S. Domalski are with the Chemical Thermodynamics Division in the Center for Chemical Physics at NBS while M. L. Reilly is with the Temperature and Pressure Division in the Bureau's Center for Basic Standards. The work described was funded by the U.S. Department of Energy (Biofuels and Municipal Waste Technology Division) from 1977 to the present, U.S. Environmental Protection Agency (Solid and Hazardous Waste Research Division) from 1977 to 1979, and the NBS (Office of Recycled Materials) from 1977 to 1982.

provides a unique capability to determine the enthalpy of combustion of heterogeneous solid materials for which further sampling and processing to obtain representative gram-size test samples may be costly or difficult. 2) The combustion of the solid sample is carried out in flowing oxygen near atmospheric pressure. Thus, the successful operation of this calorimeter revives a calorimetric technique for the combustion of solids that was discarded before 1900. The technique can now be applied to other problems which require a completeness of combustion up to 99.9%. 3) The design and operation depart from certain standard design criteria and conventional operating procedures employed in smaller, more accurate, stirred-water calorimeters.

2. The Industrial Problem and the NBS-DoE Response

Incinerator–boiler systems used to dispose of MSW are bought and sold on the basis of thermal specifications. To determine whether a system meets its thermal specifications, the calorific value of the input waste stream must be known.

At present, as well as in the past, the calorific value of MSW is determined at commercial test laboratories by bomb calorimetry using gram-size test samples. The gram-size test samples are usually prepared from kilogram-size increments. The increments are dried, sorted to remove nonmillable components (i.e., metals), and milled to 2 mm particle size (i.e., 95 mass percent passes through a 2 mm square mesh screen). In this work, the milled material is called processed MSW. The processed MSW is then subdivided, usually by coning and quartering, to obtain gram-size test samples.

For many years, combustion engineers felt that one could not sample a multi-ton quantity of MSW and extract representative gram-size test samples for bomb calorimetric measurements. The method of preparation of test samples was also in dispute because many combustion engineers believed that the composition of the test samples differed from that of the original increments. This might occur because of changes caused by excessive localized heating during milling or by nonrepresentative subdivision of processed MSW, which segregates easily. Segregation occurs because processed MSW consists of a low density component, which resembles chopped up cotton fibers, and a high density component which resembles sand. Part of the high density material is entrained in the low density material and this entrainment is nonuniform.

To address this dispute, NBS initiated a research program in collaboration with DoE and EPA to develop test procedures for accurately determining the calorific values of MSW and fuels derived from MSW. This research was also part of the NBS response to the Resource Conservation and Recovery Act of 1976. Subtitle E of this legislation mandated NBS to provide guidelines for the development of specifications for classification of materials destined for disposal.

To resolve the dispute, two questions were addressed. The first was the sampling question: How does one obtain a representative gram-size sample from a kilogram-size quantity of processed MSW? The second was the processing question: Does milling MSW down to 2 mm particle size alter its calorific value significantly? The remaining problem of extraction of kilogram-size increments in sufficient number and in such a manner as to characterize a multi-ton pile of MSW was considered beyond the scope of this study. However, in order to address the two questions, increments were extracted from a multi-ton stream of MSW using a selected sampling method.

An initial study of the day-to-day variability of the calorific value of MSW was carried out at NBS in 1980 [1][1] using the selected sampling method. We concluded from the results of that work that the sampling and processing questions could be answered with a calorimeter in which we could burn a kilogram-size sample with a total uncertainty of less than 1% in the enthalpy of combustion.

We chose to build a calorimeter for the combustion of kilogram-size samples in flowing oxygen near atmospheric pressure rather than scale-up the conventional oxygen combustion bomb for reasons of safety. Instrumentation of a small commercial incinerator was rejected because it was felt the time required to modify such a unit and validate the calorimetry would be longer than that needed to build a new calorimeter. A small combustion calorimeter [2,3] was built to demonstrate that the oxygen flow technique could be used to obtain complete combustion of pellets of MSW. The pellet mass used in the calorimeter was 25 g. Combustion of MSW which has been compressed into a pellet rather than left in loose form was adopted because this configuration reduces the dispersion of the sample and, thus, simplifies the collection of ash. To reduce the ambiguity in the scale-up of the 25 g capacity flow calorimeter, the burning characteristics of kilogram-size pellets of unprocessed MSW were studied in a prototype combustor [4].

---

[1] Numbers in brackets indicate literature references.

Unprocessed MSW in that work, and also in the present study, was prepared by withdrawing increments from the output of the primary shredder of the Baltimore County Resource Recovery Facility at Cockeysville, MD. The increments were dried at 105 °C for 12 hours and then sorted to remove metals. The particle size was 15 cm.

After designing, fabricating, and assembling the multi-kilogram flow calorimeter, a study consisting of 25 experiments was carried out to answer the processing and sampling questions. After drying the increments of unprocessed MSW, we attempted to prepare identical increments by hand sorting groups of four or more increments of MSW into categories (i.e., paper, metals, wood, vegetable matter, etc.) and reconstituting the categories (except for metals) into 2.5 kg samples having the same mass composition as the whole. Two of the 2.5 kg samples from each group were milled to 2 mm particle size and then, to obtain gram-size test samples, each of these parent samples was subdivided using a rotary riffler rather than the usual method of coning and quartering. The results, which we believe resolve the processing and sampling questions, are discussed in detail elsewhere [5]. In brief, the results are as follows:

1) The average difference of the calorific values of gram-size test samples of dry, processed MSW minus that of their kilogram-size parent of dry, processed MSW is −0.1% of the mean calorific value of the parent sample. The imprecision[2] of the average difference is 1.1% of the average calorific value and can be accounted for by the percent coefficient of variation,[3] *% CV*, of the bomb calorimetry measurements, 0.5%, and the flow calorimetry measurements, 0.4%, on these MSW samples. The subdivision process using the rotary riffler is less sensitive to the effects of segregation than the subdivision process carried out by the usual method of coning and quartering.

2) The average difference in the calorific values of MSW of kilogram-size samples of dry, unprocessed MSW minus that of dry, processed MSW is −0.5% of the average calorific value of the processed MSW. The imprecision of the difference is 2.9% of the average calorific value. We avoided excessive localized heating during milling by adding powdered dry ice to the sample as it was fed to a Wiley[4] mill in the final step of size reduction. The larger imprecision of this second result, 2.9%, as compared to the first, 1.1%, is largely due to the fact that identical kilogram-size samples of unprocessed MSW (one of which is then milled) could not be prepared by the procedure we used.

3) We concluded that the calorific values of the gram-size test samples of processed MSW are the same as the calorific values of their kilogram-size parents of unprocessed MSW within 1%. Thus, it is not necessary to combust the entire kilogram-size increment. However, the gram-size test samples must be prepared properly. In particular, the particle size of each increment should be reduced in such a way as to avoid localized heating and the resulting processed MSW should be sampled to obtain gram-size test samples in such a way as to avoid the effects of segregation. Such effects had been observed when coning and quartering were used to obtain gram-size test samples (see reference [1]).

3. Experimental Apparatus

The flow calorimeter consists of two basic parts: a constant temperature jacket and the calorimeter proper. The latter contains the sample combustor. Heat liberated in the combustion reaction is transferred to the stirred water in the calorimeter vessel, the outermost container of the calorimeter proper. The rise in temperature of the calorimeter water, after correction for heat exchange with the jacket, is proportional to the enthalpy of combustion of the sample. The calorimeter is calibrated by determining the temperature rise produced by combustion of a known mass of homogeneous, microcrystalline cellulose whose enthalpy of combustion has been measured by bomb calorimetry. (See reference [5], pp. 22–26.)

The main features of the flow calorimeter are described in section 3.1. The analysis system used to determine the completeness of combustion (i.e., the CO concentration in the product gas) and the amount of water vaporized from the calorimeter is described in section 3.2. The data acquisition system used with the calorimeter is described in section 3.3.

---

[2] For this and all other statements labeled "imprecision," we use the product of the standard deviation of the mean and the appropriate Student *t* factor at the 95% confidence level.

[3] For this and all other statements labeled *% CV*, we use 100×*s* average where *s* is the standard deviation of a single experiment.

[4] Certain facilities, commercial equipment, instruments, or materials are identified in this paper in order to adequately specify the experimental procedure. Such identification does not imply recommendation or endorsement by the National Bureau of Standards, nor does it imply that the materials or equipment are necessarily the best available for the purpose.

3.1 Description of the Multi-kilogram Capacity Flow Calorimeter

A cross-section of the entire flow calorimeter is shown in figure 1. The important dimensions and calorimeter properties are listed in table 1. All metal components are fabricated from type 316 stainless steel.

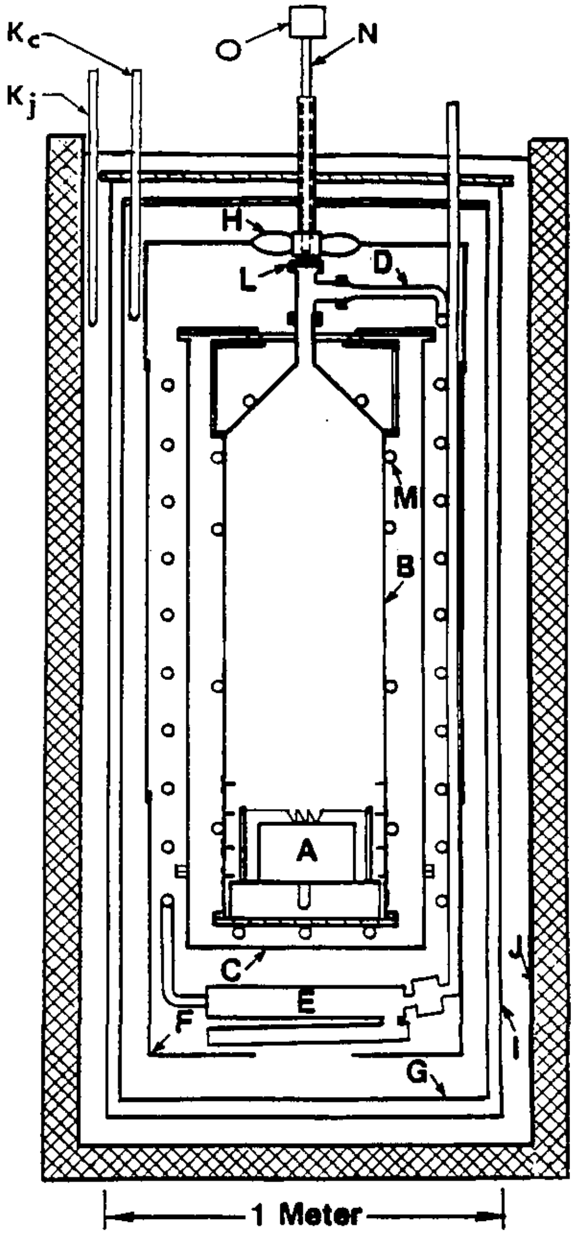

Figure 1–Diagram of the multi-kilogram capacity flow calorimeter. A denotes the sample pellet, B the combustor, C the combustor enclosure, D the heat exchange coil, E the collector, F the flow shield, G the calorimeter vessel, H the stirrer, I the submarine vessel, J the jacket, K_c the inner quartz oscillator thermometer for the calorimeter water, K_j the outer quartz oscillator thermometer for the jacket water, L the window, M the quick-cool heat exchange tube, N the boroscope, and O the TV camera.

The cylindrical compressed sample pellet (nominally 23 cm diameter and 15 cm high), A, is located inside and near the bottom of the combustor, B. A detailed cross-section of the sample and neighboring parts of the combustor is given in figure 2. Referring to that figure, the pellet, A, is supported on a parallel array of nine horizontal, alumina rods, r, (6 mm diameter) resting in notches cut in the top edge of a cup-shaped ash pan, p. The ash pan, which retains the residual ash from the burned MSW, sits on the base plate, b, that forms the bottom of the combustor. An iron fuse wire, f, having a four turn coil touching the top of the sample at the center, is stretched horizontally between two vertical electrodes of which one, e, is shown. The electrodes pass through open-ended tubes of which one, t, is shown. The tubes are welded into the bottom of the ash pan. The sample is ignited by passage of electrical current through the fuse wire.

Flowing oxygen is supplied to the sample by an array of nozzles arranged in five horizontal tiers, o_1 through o_5 (o_5 is not shown in fig. 2). Each tier contains six symmetrically spaced nozzles located in the combustor wall. The bottom tier, o_1, supplies

Table 1. Specifications for the multi-kilogram capacity flow calorimeter.

Component	Dimensions Height (cm)	Outside Diameter (cm)	Wall Thickness (mm)	Total Mass (kg)
Combustor	155	41	3.2	74
Combustor Enclosure	163	61	4.8	196
Flow Shield	213	79	1.6	73
Calorimeter Vessel	236	91	4.8	390
Submarine Vessel	243	97	4.8	454

Additional Specifications

Calorimeter water	980 liters	
Jacket water	2160 liters	
Heat capacity of calorimeter	0.4 MJ/K	(assembly)
	4.1 MJ/K	(water)
	4.5 MJ/K	(total)

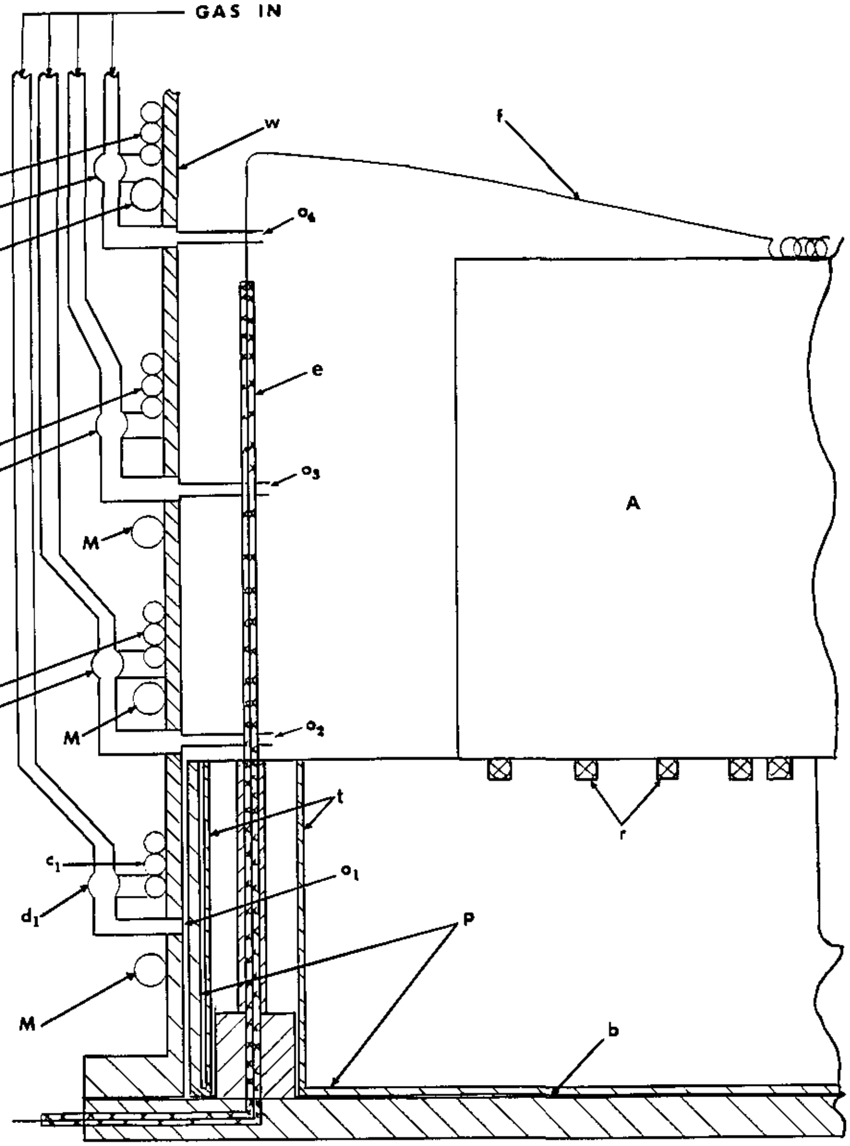

Figure 2–Cross section of the sample and neighboring parts of the combustor (to scale; pellet height is 15 cm). A denotes the pellet, b the combustor base plate, c_1 through c_4 the oxygen preheat coils, d_1 through d_4 the oxygen distribution rings, e one of the two electrodes, f the iron fuse wire, M the helical tube of the quick-cool heat exchange system, o_1 through o_4 the oxygen inlet nozzles, p the ash pan, r the alumina support rods, t an open tube in the ash pan, and w the wall of the combustor. A and M designate the same components in figures 1 and 2.

oxygen through slots in the ash pan as a diffuse stream that is directed at the bottom of the sample. The other tiers supply narrow jets of oxygen that are either directed at the sides of the sample or into the space above the sample. The oxygen inlet line for each tier feeds a distribution ring, d_1 through d_5, (d_5 is not shown in fig. 2) which supplies the oxygen to the nozzles of that tier. The oxygen entering the distribution rings of the top four tiers is first preheated by passing it through separate sets of three coils, c_1 through c_5, (c_5 is not shown in fig. 2) wound around and welded to the outside of the combustor wall, w.

Referring back to figure 1, the combustor, B, is surrounded by a concentric cylindrical vessel, the combustor enclosure, C. The space between the combustor and the combustor enclosure contains the tubes that supply oxygen to the combustor, leads for the thermocouples to monitor the temperature of the oxygen as it enters each distribution ring and the temperature at various locations on the combustor wall, and the fuse ignition leads. The space also contains the helical tube, M, of the quick-cool heat-exchange system (the tube is welded to the outside of the combustor with a pitch as shown in fig. 2), and argon gas to reduce oxidation of these components.

A submersible pump circulates the calorimeter water through the quick-cool tube, M, before and after the combustion reaction to ensure that the combustor wall and calorimeter water are at the same temperature during drift periods. Prior to ignition, the quick-cool tube is purged of water. The relatively poor heat transfer between the combustor enclosure and the combustor allows the temperature of the walls of the combustor to rise during the combustion and, thus, promotes the combustion of any soot deposited on the cold combustor walls during the initial stage of the sample combustion.

The product gas leaves the top of the combustor and then passes downward through a heat-exchange coil, D, having 10 turns. The product gas then passes through the collector, E, through the exit tube, and, finally, out of the calorimeter. The heat exchange coil transfers heat from the product gas to the calorimeter water contained in the space bounded by C and G. Most of the water formed in the combustion reaction condenses and is trapped in the collector, E. An enlarged cross-section of the collector, E, is shown in figure 3. Referring to that figure, the product gas enters the larger, upper, toroidal tube, v_1, from the 10-turn heat-exchange coil. Condensate drains from v_1 into a second, smaller, lower, toroidal tube, v_2. The product gas then leaves the collector and passes through glass wool backed by a screen, s, in the cylindrical stuffing box, w. The wool reduces the entrainment of condensate droplets in the product gas. Auxiliary dry dilution oxygen is added through a port, i, in the stuffing box to reduce the partial pressure of water vapor in the product gas so that it will not condense after the product gas is cooled to room temperature.

Referring back to figure 1, the calorimeter water is directed past the heat exchange coil by means of the flow shield, F. Water is drawn through the bottom port (20 cm diameter) in the flow shield, past the heat exchange coil, D, and is mixed by blades of the stirrer, H, mounted in the top port of the shield. Water returns to the bottom port via the annular space between the calorimeter vessel, G, and flow shield at a water flow rate of about 180 L/min. Thus, the calorimeter water makes a complete circuit of the flow path about every 5.4 min.

The calorimeter vessel is surrounded by the concentric cylindrical submarine vessel, I, which constitutes the innermost portion (i.e., surface) of the constant temperature jacket. The "interspace" between the vessels, which is 2.5 cm wide, is filled with air which serves to reduce the rate of heat exchange between the jacket and the calorimeter proper. (The top interspace which is between the lids of the calorimeter and the submarine is 5 cm.) The submarine vessel is submerged in the stirred water of the jacket, J. The jacket is a fiberglass covered container whose walls consist of a steel framework covered by polyurethane foam.

The calorimeter water temperature is monitored by the inner quartz oscillator thermometer, K_c. The outer quartz oscillator thermometer, K_j, monitors the temperature of the jacket water. Temperatures of the inlet oxygen supply and the product gas are monitored with thermocouple probes whose junctions are located in the gas tubes at the level of the calorimeter vessel lid. The temperatures of the calorimeter water at the top and bottom of the flow shield are monitored to measure the nonuniformity in the calorimeter water temperature. The measurement junctions of the two separate thermocouples are placed between the calorimeter vessel and the top and bottom edges, respectively, of the flow shield.

The combustion reaction is monitored visually through the window, L, sealed to the inline port of a tee in the product gas line at the top of the com-

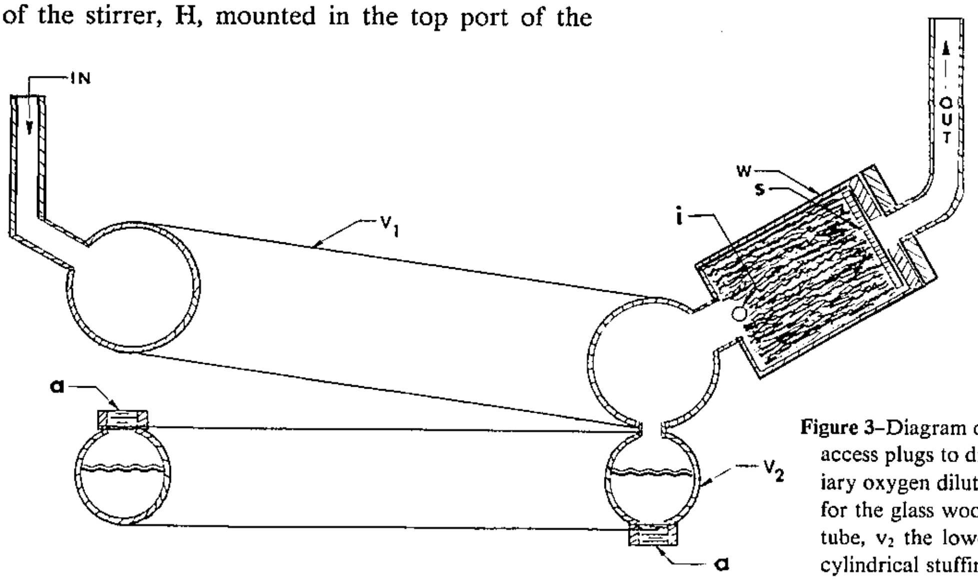

Figure 3–Diagram of the collector. a denotes the access plugs to drain the collector, i the auxiliary oxygen dilution port, s the backup screen for the glass wool filter, v_1 the upper toroidal tube, v_2 the lower toroidal tube, and W the cylindrical stuffing box.

bustor and through the adjacent second window sealed to the end of the hollow stirrer shaft in the water. The boroscope, N, which extends downward through the hollow stirrer shaft, is used to view the combustion. The boroscope is attached to a TV camera, O, which is connected to a video monitor-recording system. Oxygen is supplied to the underside of the viewing window to prevent condensation of water on the window during the combustion.

Oxygen is supplied to the calorimeter from six independent sources, each consisting of one or more standard 6200 liter (STP) oxygen tanks that is equipped with reducing and shut-off valves. The oxygen flow from each source is monitored with a mass flow controller. Flowmeters are intercompared by connecting them in parallel and series in appropriate combinations. Two of the meters were calibrated at NBS with an uncertainty of 0.5%.

To simplify the assembly and disassembly of the calorimeter, all the components inside the calorimeter vessel were designed to be suspended from the calorimeter vessel lid and this lid was, in turn, suspended from (beneath) the submarine lid. Motors for the calorimeter stirrer and quick-cool water pump, the boroscope, and the TV camera are mounted in a lifting frame attached to the top of the submarine vessel. The calorimeter plus the submarine vessel at various stages of assembly are raised and lowered with a gantry crane whose hoist chain is connected to the top of the lifting frame. The empty submarine vessel is restrained against the buoyant force of the jacket water by three chains connected between the vessel and eyebolts anchored to the bottom of the jacket. When the calorimeter vessel is unbolted from its lid and the internal calorimeter components are withdrawn, the calorimeter vessel is nested inside the submarine vessel on a removable, concentric collar placed between the top flange of the calorimeter vessel and the top flange of the submarine vessel.

Three features of the calorimeter hardware are significant. First, holes where tubes (containing thermocouple leads, electrical leads, supply oxygen, or product gas) pass through the various lids (e.g., submarine vessel, calorimeter vessel, or combustor enclosure) are closed with stationary O-ring seals. Motor drive shafts pass through chimneys in the submarine vessel lid and rotary O-ring seals in the calorimeter vessel lid. The rotary seals reduce evaporative loss of the calorimeter water when it is warmer than the submarine vessel.

Second, to reduce leakage of gas between the inside of the combustor and the gas space between the combustor and the combustor enclosure, the combustor base plate is sealed to the rest of the combustor by a gasket that is a composite of graphite and 316 stainless steel. The combustor enclosure itself is made gas-tight by use of Viton O-ring seals. Electrical leads to the inside of the combustor enclosure are hermetically sealed with epoxy cement in their feed-through tubes.

Third, the reference junctions of all thermocouples on the combustor, in the calorimeter water, and in the flow lines (exclusive of those in the product gas analysis train) are mounted on an aluminum reference block which is inside a hermetic chamber that connects by tubes to the combustor enclosure. These tubes feed the thermocouple leads from the combustor through the various lids and support the block and chamber above the level of the jacket water. The hermetic seal in the chamber completes the gas-tight seal of the combustor enclosure. The temperature of the block is allowed to float (i.e., it is not controlled) but its temperature is monitored by the calorimeter water thermocouple whose junction is located at the top edge of the flow shield and is close to the inner quartz oscillator thermometer, K_c. During an experiment, the block temperature changes by less than 0.1 °C.

3.2 Analysis Systems

After leaving the submarine vessel, the product gas passes through a mixing chamber. Just beyond the chamber, a portion of the gas is continuously withdrawn for analysis; the product gas at this point is at or near room temperature. A block diagram of the analysis system is shown in figure 4. Part of the gas withdrawn for analysis is dried and passed at a flow rate of about 2 L/min through dedicated infrared detectors for CO and CO_2. A second part of the gas is passed at a flow rate of about 2 L/min through a cooled-mirror type of automatic dew point detector to monitor water vapor. The remaining part of the analysis gas is passed at a flow rate of about 5 L/min through a scanning infrared detector used to monitor various trace components (such as hydrocarbons, SO_2, HCl, etc.). These detectors in combination with three manometers and four thermocouples (to monitor gas temperatures) are used to determine the composition of the product gas.

3.3 Data Aquisition Equipment

The enormous amount of data generated during each experiment was monitored and recorded using the system shown schematically in figure 5. Because of the delays associated with displaying and

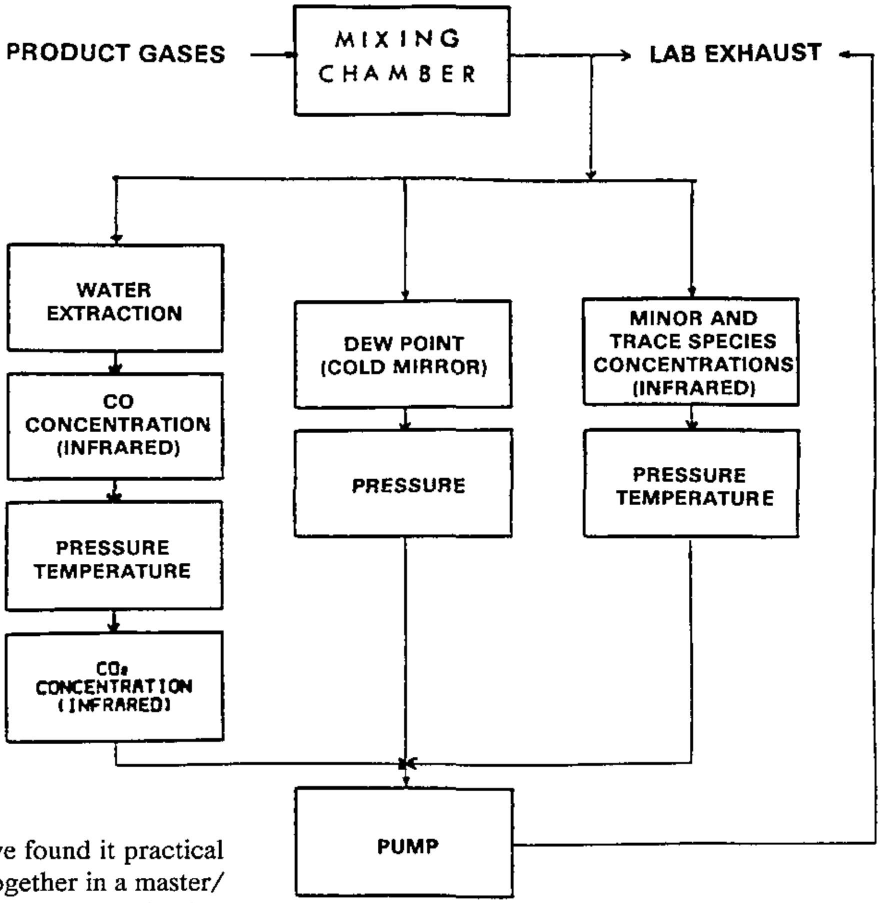

Figure 4–Block diagram of the product gas analysis system.

printing the data in real time, we found it practical to couple two minicomputers together in a master/slave configuration via a RS-232 communication link. All the software for both computers was written in BASIC programming language.

The low-level signals generated by the 27 thermocouples of the calorimeter were sequentially sensed with a digital voltmeter via a scanner. The frequency of each quartz oscillator thermometer was monitored with a counter using the NBS 100 kHz Standard Frequency as the time base. These instruments were connected via an IEEE-488 data bus to the master minicomputer which controlled the acquisition and logging of all the data. Each of the above signals was measured at least once every minute throughout the entire duration of the experiment.

The signals generated by the meters monitoring the inlet oxygen flow rates plus the various detectors in the analysis system were sequentially sensed with a second digital voltmeter connected to the second minicomputer operated in a slave mode. The one scanner controlled the input to both voltmeters. These signals were recorded at least once every minute during the time interval for which they were significant. Because of the more rapid variation of the concentrations of CO, CO_2, and water vapor in the product gas and the need to accurately correct for the enthalpy of vaporization of water lost from the calorimeter, the signal from each of these detectors was recorded at least three times every minute.

For the experiments described in this paper, it was convenient to record the ouput signal of the scanning infrared detector on a strip chart. No significant energy loss was associated with very small concentrations of the trace components in the product gas.

4. Description of an Experiment and Typical Results

The time frame, operating parameters, and significant outputs of a typical experiment are described in section 4.1. An idea of the time frame of preparation for an experiment and some of the details of the assembly of the calorimeter are given as the large size of the calorimeter magnifies time and manpower needs and produces problems in otherwise trivial operations. A summary of data reduction procedures is given in section 4.2. Typical calculated results for calibration and "unknown" experiments are given in section 4.3.

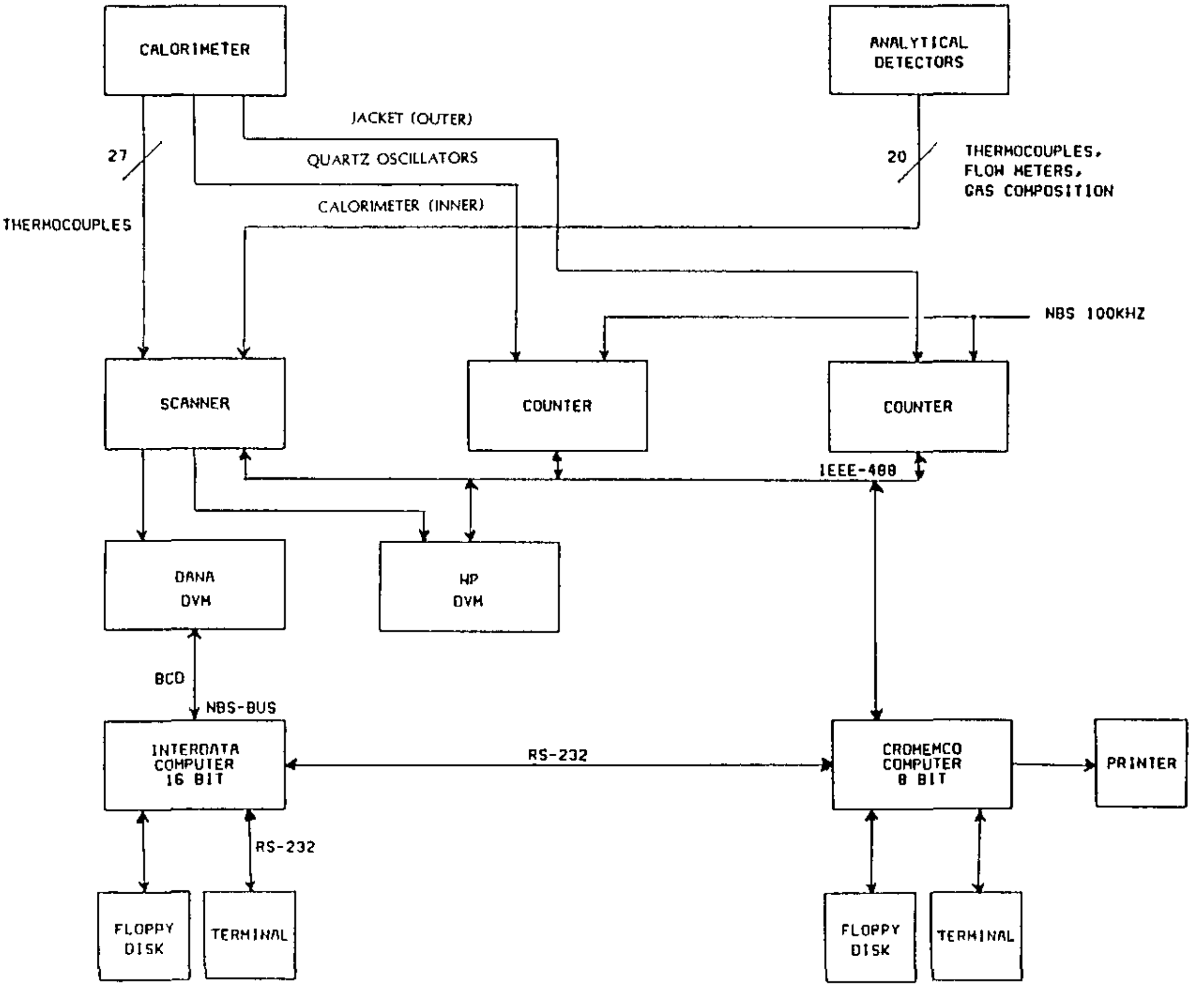

Figure 5-Block diagram of the data acquisition system.

4.1 Experimental Procedure

On the day prior to the experiment, the sample pellet is prepared and the components inside of the calorimeter vessel are assembled.

On the day of the experiment, the calorimeter water is heated (or cooled) in a separate holding tank to a temperature within ±0.3 °C of that of the jacket water which is within ±1 °C of room temperature (22 °C). A fixed volume of water from the holding tank is added to partially fill the empty calorimeter vessel; the volume is the maximum amount that experience shows will not splash or overflow as the internal components of the calorimeter are lowered into the calorimeter vessel. The volume is determined with a jig, shown in figure 6, which has a filling cup, fc, having a conical bottom and an overflow hole, oh, located in its side. The upper supports, sp, are bolted to the top surface of the calorimeter vessel, G, so that the cup is inside (1.3 cm radial clearance) and at a fixed distance (about 75 cm) below the top flange of the vessel. After leveling the top surface of the calorimeter vessel to within ±20 seconds of arc using the spirit level, I, water is added until it just overflows into the inside of the filling cup. After the jig is removed, the internal components of the calorimeter are gently lowered into the vessel. The calorimeter vessel and submarine vessel are bolted to their respective lids. After lowering the entire assembly into the jacket water, the final 20 liters (fixed for all runs) of water needed to fill the calorimeter vessel to within 0.3 cm of its lid are added.

The stirrers for the calorimeter and jacket water are turned on, and the calorimeter water temperature is monitored for one hour after the drift rate becomes constant. During this time interval, the calorimeter water is pumped through the quick-cool heat exchange tube on the combustor wall.

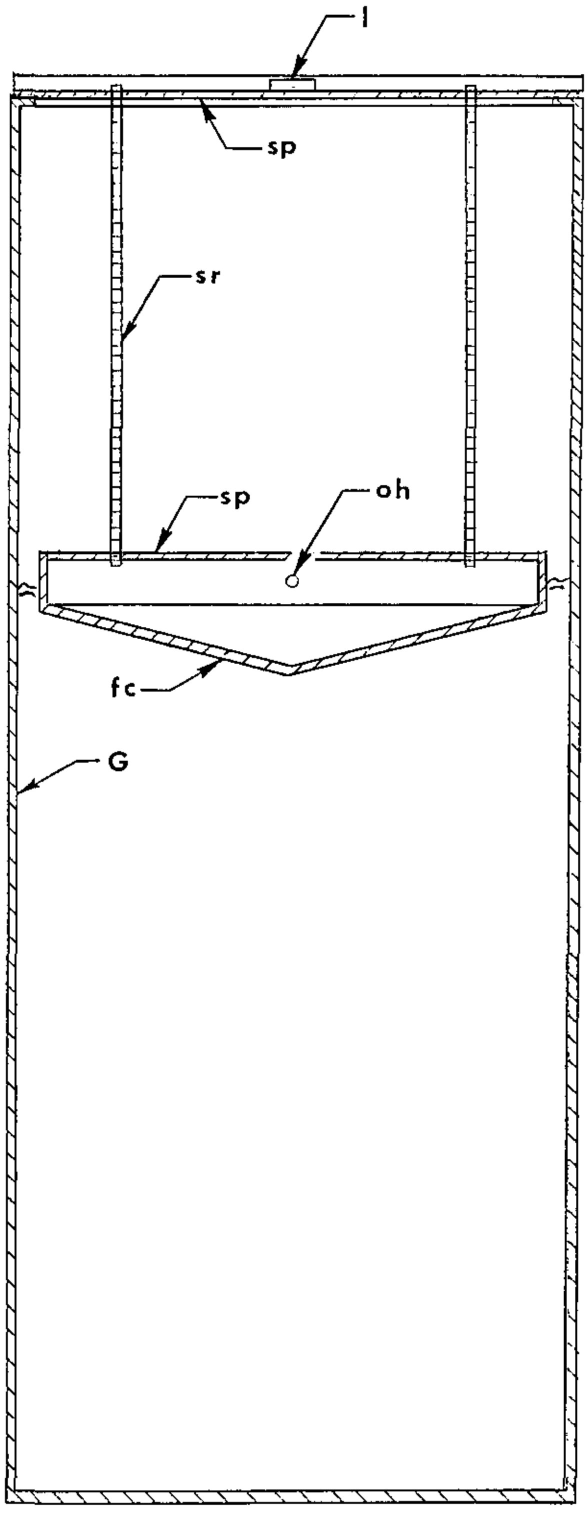

Figure 6–Diagram of the calorimeter water loading jig. fc denotes the filling jig cup (cup-shaped pan), G the calorimeter vessel, I the spirit level, oh the overflow hole in filling jig cup, sp the filling jig cup supports, and sr the filling cup spacing rods.

The last 30 minutes of the time interval is the initial drift period.[5]

Twelve and one-half minutes prior to ignition, the flow of water to the quick-cool heat exchange tube is diverted to the calorimeter vessel and the water remaining in the quick-cool tube is flushed out with compressed air. The combustor is then flushed with oxygen for 10 minutes at a flow rate of 30 L/min. (Flow volumes are expressed in liters at 0 °C and 101.325 kPa.) Two and one half minutes prior to ignition, the flow rates are increased to the levels used during combustion when oxygen is supplied at constant rates of 150 L/min to the combustor, 10 L/min to the viewing window, and 110 L/min to the dilution port at the collector exit for a total flow of 270 L/min.

Sample burning times were approximately 32 minutes for pellets of unprocessed MSW or microcrystalline cellulose, and about 42 minutes for processed MSW. The CO_2, H_2O, and CO concentrations in the product gas during the combustion of a processed MSW pellet are shown in figure 7. The peak and average CO_2 concentrations over the first 10 minutes of the combustion are 52 and 38 mole percent, respectively. The latter concentration corresponds to an inlet oxygen flow rate of about 2.5 times stoichiometry.

The H_2O concentration reaches a maximum of 2.4 mole percent (i.e., dew point of 16 °C) at 30 minutes; the abrupt fall in concentration at 42 minutes indicates that the combustor has been completely flushed of product gas. The inlet oxygen flow rate is maintained at the same level as during the combustion reaction for another 10 minutes to assist in the "cool off" of the combustor. The total inlet oxygen flow rate is then reduced to about 20 L/min to prevent excessive evaporation of water from the collector. This flow, which is supplied only to the combustor, maintains a positive pressure in the combustor with respect to the collector and thus prevents backflow of condensate into the combustor. The inlet oxygen flow is stopped prior to the beginning of the final drift period.

The occurrence of two peaks in the CO concentration versus time is typical of all the MSW samples. In figure 7, the initial and final maximum CO concentrations are 0.016 and 0.027 mole percent, respectively. The initial peak always occurs near the time of the maximum rate of production of CO_2; the final peak occurs near the end of the vi-

---

[5] Strictly, the initial drift period ends 12.5 minutes prior to ignition when the oxygen supply used to flush out the calorimeter is turned on. In practice, the error incurred in ΔT_c of eq (3) and ΔH_g of eq (1) by assuming that the initial drift period ends at the time of ignition has a negligible effect on our results.

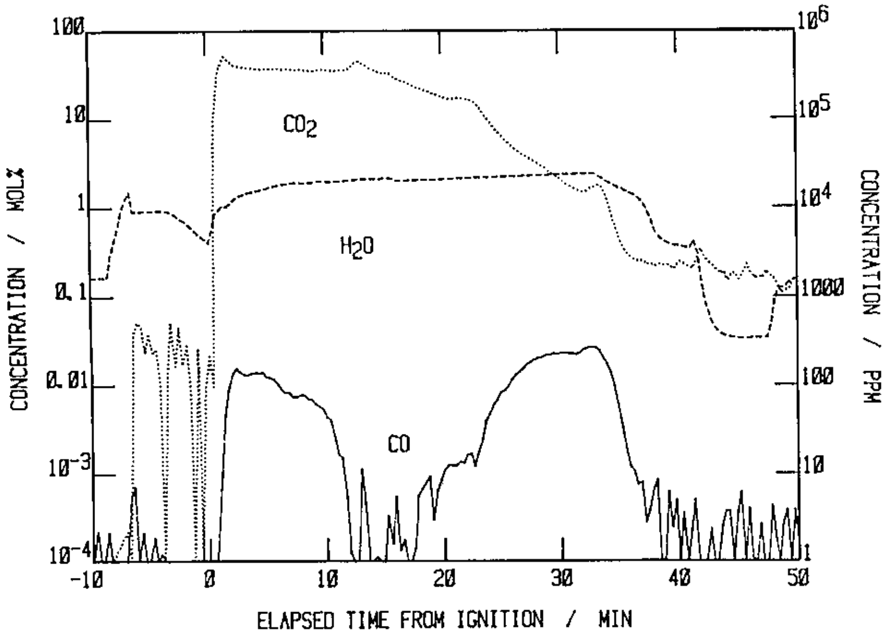

Figure 7–A plot of the concentrations of gaseous carbon dioxide, water, and carbon monxide as a function of time for a typical experiment on MSW.

sual burning when the ash tends to inhibit the combustion. The average CO concentration in a cellulose combustion is about a factor of 50 smaller than that shown in figure 7.

The temperature of the product gas as it leaves the top of the combustor rises to about 400 °C within the first minute of the combustion, gradually increases to a maximum of about 450 °C between 12 and 15 minutes after ignition, and then decays exponentially thereafter. The temperatures of the combustor wall and of the oxygen gas as it leaves the preheat coils increase more gradually to their peak values at about the same time and decay similarly. The peak values of the temperatures of the wall and adjacent preheat coils within 25 cm of the ash pan are between 600 and 700 °C.

When the temperature of the combustor base plate has decreased to 220 °C, the calorimeter water is again circulated through the quick-cool heat exchange tube. This safely removes the appreciable excess heat stored in the combustor. A plot of the calorimeter water temperature versus elapsed time for the experiment that corresponds to figure 7 is shown by the solid line of figure 8. When the quick-cool system was activated, which occurred at an elapsed time of 65 minutes, the temperature of

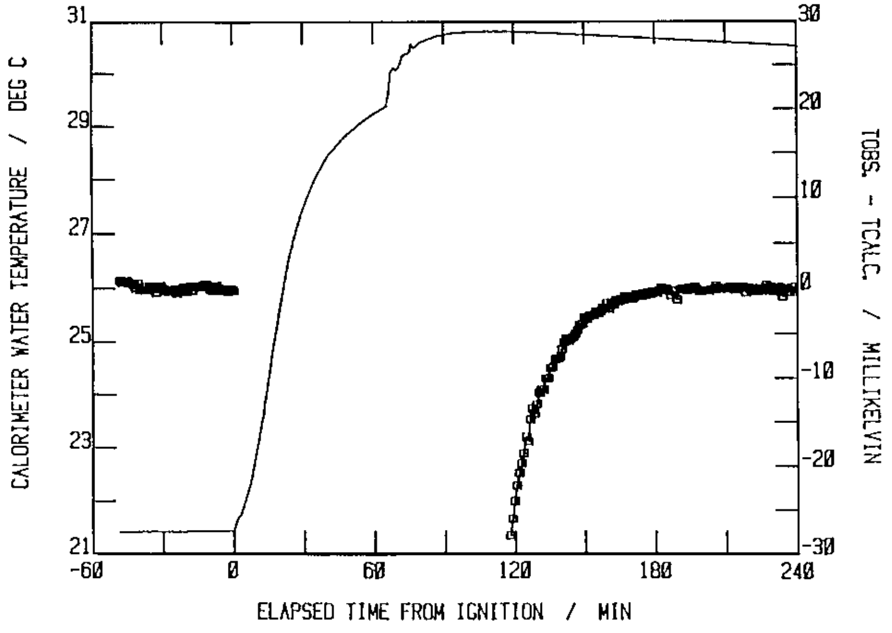

Figure 8–A plot of the observed temperature rise of the calorimeter water plus the deviation of the observed data points from the smooth curve fit to the data during the drift periods. The effect of activation of the quick-cool system is seen at about 65 minutes.

the calorimeter water has increased 8 °C. During the next 10 minutes, when most of the excess heat was removed, the temperature of the calorimeter water increased by another 1.2 °C. The latter increase indicated that 13% of the total heat liberated by the combustion reaction was stored in the walls and base plate of the combustor.

After the drift rate of the calorimeter water attains a steady value (which occurs about three hours after ignition) the inlet oxygen flow is stopped and temperature readings are made for an additional hour. At this point, the combustor and calorimeter water are at the same temperature to within 0.1 °C. The last 30 minutes of this time interval corresponds to the final drift period.

Before assembly and after disassembly of the calorimeter, the ash pan with its contents was weighed to determine the mass of ash formed in the combustion experiment. Similarly, the collector was weighed to determine the mass of water which was formed in the combustion reaction and remained in the calorimeter. The ash was milled, homogenized, and a sample was analyzed for moisture, carbon, and hydrogen content. The condensate in the collector was analyzed for total H^+, Cl^-, $SO_4^=$, and NO_3^- contents.

4.2. Data Reduction

Results are calculated using a format adopted from the work of Prosen et al. [6]. The basic measurement equation is:

$$E\Delta T_c = -(M\cdot\Delta\bar{H}_{st}+\Delta H_v+\Delta H_g+\Delta H_{ic} +\Delta H_{ig}+\Delta H_x)+W. \quad (1)$$

In eq (1), E is the energy equivalent of the calorimeter. The parameter ΔT_c is the corrected temperature rise of the calorimeter. The parameter M is the mass of the sample. The parameter $\Delta\bar{H}_{st}$ is the enthalpy change per unit mass of sample for an assumed standard reaction in which all reactants and products are at some selected isothermal process temperature, T_h, and pressure of 101.325 MPa (1 atm). The remaining five terms on the right of eq (1) account for the conditions of a particular experiment. They are as follows: ΔH_v is the correction for the vaporization of water formed in the combustor that is lost from the calorimeter (i.e., in product gases). The parameter ΔH_g is the correction for the net heat transport of gas entering and leaving the calorimeter at some temperature other than T_h. The parameter ΔH_{ic} is the correction for incomplete combustion of the combustible fraction of the sample to the assumed products of the standard reaction. The parameter ΔH_{ig} is the correction for the enthalpy of oxidation of the fuse. The parameter ΔH_x is the correction for deviations of the conditions of the experiment from a constant pressure process at 1 atm assuming all gases are perfect and the kinetic energy of the flowing gases is negligible. The parameter W is the electrical work required to heat the fuse wire.

The corrected temperature rise, ΔT_c, is evaluated in the conventional manner (see reference [7], p. 2–15). The drift period equation, eq (2) below, is fitted to the observed calorimeter water temperature, $T_1(t)$, versus time, t, data of the initial and final drift periods using a computer program given in reference [8].

$$dT_1(t)/dt = k(T_\infty - T_1(t)) \quad (2)$$

In the application of eq (2), k, the cooling constant, and T_∞, the convergence temperature, are assumed to be constant and identical for both drift periods. The data points in figure 8 are the deviations of $T_1(t)$ from the integral form of eq (2). (The ordinate scale is -30 to $+30$ mK.) The set of data points on the right of the figure indicates that the final drift period begins about 150 to 180 minutes after ignition. The corrected temperature rise is given by eq (3).

$$\Delta T_c = T_1(t_f) - T_1(t_i) - k\int_{t_i}^{t_f}(T_\infty - T_1(t))dt \quad (3)$$

In eq (3), t_i and t_f are times at the end of the initial drift period (ignition of the sample, see footnote 5) and at the beginning of the final drift period, respectively. $T_1(t_i)$ and $T_1(t_f)$ are called the initial and final temperatures of the calorimeter, respectively. The observed temperature rise is $T_1(t_f)-T_1(t_i)$, and the correction for the heat exchange with the surroundings is the last term on the right of eq (3). The sample size was chosen so that the observed temperature rise was between 6.0 and 9.5 °C for all experiments. The heat exchange correction amounted to about 4% of the observed temperature rise. The cooling constant, k, is typically about $3\times10^{-4}\text{min}^{-1}$ and T_∞ is about 22 °C (near room temperature).

Whether the energy equivalent, E, refers to the calorimeter when the products or reactants are present is, in principle, determined by the selection of the isothermal process temperature, T_h (see reference [7], p. 2–6 and reference [9]). For this calorimeter, the difference in E for $T_h = T_1(t_i)$ or $T_h = T_1(t_f)$ is negligible. In our work, it is convenient to take T_h equal to the initial calorimeter temperature $T_1(t_i)$ so that E refers to the calorimeter after the combustion reaction.

Since the value of E varies with the amount of ash remaining in the combustor (e.g., none in a calibration reaction) and water remaining in the collector, these variations are taken into account by adding the appropriate heat capacity difference, denoted by δE, to the value of E calculated from each calibration run to obtain E_s. The parameter E_s is the energy equivalent under an arbitrary but fixed set of so-called "standard calorimeter conditions." A different but appropriate δE is subtracted from the average E_s to obtain the energy equivalent for each MSW combustion experiment.

For the calibration reaction with microcystalline cellulose, the products of the standard reaction are taken to be $CO_2(g)$ and $H_2O(l)$. For the combustible fraction of MSW, that contains primarily C, H, O, N, S, and Cl, the products of the standard reaction are taken as $CO_2(g)$, $H_2O(l)$, $N_2(g)$, $SO_2(g)$ and HCl(aq). (Gases are assumed to be perfect and solutions are assumed to be ideal.) As a consequence, ΔH_{ic} contains the corrections for the presence of CO(g) in the product gases, carbon in the ash, and a correction for the presence of any appreciable $SO_4^{=}$ and NO_3^- in the collector condensate. Separate experiments using a flame ionization detector show that the concentration of gaseous hydrocarbons in the product gas is negligible.

The reactions that correspond to $\Delta \bar{H}_{st}$, ΔH_v, and ΔH_g and the method used to calculate the correction terms in eq (1) are similar (see reference [10]) to those given in reference [3].

4.3 Typical Results

Calibration results are given in table 2. The second column is the standard enthalpy of combustion per unit mass of dry cellulose as determined by bomb calorimetry after correction to the value of T_h appropriate to each experiment (i.e., $T_h = T_1(t_i)$). The third column is the dry sample mass, M. Quantities in columns five through nine were defined in the previous section. The ten are column entries in the correction, δE, added to the energy equivalent calculated according to eq (1) to obtain the energy equivalent, E_s, for standard calorimeter conditions. The standard calorimeter conditions are defined to be: the calorimeter water is 21 °C immediately after it has been assembled and filled with water, no ash remains in the ash pan, and the mass of condensate remaining in the collector after the reaction is 1215 g. E_s is given in the last column of table 2. The average energy equivalent, E_s, and the standard deviation of a single measurement are listed at the bottom of the table.

The % CV of the determination of E_s, 0.19%, is comparable in magnitude to the % CV of the 11

Table 2. Calculation of the energy equivalent of the calorimeter.

Col. Exp. No.	(2) $-\Delta \bar{H}_{st}$ MJ/kg	(3) M (dry) kg	(4) $-M \cdot \Delta H_{st}$ MJ	(5) ΔH_v MJ	(6) ΔH_g MJ	(7) ΔH_{ic} (CO) MJ	(8) $-\Delta H_{ig} + W$ MJ	(9) ΔT_c K	(10) δE(a) MJ/K	(11) E_s(b) MJ/K
9	17.340	2.0474	35.502	(0.217)(c)	0.022	(0.000)(d)	0.002	7.8652	−0.0019	4.4818
10	17.345	2.0429	35.434	(0.263)(c)	−0.012	(0.000)(d)	do	7.8447	−0.0022	4.4830
11	17.336	2.0659	35.814	0.285	0.048	0.000	do	7.9514	0.0000	4.4625
15	17.349	2.0859	36.188	0.203	−0.042	0.001				
24	17.335	2.2856	39.621	0.304	0.043	0.001	do	8.7449	+0.0001	4.4913
29	17.335	2.2883	39.667	0.367	0.077	0.000	do	8.7728	+0.0003	4.4715
30	17.335	2.3836	41.320	0.321	0.064	do	do	9.1495	0.0000	4.4742
35	17.337	2.3239	40.289	0.330	0.066	do	do	8.9142	−0.0006	4.4748
36	17.336	2.4584	42.619	0.313	0.065	do	do	9.4261	−0.0009	4.4806
							Average			4.4767
							Std. dev. (% CV)[e]			0.0086 (0.19%)

(a) Correction for density of water at filling temperature other than 21 °C and for the difference of the mass of water in the collector from 1215 g; add to E of eq (1) to obtain E_s.

(b) E_s is E at filling temperature of 21 °C and 1215 g water in collector after the reaction.

(c) Estimated assuming that the mass of water vaporized is the water formed (as calculated from the empirical formula) minus that remaining in the collector.

(d) CO detector not functioning properly; CO assumed to be zero.

(e) Includes variance of mean ΔH_{st} of cellulose. Without latter, the standard deviation is 0.0084 and % CV is 0.19%.

bomb calorimetric determinations of $-\Delta\bar{H}_{st}$ of cellulose, 0.15%. For the bomb calorimeter used in the latter measurements, the *% CV* for the determination of its energy equivalent by combustion of standard reference material (SRM) benzoic acid was 0.05%. (A state-of-the-art bomb calorimeter has a *% CV* of 0.01% or less for the determination of its energy equivalent by SRM benzoic acid.)

The magnitudes of the average corrections to the calibration data are listed in the third column of table 3. The correction to the observed temperature rise to obtain ΔT_c, 4% of ΔT_c, is the largest correction. The next largest correction is the vaporization correction, ΔH_v, which is 0.75% of $M\cdot\Delta\bar{H}_{st}$ followed by the gas heat transport correction, ΔH_g which is about 0.1% of $M\cdot\Delta\bar{H}_{st}$. The correction for CO is negligible and no ash or residue remained from the combustion reaction.

As indicated in the third row of table 3, an average of 91.0% of the total water formed in the reaction is retained in the collector. The measured total water formed in the combustion reaction was 100.67±0.42% (imprecision of the mean of experiments 11 through 36 of table 2) of the water produced by the combustion of cellulose as calculated from its empirical formula of $C_6H_{10}O_5$(s). The measured CO_2 was 99±3% (imprecision of the mean of experiments 11 through 36 of table 2) of the calculated value of CO_2.

The results for the enthalpy of combustion of four sets of paired samples of processed MSW are given in table 4. The pairs of samples designated as E and E′ followed by the same number were prepared in such a way that each sample is "identical" (see reference [5], p. 19–22). The energy equivalent, E in column 3 is the average value of E_s taken from table 3 plus a correction for the variation in filling temperature from 21 °C and for the difference between the amount of water retained in the collector and ash in the combustor in these experi-

Table 3. Magnitudes of average enthalpy corrections of the basic measurement equation, eq (1).

Type of Correction	Symbol Form	Cellulose	Processed MSW
Correction for heat exchange	$\lvert(\Delta T_c-\Delta T_l)/\Delta T_c\rvert$[(a,b)]	4.00%	3.50%
Vaporization of water	$\lvert\Delta H_v/M\cdot\Delta H_{st}\rvert$	0.75%	1.42%
(water in collector/total water)		(91.0%)	(81.4%)
Gas heat transport correction	$\lvert\Delta H_g/M\cdot\Delta\bar{H}_{st}\rvert$	0.12%	0.13%
Correction for imcomplete combustion	$\lvert\Delta H_{ic}/M\cdot\Delta\bar{H}_{st}\rvert$		
CO(g)		0.00%	0.13%
carbon in ash		—[(c)]	0.03%[(d)]
$SO_4^=$ (aq) rather than SO_2(g)		—	0.01%
NO_3^- (aq) rather than N_2(g)		—	—

[(a)] ΔT_l is the observed temperature rise, $T_l(t_f)-T_l(t_i)$.

[(b)] | | indicates absolute value.

[(c)] no ash formed.

[(d)] carbon in ash is assumed to be elemental carbon.

Table 4. Calculation of $-\Delta H_{st}$ for processed MSW samples.

Column No.	(2)	(3)	(4)	(5)	(6)	(7)	(8)	(9)	(10)	(11)	(12)
							ΔH_{ic}				
Sample No.	ΔT_c K	E MJ/K	$E\Delta T_c$ MJ	ΔH_v MJ	ΔH_g MJ	(CO) MJ	C(ash)[(a)] MJ	$SO_4^=$(aq) MJ	$(\Delta H_{ig}-W)$ MJ	M(dry) Kg	$-\Delta\bar{H}$st MJ/Kg
E4	7.1030	4.4753	31.788	0.547	0.059	0.048	0.007	−0.003	−0.002	2.2032	14.726
E′4	7.1537	4.4758	32.019	0.464	0.046	0.050	0.008	−0.004	do	2.1984	14.820
E6	6.8905	4.4749	30.834	0.498	0.046	0.065	0.015	−0.002	do	2.1761	14.454
E′6	6.7822	4.4758	30.356	0.506	0.032	0.101	0.016	−0.003	do	2.1381	14.502
E7	8.2678	4.4758	37.005	0.492	0.054	0.042	0.016	−0.003	do	2.2520	16.698
E′7	8.2695	4.4752	37.007	0.602	0.048	0.033	0.014	−0.002	do	2.2564	16.708
E9	9.2526	4.4771	41.425	0.486	0.052	0.011	0.005	−0.005	do	2.2849	18.369
E′9	9.2217	4.4766	41.282	0.399	0.042	0.006	0.008	−0.006	do	2.2899	18.223

[(a)] Carbon in ash is assumed to be elemental carbon.

ments and the calibration experiments. To illustrate typical magnitudes of the individual corrections to E_s, the heat capacity correction for the water filling temperature, water in the collector, and ash in the combustor for experiment E6 are −0.5 kJ/K, −1.9 kJ/K, and +0.6 kJ/K, respectively. The definitions of the enthalpy corrections in columns 5 through 7 and in column 10 are the same as those in the corresponding columns in table 2. The correction for incomplete combustion given in column 8 is for the presence of carbon (assumed to be elemental carbon) in the ash. The correction given in column 9 is for the formation of $SO_4^{=}(aq)$ rather than $SO_2(g)$.

The enthalpy of combustion per unit dry mass, $-\Delta \bar{H}_{st}$, is listed in the last column. Using pair differences, a pooled estimate [11,12] of the standard deviation of a single measurement of $-\Delta \bar{H}_{st}$ of "identical" processed MSW samples was calculated. The resulting % *CV*, 0.4%, is the measurement error of the calorimeter with an actual sample of MSW. For comparison, the % *CV* for measurements of $-\Delta \bar{H}_{st}$ on the corresponding pairs of "identical" gram-size samples of MSW obtained with the same bomb calorimeter used in the cellulose measurements was 0.5% [5].

Average corrections for the processed MSW measurements are listed in the fourth column of table 3. The water vaporization correction is about twice as large as that for the calibration measurement due to the longer reaction time (and consequent flow of oxygen for a longer time interval). The longer reaction time is due to the deceleration of the rate of combustion during the last stages of the reaction by the intimate contact of the noncombustible and combustible components in the highly processed MSW. This is also reflected in a much larger CO correction and an appreciable correction for carbon in the ash. The ash ranged from 18 to 35% of the initial sample mass.

As indicated in the third row of table 3, an average of 81.4% of the total water formed in the combustion reaction of the processed MSW is retained in the collector. No reliable value for the hydrogen content of these samples (as in the case of cellulose) was available to compare the total collected water with that calculated from the empirical formula for the sample. However, the consistency of the experimental measurements can be checked by comparing the measured hydrogen contents of samples from the same day. The pooled estimate of the standard deviation of the hydrogen content of the pairs of samples was 0.045% of the dry pellet weight. Since the average hydrogen content was 5.15% of the dry pellet weight, the % *CV* of the measured hydrogen contents of all four sets of paired samples was 0.9%.

5. Design Basis and Performance Characteristics

As indicated in section 2, our initial assessment of the industrial problem showed that a satisfactory solution would be obtained with a kilogram capacity calorimeter that could provide an enthalpy of combustion having an overall uncertainty of less than 1% for a single measurement. As flow calorimetry requires more auxiliary measurements than bomb calorimetry, the strategy adopted to achieve this goal was to design and operate the instrumentation so that contributions of individual errors would be held to 0.1% or less. This section documents the extent to which this strategy was achieved.

Measures are described in section 5.1 which ensure that the energy equivalent of the calorimeter for standard calorimeter conditions is the same for both calibration and "unknown" experiments. Errors associated with the corrected temperature rise are described in section 5.2, and an overall uncertainty estimate is discussed in section 5.3.

5.1 *Design Basis*

The large sample flow calorimeter described is a stirred-water, isoperibol[6] calorimeter of the Coops-Van Nes design (see reference [13]). Coops and Van Nes [14] devised the "flow pattern control shield" cited in [13] which we call the flow shield, for short. The design basis for closed isoperibol calorimeters (i.e., those for which no reactants or products flow across the calorimeter boundary) has been reviewed elsewhere [13]. From a review of some previous work on calorimeter theory [15] and on the design practice and data analysis of flow calorimetry [16], we concluded that the design basis of open calorimeters (i.e., those for which reactants or products do flow across the calorimeter boundary) are essentially the same as those for closed calorimeters. In particular, to account for the enthalpy of the gases entering or leaving the calorimeter proper, the gas flow tubes should be in good thermal contact with the calorimeter water and jacket water, and the measurement junctions of the thermocouples used to monitor the temperatures of the fluids entering and leaving the

---

[6] Isoperibol indicates the presence of a constant temperature environment, i.e., a calorimeter with a constant temperature jacket.

calorimeter should be located at the interspace. Since the oxygen entering our calorimeter is passed through coils immersed in the jacket water, the temperature of the entering gas is equal to the jacket water temperature. By virtue of the product gas heat exchange coil and the collector, the temperature of the exit gas is equal to that of the calorimeter water. From measurements with thermocouples, it was found to be within 0.1 °C of the temperature of the calorimeter water at the location of the inner quartz oscillator thermometer.

The primary calorimeter design problem is to meet the requirement that the energy equivalent for standard calorimeter conditions be the same for both the calibration and "unknown" experiments. This design problem is referred to as the problem of equivalent sources and the associated error is referred to as the nonequivalent source error. In the following four sections (5.1.1 through 5.1.4) we review the measures taken to ensure that the nonequivalent source error is less than 0.1%.

5.1.1 Flow Shield. The flow shield, F of figure 1, was introduced because it provides efficient circulation of water within the cylindrical calorimeter vessel. Its purpose [13] is to make the temperature gradients in the water of the annular space between the flow shield and the calorimeter vessel, which we shall call the liquid shell, independent of the difference in temperature gradients on the heat sources (i.e., the combustor, combustor enclosure, heat-exchange coil, and collector) between the calibration and "unknown" reactions. This requires: 1) that the calorimeter water enters the liquid shell from the stirrer port in the flow shield (the temperature of the stirred water is uniform) and, that 2) the heat that is transferred from the liquid inside the flow shield to the liquid shell by heat transfer across the flow shield be negligible in comparison with that by forced convection due to stirring. For ease of assembly and substantial reduction in cost and fabrication time, we elected to depart from the second requirement, which would require the flow shield to be, in effect, a Dewar vessel. We made the flow shield from a sheet of 1.6 mm thick 316 stainless steel.

To compensate for this decision, we chose to minimize the nonequivalent source error by reducing the difference in termperature gradients inside the flow shield between the calibration and "unknown" experiments as discussed in sections 5.1.2 through 5.1.4.

5.1.2 Combustor Enclosure. The calorimeter is calibrated with a pellet of solid micro-crystalline cellulose that is burned in the same location as the "unknown" sample of MSW. As a steady-state approach is sufficient to analyze the equivalent source problem (see reference [13], p. 3–7), we note that, for the same rate of heat evolution by the calibration and "unknown" samples, the differences between the temperature gradients on the combustor enclosure in a calibration and "unknown" experiment are substantially less than on the combustor wall. This is due to the relatively poor heat transfer by gaseous conduction and convection between the combustor and the combustor enclosure during the main period.

5.1.3 Cellulose as a Calibrant. The only difference in the temperature gradients on the product gas heat-exchange coil is that caused by the different concentrations of water in the product gas stream from the combustion of calibration and "unknown" samples. (The differences are compared at the same rate of heat evolution.) This difference is nearly completely eliminated by using cellulose as a calibrant because paper is the major component, about 80 mass percent, of the combustible components in MSW. (The ratio of the number of moles of water to the number of moles of CO_2 produced in a combustion of the MSW samples given in table 4 is 0.78. The corresponding value for the microcrystalline cellulose samples is 0.83.)

5.1.4 Calorimeter Water Heat Transfer. To guarantee a small equivalent source error, the flow pattern of the calorimeter water must be the same (i.e., the same heat transfer characteristics) for both the calibration and "unknown" reactions (see reference [13] p. 3–4). This requirement is met by: a) adjusting the stirring rate of stirrer, H of figure 1, to be the same in every experiment with a tachometer and b) by filling the calorimeter vessel with the same volume of water at nearly the same temperature in every experiment. The point of procedure b) is that the coefficient of heat transfer between the calorimeter vessel lid and the liquid shell shall be the same in every experiment and preferably large to reduce possible errors due to differences in the coefficients of heat transfer.

The coefficient of heat transfer between the calorimeter water and the vessel lid was made large through the following three measures.

1) The "topping off" procedure described in section 4.1 was used to fill the calorimeter vessel as completely as possible, while allowing for the thermal expansion of the water during the run. Measurement of the level of the water inside the assembled calorimeter vessel established that the height of liquid in the various fillings varied by less than 1.6 mm.

2) A 3 mm thick sheet of copper was bonded with epoxy cement and bolted to the underside of

the 316 stainless steel calorimeter vessel lid to improve the radial heat transfer in the lid. The stirring action lifts calorimeter water up against the central portion of the underside of the vessel lid.

3) The stirring rate was made as large as was consistent with keeping the fluctuations in calorimeter water temperature less than 0.0001 °C.

5.1.5 Nonequivalent Source Error. The nonequivalent source error was estimated from an analysis of a simple model that takes into account the temperature gradients in the calorimeter water and temperature gradients on the combustor enclosure, flow shield and calorimeter vessel. The calculated result was of the order of $\pm 0.01\%$ of $\Delta \bar{H}_{st}$. To allow for the possibility that the simplicity of the model results in an underestimate of the nonequivalent source error, we increased the estimate of the uncertainty due to this source of error to $\pm 0.05\%$ of $\Delta \bar{H}_{st}$.

5.2 Heat Exchange Correction

Small deviations of the measured rate of change of the calorimeter water temperature from the drift period equation, eq (2), were expected for three reasons. First, the jacket water temperature, $T_2(t)$, changed with time. This, in effect, causes T_∞ to vary with time because the calorimeter is designed so that its effective environment temperature is equal to $T_2(t)$ to a good first approximation. Thus, T_∞ is given by eq (4)

$$T_\infty = T_2 + p_0/k \tag{4}$$

In eq (4), p_0 is the time rate of change of the calorimeter water due to stirring. The change in jacket temperature was allowed because the total increase of $T_2(t)$ from t_i to t_f is generally less than 0.2 °C and the expected correction for this effect is of the order of 0.03% of the corrected temperature rise and should be very nearly the same for both the calibration and "unknown" experiments.

The second reason for expecting the deviations from the drift period equation is that the cooling constant, k, should vary with temperature because the maximum difference between the calorimeter and jacket water temperatures for our experiments is from 6 to 9 °C. Nonlinear heat transfer by free convection in the interspace between the calorimeter vessel and the submarine vessel cannot be assumed to be negligible (i.e., not greater than 5% of conductive heat transfer) unless the width of the interspace is less than 1.1 cm (see reference [17], p. 104). The selected interspace separations, 5 cm on the top and 2.5 cm on the side of the calorimeter, were dictated by manufacturing and assembly considerations.

The third reason for expecting deviations from eq (2) is that the temperature of the calorimeter water was greater than the temperature of the jacket water throughout the last 80% of the experiment—shortly after ignition to the end of the final drift period. A slight water leak in the static O-ring seals of the various flow and thermocouple lead tubes or in the rotary O-ring seal of the drive shafts of the calorimeter stirrer or quick-cool pump would allow mass transfer by evaporation of the calorimeter water to occur which results in nonlinear heat transfer. The calorimeter was operated so that its initial temperature was within 0.3 °C of the jacket in order to reduce the time required to reach a steady initial drift rate and, thus, keep the time duration of an experiment within tolerable limits.

A study of the deviations from eq (2), which is often called a Newton's cooling law test, was made in the usual manner [18]. The calorimeter was forced to pass through a sequence of drift periods having average calorimeter water temperatures spanning the range of operation. This was accomplished by assembling the calorimeter vessel in the usual manner except that a cooling coil was placed inside the bottom port of the flow shield and the calorimeter water was preheated to 10 °C warmer than the jacket water. The supply and exit lines of the cooling coil leave and enter the calorimeter through auxiliary chimneys (normally capped) in the calorimeter vessel lid. The lines end in quick-disconnect couplers located just outside the chimneys. After the first equilibration period of slightly more than two hours (only the last 30 minutes is the actual drift period), the supply and exit couplers of the cooling coil were connected to a chilled water supply, the calorimeter water was cooled about 2 °C, the supply and exit couplers were disconnected, and another equilibrium period was started. The quick-cool pump was run throughout the entire test. No oxygen was supplied to the calorimeter in the test.

Analysis of the results of the above Newton's cooling law test shows that the data can be represented by eqs (5a) through (5d).

$$dT_1(t)/dt = p_0 - k_0(1 + f(\beta))\,\beta \tag{5a}$$

where

$$\beta = T_1(t) - T_2(t) \tag{5b}$$

$$f(\beta) = a_0\beta + a_1\beta^2\,;\ 10\ ^\circ\mathrm{C} \geqslant \beta \geqslant 1.5\ ^\circ\mathrm{C} \tag{5c}$$

$$f(\beta)=0 \qquad ; 1.5\ ^\circ\text{C} \geqslant \beta \geqslant -3\ ^\circ\text{C} \tag{5d}$$

In eqs (5), p_0, k_0, a_0 and a_1 are positive constants. The parameter $T_2(t)$ is the jacket water temperature. The eqs (5) are identical with eq (2) if T_∞ is given by eq (4) and the cooling constant, k, is replaced with the temperature dependent expression:

$$k=k_0\,(1+f(\beta))\,. \tag{6}$$

Equation (5a) indicates that heat transfer between the calorimeter and the jacket is nonlinear and eqs (5c) and (5d) indicate that the larger portion of this nonlinearity is probably due to heat transfer by evaporation of the calorimeter water and condensation on the inner surface of the submarine vessel (i.e., when $\beta>0$) rather than heat transfer by free convection. If free convection predominated, the observed value of $f(\beta)$ would tend to be symmetric around $\beta=0$. The estimated contribution of heat transfer by free convection to $f(\beta)$ is less than 25% of the $f(\beta)$ used to estimate the maximum correction to ΔT_c (see below). The estimated contribution of radiative heat transfer to the same $f(\beta)$ is about 2%. The nonlinear heat transfer is taken into account by a temperature dependent cooling constant as shown by eq (6). The variation of the jacket water temperature with time is taken into account by the second β on the right hand side of eq (5a) independent of whether $f(\beta)$ is or is not zero.

The correction, $\delta\Delta T_c$, to be added to the corrected temperature rise calculated according to eq (3) to yield the corrected temperature rise when eqs (4) and (6) are inserted into eq (3) was carried out by calculating p_0 and k_0 of eqs (5) from k and T_∞ derived from a fit of the drift data using eq (2). he parameter $f(\beta)$ was approximated by setting $a_1=0$ and increasing a_0 equal to 0.067 because this provides an upper bound to $f(\beta)$ for all the data obtained in the Newton's cooling law test and simplifies the calculation of the correction. Refitting the drift period data with eqs (5) is not necessary because the value of k, about 3×10^{-4} min^{-1}, is sufficiently small that the fit of the integral form of eq (2) to the experimental drift data amounts to a straight line fit of the temperature as a function of time in each drift period. The expression for $\delta\Delta T_c$ can be derived by a straightforward extension of the arguments used to derive eqs e7–e11 of reference [13].

A summary of the results of the corrections to the corrected temperature rise for six experiments is given in table 5 for two calibration experiments and for four "unknown" experiments (two for each type of MSW sample, unprocessed and processed). The second through fourth columns of table 5 list the corrected temperature rise of the calorimeter, the observed temperture rise of the calorimeter, and the corresponding observed change in temperature of the jacket water between t_i and t_f, respectively. The fifth and sixth columns list the contribution to $\delta\Delta T_c$ due to the change in jacket water temperature, and to the variation of the cooling constant with temperature. The next to last column is the total $\delta\Delta T_c$ and the last column is $\delta\Delta T_c$ expressed as a percent of ΔT_c. It can be seen that the total correction to ΔT_c is +0.04% or less and the net correction for "unknown" experiments is expected on the average to be less than 0.02%. Thus, the net correction is small in comparison to 0.1%.

Apart from the change in jacket water temperature with time and the change in cooling constant with β, the drift period data of the experiments are remarkably normal. For example, during the drift periods, the thermocouples indicate that compo-

Table 5. Correction for change in jacket temperature and cooling constant.

Experiment	ΔT_c(a)	ΔT_1(b)	ΔT_2(c)	$\delta\Delta T_c$(d)			$(\delta\Delta T_c/\Delta T_c)$
				Jacket Water(e)	Cooling Constant(f)	Total	
Sample No.	°C	°C	°C	°C	°C	°C	%
Cellulose (35)	8.9142	8.5746	0.1872	0.0050	+0.0081	+0.0031	+0.035
Cellulose (36)	9.4261	9.0560	0.1832	−0.0049	+0.0086	+0.0037	+0.039
Processed MSW (E'9)	9.2217	8.8160	0.2379	−0.0065	+0.0064	−0.0001	−0.001
Processed MSW (E6)	6.8905	6.6412	0.1556	−0.0039	+0.0058	+0.0019	+0.028
Unprocessed MSW (A4)	9.6576	9.2598	0.1994	−0.0059	+0.0084	+0.0025	+0.026
Unprocessed MSW (B2)	7.1685	6.9262	0.1235	−0.0032	+0.0060	+0.0028	+0.040

(a) Corrected temperature rise according to eq (3).

(b) Observed temperature rise, calorimeter water.

(c) Observed change in temperature of the jacket water.

(d) Correction to be added to ΔT_c for change in jacket water temperature and temperature dependence of the cooling constant.

(e) Contribution to $\delta\Delta T_c$ due to change in jacket water temperature.

(f) Contribution to $\delta\Delta T_c$ due to temperature dependence of cooling constant.

nents of the combustor and the various parts of the calorimeter and liquid shell are isothermal to between 0.1 and 0.03 °C. This is true even when β is about 9.5 °C and in spite of the enormous size of the calorimeter. (Even during the main period, the maximum temperature difference in the liquid shell near the top and bottom of the water flow shield is only 0.25 °C.) The exponential decay of the calorimeter temperature in the approach to the final drift period is normal in the sense that the decay time constant, 15 minutes, is a small multiple of the water circulation time of 5.4 minutes.

5.3 Uncertainty Estimates

Estimates of the systematic errors in the experiments are given in table 6. The first column contains the symbol in eq (1) associated with the source of the error. The second column lists the type of uncertainty. The values given in the third column are the net effect of the estimated systematic error on $-\Delta\bar{H}_{st}$ for dry MSW samples. Unless stated otherwise, the errors are the same for processed and unprocessed MSW samples.

The error estimate given in the first row is the overall error cited in section 5.1.5. The error given in the second row is the average calculated from table 5 for processed MSW. The corresponding value for unprocessed MSW is 0.00%.

The value of the error given in the third row is the uncertainty associated with the assumption that the residual moisture in the kilogram-size flow calorimeter samples of processed MSW and cellulose is the same as in the gram-size test samples. Moisture content determinations were only made on the gram-size test samples which were taken from each parent and stored in moisture proof containers. The moisture was determined by ASTM method E790-81, which involves weighing the test samples and then drying the samples in loose form at 105 °C for an hour in a mechanical convection oven. Samples were weighed after they cooled in a desiccator. The moisture content of each parent sample was corrected for any weight change between the time of its riffling and the time the parent was pelleted and combusted.

Table 6. Estimates of systematic error.

	Source of Error	Percent Effect on
Quantity	Type of Uncertainty	$-\bar{H}_{st}$ of MSW
1. E	Nonequivalent sources	±0.05
2. ΔT_c	Change in jacket water temperature and Temperature dependence of the cooling constant (see $\delta\Delta T_c$).	$-0.02^{(a)}$
3. M	Moisture same in processed MSW parent and gram-size test samples or Moisture same in unprocessed MSW and gram-size test samples.	±0.20
4. ΔH_v	Oxygen flow rate.	±0.03
5. ΔH_g	Oxygen flow rate.	±0.00
6. ΔH_{ic}	Oxygen flow rate, effect on measurement of CO (g).	±0.01
7. ΔH_v	Input and output gas moler flow rates equal.	0.002
8. ΔH_{ic}	Input and output gas molar flow rates equal, effect on measurements of CO(g)	−0.001
9. ΔH_{ic}	Carbon in ash is cellulose rather than free carbon.	$0.01^{(b)}$
10. M	Dispersion of sample in combustion zone.	±0.05
11. ΔH_x	Kinetic energy loss and Joule-Thompson cooling.	−0.000
12.	Heat of wetting:	
	Effect on gram minus kilogram samples of processed MSW	$-0.000^{(c)}$
	Effect on unprocessed minus processed kilogram samples	$-0.002^{(c)}$
	Total Systematic Error	±0.37

(a) applies to processed MSW, value for unprocessed is 0.00%.
(b) applies to processed MSW, value for unprocessed is 0.02%.
(c) error in appropriate average difference in calorific value, expressed as % of average processed calorific value.

For unprocessed MSW samples, the error in the third row is the uncertainty associated with the assumption that the moisture is equivalent to that which would have been obtained had the sample been processed and its moisture content determined with a gram-size test sample. The moisture content of each increment of unprocessed MSW was determined by drying the entire increment in loose form in a large open pan for 12 hours at 105 °C in a large, mechanical convection oven. The sample was weighed after it had cooled (about one hour later). Then, a known mass of water was added to the sample to return the moisture content to about 3 to 4%, the sample was pelleted, weighed, and burned. The water added after drying improves the cohesion of the pellet. The error estimate is believed to take into account moisture pick-up during the cooling of the increment (studied in an auxiliary experiment) as well as other possible errors due to differences between this procedure and that employed for the gram-size test samples.

It should be noted that the "moisture" error in the third row does not involve questions about absolute moisture content. Only errors associated with differences in moisture content are pertinent to the results (see end of section 2). Further, vaporization of different amounts of moisture initially present in a sample during different combustion runs contributes no error since the dew point of the gases leaving the calorimeter is continuously monitored.

The error values given in the fourth through sixth rows are due to the estimated uncertainty in the total oxygen flow rate which is estimated to be, at most, 5%. This estimate is believed to take into account that the total flow rate is the sum of the measured flow rates through six flow meters as well as assumptions about the nonlinearity of some of the uncalibrated flow meters.

The error values given in the seventh and eighth rows are associated with the error in the assumption that the total input oxygen and output product gas flow rates are equal. The correct product gas flow rate was calculated from the sum of the input oxygen flow rate, the flow rate of water vapor in the product gas (based on the measured water concentration), and the correction for the moles of oxygen consumed in the production of water. The latter correction was estimated from the measured CO_2 concentration in the product gas and the stoichiometric coefficients of the standard combustion reaction using an empirical formula for MSW. The error is very small because the combustible fraction of the MSW is such that the amount of oxygen consumed to oxidize hydrogen to water is small and most of the water produced in the reaction remains trapped in the collector.

The error value given in the ninth row is the effect of treating the carbon component of the ash as cellulose rather than elemental carbon. In the 10th row, we list the error associated with the amount of sample (about 1 g) that may be dispersed by the flowing gas prior to ignition and does not get burned after the reaction starts.

The error in the 11th row is that associated with the assumption that ΔH_x of eq (1) is zero. The magnitude of the contribution to ΔH_x by the expansion cooling (i.e., Joule-Thompson cooling) of the inlet oxygen was estimated from the calculated mean pressure drop of the inlet oxygen (0.34 atm) to be 34 $\text{J/min} \times \Delta t$ where Δt is the time during which the inlet oxygen flow rate is 270 L/min. The kinetic energy loss contribution to ΔH_x is estimated to be -31 $\text{J/min} \times \Delta t$. The net effect on $-\Delta \bar{H}_{st}$ is 0.000%.

The error in the 12th row is that associated with the heat of wetting of the samples. The mean difference in the moisture content of the gram-size test samples and the same parent processed MSW samples is 0.00%. The mean difference in the moisture contents of the unprocessed MSW minus that of the corresponding "identical" processed increments is -0.07%. Using the data analysis given in reference [19] and assuming the combustible components are given cellulose the -0.07% moisture difference, for example, corresponds to an estimated systematic error of -0.002% to be added to the average difference of -0.5% (see section 2).

The overall systematic error given at the bottom of the table is calculated by adding the individual errors algebraically. No error is given for degradation association with preparation (milling) of the processed MSW samples from the unprocessed MSW samples since the purpose of one of the sets of the experiments was to determine this change. The results as cited in section 2 indicate the error is of the order -0.5% of $-\Delta \bar{H}_{st}$.

The standard deviation of a single calibration experiment is 0.2% of the average energy equivalent. It is worth noting that this % *CV* is not primarily due to the variation in the amount of water added to the calorimeter. Separate tests of the filling technique were carried out using a load cell to intercompare the mass of the calorimeter vessel filled with water with a 6000 kg tare mass. The % *CV* of the ratio of the mass of the tare divided by the mass of the full (water) calorimeter vessel was 0.01%.

The standard deviation of a single measurement of $\Delta \bar{H}_{st}$ for MSW samples is 0.4% of $\Delta \bar{H}_{st}$. Thus, the overall uncertainty in a single measurement of $\Delta \bar{H}_{st}$ is $\pm 0.8\%$, which is the sum of the standard deviation of $\pm 0.4\%$ and the systematic error of $\pm 0.37\%$.

6. Conclusions

1) A calorimeter capable of determining the enthalpy of combustion of kilogram-size samples of MSW has been successfully constructed and operated. The number of experiments carried out to date (April 1986) is approximately 60.

2) Samples have been successfully burned in flowing oxygen near atmospheric pressure. Combustion of the organic portion of the MSW to CO_2 and H_2O is complete, in terms of the enthalpy of

combustion, to 99.9+% even when the initial mass contains 35 mass % of noncombustible components in intimate contact with the combustible components. In the absence of these noncombustible components, oxidation is complete to 99.99%.

3) The above degree of completeness of oxidation is accomplished in spite of the fact that the sample is burned as a single, multi-kilogram pellet rather than in loose form. Combustion of the material in pellet form has the major advantage of simplifying the quantitative collection of ash and also restricts the reaction zone to a smaller volume.

4) The % *CV* for calibration experiments is 0.2% and for measurements of $-\Delta\bar{H}_{\rm st}$ of "unknown" MSW samples is 0.4%.

5) Because of cost and time considerations, we departed from a number of design and operation dictums for stirred-water calorimeters with a constant-temperature jacket. Because of manufacturing considerations, the calorimeter design did not exclude heat transfer by free convection with the surrounding jacket. The calorimeter was operated at a temperature above its jacket temperature to reduce the duration of an experiment. The jacket water temperature was allowed to drift about 0.2 °C. An error analysis shows that the effect of all these departures is each less the 0.1%.

6) The overall uncertainty of a single calorimetric result is judged to have an absolute value of less than 1% by virtue of the calorimeter having been designed and operated so that the cumulative contribution of the individual possible sources of systematic error is of the order of ±0.4%.

Technical support for this project was provided by members of the ASME Research Committee on Industrial and Municipal Wastes, the ASME Performance Test Code Committee (PTC-33) on Large Incinerators, and the ASTM Committee (E-38) on Resource Recovery and its Subcommittee E-38.01 on Energy. These committees helped to identify this work as an important industrial research need.

We acknowledge the contributions of the following members of the Chemical Thermodynamics Division of the Center for Chemical Physics: J. C. Colbert performed the bomb calorimetry measurements, T. J. Buckley assisted in the data reduction computations, and S. S. Bruce assisted in the execution of the experiments. R. C. Paule of the NBS National Measurement Laboratory provided statistical consultation.

7. References and Notes

[1] Kirklin, D. R.; J. C. Colbert, P. H. Decker, A. E. Ledford, Jr., R. V. Ryan, and E. S. Domalski, The variability of municipal solid waste and its relationship to the determination of the calorific value of refuse-derived fuels, Resources and Conservation **9**, 281 (1982); see also Part A of NBSIR 82-2491, U.S. Natl. Bur. Stand., Washington, DC (1982).

[2] Reilly, M. L.; K. L. Churney, D. R. Kirklin, A. E. Ledford, and E. S. Domalski, An oxygen flow calorimeter for kilogram-size samples of municipal solid waste, Part I. A 25 gram capacity combustion flow calorimeter for determining the calorific value of refuse-derived fuels, Resources and Conservation **8**, 147 (1982).

[3] Domalski, E. S.; K. L. Churney, M. L. Reilly, D. R. Kirklin, A. E. Ledford, and D. D. Thorton, 25 gram capacity combustion flow calorimeter, NBSIR 84-2457, U.S. Natl. Bur. Stand., Washington, DC (1982).

[4] Ledford, A. E.; R. V. Ryan, M. L. Reilly, E. S. Domalski, and K. L. Churney, An oxygen flow calorimeter for kilogram-size samples of municipal solid waste. Part II. Trial combustions of kilogram-size samples of municipal solid waste, Resources and Conservation **8**, 159 (1982).

[5] Churney, K. L.; E. S. Domalski, A. E. Ledford, J. C. Colbet, S. S. Bruce, T. J. Buckley, R. C. Paule, and M. L. Reilly, Assessing the credibility of the calorific value of municipal solid waste, NBSIR 84-2825 (DoE), U.S. Natl. Bur. Stand., Washington, DC (1984).

[6] Prosen, E. J.; F. W. Maron and F. D. Rossini, Heat of isomerization of the two butadienes, J. Res. Natl. Bur. Stand. **42**, 269 (1949).

[7] Sunner, S., Basic principles in combustion calorimetry, Chap. 2 in *Combustion Calorimetry*, Experimental Chemical Thermodynamics, Volume 1, S. Sunner and M. Manson, editors, Pergamon Press: Oxford (1979).

[8] Goldberg, R. N.; R. L. Nuttall, E. J. Prosen, and A. P. Brunetti, Digital data acquisition and computer computation applied to calorimetric experiments, Natl. Bur. Stand. (U.S.) Report 10-437, June 1971. See Program TEMPQTZ. See also Steckler, D. K.; R. N. Goldberg, R. B. Tewari, and T. J. Buckley, Computer software for the acquisition and treatment of calorimetric data, NBS Technical Note 1224, U.S. Natl. Bur. Stand., Washington, DC (1986).

[9] Vanderzee, C. E., Reduction of results to the isothermal calorimetric process and to the standard-state process in solution-reaction calorimetry, J. Chem. Thermodynamics **13**, 947 (1981); Evaluation of corrections from temperature-time curves in isoperibol calorimetry under normal and adverse operating conditions, ibid. **13**, 1139 (1981).

[10] Equations (9a) and (9b) and the enthalpy change of reaction (6) of reference [3] are in error. The correct expressions are:

$$Z(\text{soln},\ T_i)=(N_7+N_3^i-N_3^f)\,\text{H}_2\text{O}(g,T_i)+ [Z-(N_7+N_3^i-N_3^f)\,\text{H}_2\text{O}]\,(\text{soln},\ T);\quad p=1\ \text{atm}. \tag{9a}$$

$$Z=N_9\text{HCl}+N_{10}\text{H}_2\text{O}\,. \tag{9b}$$

ΔH for eq (6) when $N_4=1$ is -282.98 kJ/mol.

It should be noted that this work, $\Delta H_{\rm g}$ was calculated as the time integral of the expression $\dot{N}_{\rm in}\,C_2\,(T_1-T_2)$ where $\dot{N}_{\rm in}$ is N_1+N_2 of reference [3], $\dot{N}_{\rm in}$ is the total molar input oxygen flow rate, C_2 is the heat capacity of oxygen, and T_2 is the jacket water temperature. This differs by less thn 2% from ΔH_g given by eqs (8) of reference [3], as determined from the results of the calculations for entry 7 of table 6. It should also be noted that in the present work both $N_{10} - N_7$ as well as N_7 are measured in each experiment and no gas flow is permitted during the final drift period (see p. 23, reference [3]).

[11] Mandel, J., and R. C. Paule, Interlaboratory evaluation of a material with unequal numbers of replicates, Analytical Chemistry **42**, 1194 (1970) and Correction, Analytical Chemistry **43**, 1287 (1971).

[12] Mandel, J., and R. C. Paule, Statistical analysis of sampling and measurement errors in the characterization of refuse-derived fuel, Proceedings of the Second International Conference on Materials and Energy from Refuse, Antwerp, Belgium, p. 6.25 (1981).

[13] Mosselman, C., and K. L. Churney, Calibration of combustion calorimeters, Chap. 3 in *Combustion Calorimetry*, Experimental Chemical Thermodynamics, Volume 1, S. Sunner and M. Mansson, editors, Pergamon Press: Oxford (1979).

[14] Coops, J., and K. Van Nes, Researches on heat of combustion II. Internal lag and method of stirring in isothermally jacketed calorimeters, Rec. Trav. Chim. **66**, 131 (1947).

[15] Churney, K. L.; E. D. West, and G. T. Armstrong, A cell model for isoperibol calorimeters, NBSIR 73-184, U.S. Natl. Bur. Stand. (1973).

[16] Pilcher, G. Oxygen flame calorimetry, Chap. 14 in *Combustion Calorimetry*, Experimental Chemical Thermodynamics, Volume 1, S. Sunner and M. Mansson, editors, Pergamon Press: Oxford (1979).

[17] Ginnings, D. C., and E. D. West, Principles of calorimetric design, Chap. 4 in *Experimental Thermodynamics*, Volume 1, Calorimetry of Non-Reacting Systems, J. P. McCullough and D. W. Scott, editors, Plenum Press: New York (1968).

[18] Churney, K. L., and G. T. Armstrong, Studies in bomb calorimetry. A new determination of the energy of combustion of benzoic acid in terms of electrical units. J. Res. Natl. Bur. Stand. **72A**, 453 (1968).

[19] Colbert, J. C.; He Xiheng and D. R. Kirklin, Enthalpy of combustion of microcrystalline cellulose, J. Res. Natl. Bur. Stand. **86**, 665 (1981).

Journal of Research of the National Bureau of Standards

Possible Changes in the U.S. Legal Units Of Voltage and Resistance

Volume 91 Number 5 September–October 1986

B. N. Taylor

National Bureau of Standards
Gaithersburg, MD 20899

The Consultative Committee on Electricity of the International Committee on Weights and Measures is considering adopting sometime in the future 1) a new value for the Josephson frequency-voltage ratio $2e/h$ (e is the elementary charge and h is the Planck constant) and 2) a value for the quantized Hall resistance $R_H \equiv h/e^2$. Both values are to be chosen as consistent with their International System of Units (SI) values as possible and would be used by every national standards laboratory which employs the Josephson and quantum Hall effects to define and maintain their national or legal units of voltage and resistance. Based on current knowledge, this would lead to an increase in the U.S. Legal Volt of about nine parts-per-million (ppm) and an increase in the U.S. Legal Ohm of about 1.5 ppm. Comparable changes would be required in the voltage and resistance units of most other national, governmental, and industrial standards laboratories throughout the world. Many high-precision instruments would also have to be readjusted to make them consistent with the new units. It is the purpose of this paper to review in some detail the basis for these proposed and potentially significant changes.

Key words: electrical units; Josephson effect; ohm; quantum Hall effect; volt.

Accepted: July 31, 1986

1. Introduction

The dominant system of units used throughout the world to express the results of physical measurements is *Le Système International d'Unités* or International System of Units, abbreviated SI. The seven *base* units of the SI from which all other units are *derived* are the meter (m), kilogram (kg), second (s), ampere (A), kelvin (K), mole (mol), and candela (cd) [1][1]. These are, respectively, the unit of length, mass, time, current, temperature, amount of substance, and luminous intensity.

About the Author: B. N. Taylor is a physicist and Chief of the Electricity Division. The division is within the NBS National Measurement Laboratory.

The SI electrical units most commonly used in practice are those of potential difference (or electromotive force) and resistance; the volt (V) and ohm (Ω). These two units are derived from the three SI base mechanical units (m, kg, s) and the SI base electrical unit (A), the specific relationships being

$$1\ \mathrm{V} = 1\ \mathrm{m}^2 \cdot \mathrm{kg} \cdot \mathrm{s}^{-3} \cdot \mathrm{A}^{-1} \qquad (1)$$

$$1\ \Omega = 1\ \mathrm{m}^2 \cdot \mathrm{kg} \cdot \mathrm{s}^{-3} \cdot \mathrm{A}^{-2} \qquad (2)$$

Because the SI definitions of the volt and ohm embodied in eqs (1) and (2) are extremely difficult to realize with high accuracy, national standards laboratories such as NBS have historically used practical representations of them to serve as the

---

[1] Numbers in brackets indicate literature references.

national or legal electrical units. For example, the mean emf of a particular group of electrochemical standard cells of the Weston type (each with an emf of order 1.018 V) has traditionally been used to define a laboratory or as-maintained national unit of voltage V_{LAB}, and the mean resistance of a particular group of precision wire-wound resistors of the Thomas or similar type (each with a resistance of order 1 Ω) has similarly been used to define a laboratory or as-maintained national unit of resistance Ω_{LAB}. The national unit of current A_{LAB} is then defined in terms of V_{LAB} and the Ω_{LAB} by means of Ohm's law, $A_{LAB}=V_{LAB}/\Omega_{LAB}$, and does not require its own separate representation.

A laboratory or as-maintained national system of practical electrical units immediately raises two questions: 1. How does one ensure that V_{LAB} and Ω_{LAB} are *constant in time* when they are based on artifacts? 2. How does one ensure that V_{LAB} and Ω_{LAB} are *consistent with their SI definitions*? Problem 1 leads to the idea of monitoring or *maintaining* laboratory units while Problem 2 to the idea of carrying out *absolute realizations* of the SI electrical units. Ideally one would like to solve both problems simultaneously, that is, to maintain a laboratory unit constant in time and consistent with its SI definition by the same means and at the same time, and at a level of accuracy which is in keeping with the inherent stability of the artifacts used to define it. However, because this stability is at the level of parts in 10^7 per year (or for some very well aged cells and resistors at the level of parts in 10^8 per year), it has not yet proved feasible to do so in most laboratories.

It is important to recognize that Problems 1 and 2 *both* require solution. If the various national units of voltage and resistance (and hence current) *vary with time*, it will be difficult to make reproducible and consistent electrical measurements within a particular country as well as between different contries. If the units are *inconsistent with their SI definitions*, electrical and mechanical measurements of force, energy, and power will not yield the same results. While there are no practical situations at present where measurement accuracy is high enough to make visible the known inconsistencies between the SI mechanical and as-maintained electrical units, it is inevitable that such situations will arise as science and technology advance. Moreover, if all national units are consistent with the SI they will be consistent with each other. This will help ensure that electrical measurements made throughout the world are compatible.

2. Maintaining Laboratory Units

2.1 Josephson Effect

The national standards laboratories of most major industrialized countries now use the Josephson effect [2] to define their unit of voltage and maintain it constant in time. A low-temperature, solid-state physics phenomenon, the Josephson effect occurs when two superconductors separated by 1–2 nm (achievable with an oxide layer) are cooled below their transition temperatures. If such a Josephson junction is exposed to microwave radiation of frequency f, current steps appear in its current-voltage curve at discrete or quantized values of voltage. The voltage V_n of the nth step and the frequency f are related by $2eV_n=nhf$ where e is the elementary charge and h is the Planck constant. A Josephson junction can thus be viewed as a perfect frequency-to-voltage converter with the constant of proportionality being the invariant fundamental constant ratio $2e/h$. Numerically, $2e/h\approx 484$ MHz/μV. Hence, the spacing between steps for applied radiation of 10 GHz, a commonly used frequency, is ≈20 μV. The amplitude of the current steps decreases with increasing n and there are practical limitations on the minimum useable size of a current step due to electrical noise. The maximum step number n is thus usually restricted to ≈250 for a single Josephson junction, corresponding to a maximum junction voltage of ≈5 mV. Because frequencies can be readily measured to very high accuracy, the Josephson effect can be used to define and maintain V_{LAB} to an accuracy limited only by the uncertainty with which the voltage across the Josephson device can be compared with the 1.018-V emf of a standard cell. Typically this is in the range 0.01 to 0.1 parts-per-million or ppm. (Throughout this paper all uncertainties are meant to correspond to one standard deviation estimates.) The standard cell now serves only as a "flywheel," that is, as a means of preserving or storing V_{LAB} between Josephson effect measurements.

The defining equation for V_{LAB} based on the Josephson effect is

$$(2e/h)_{LAB}=483597\ \text{GHz}/V_{LAB} \quad , \tag{3}$$

where $(2e/h)_{LAB}$ is the specific value of $2e/h$ adopted by the laboratory to define V_{LAB}. The question mark is meant to indicate that several different values are in use at the various national laboratories. For example, since 1 July 1972 NBS has defined V_{NBS} and maintained it constant in time with an uncertainty of 0.031 ppm using the value [3]

$$(2e/h)_{\mathrm{NBS}} \equiv 483593.420\ \mathrm{GHz/V_{NBS}} \quad . \tag{4}$$

This particular number was chosen in order not to introduce a discontinuity in the U.S. Legal Volt when on this date NBS officially converted from standard cells to the Josephson effect as the basis for V_{NBS}. In contrast, a large number of national laboratories, including the National Research Council (NRC), Canada, the National Physical Laboratory (NPL), U.K., the Physikalisch-Technische Bundesanstalt (PTB), Federal Republic of Germany, and the Electrotechnical Laboratory (ETL), Japan, as well as the International Bureau of Weights and Measures (BIPM), use

$$(2e/h)_{\mathrm{LAB}} \equiv 483594.000\ \mathrm{GHz/V_{LAB}} \quad , \tag{5}$$

a value recommended in October 1972 by the Consultatative Committee on Electricity (CCE) of the International Committee on Weights and Measures (CIPM) [4]. This means that the unit of voltage of these countries and of the BIPM is 1.20 ppm larger than that of the U.S.

The CCE value of $2e/h$ was chosen to be consistent with the unit of voltage of the BIPM as it existed on 1 January 1969 based on a group of standard cells. Acting upon a 1968 CCE recommendation, on this same date BIPM decreased its unit of voltage by 11.0 ppm to bring it into agreement with the SI unit [5]. Thus the CCE value of $2e/h$ was intended to be consistent with the SI. The 11 ppm decrease recommended by the CCE was initially obtained from the results of NBS and NPL current-balance absolute realizations of the SI ampere with the help of a number of calculable inductor and capacitor absolute realizations of the SI ohm [6]. (It was later supported by results from certain fundamental constant determinations [7,8].) Most national laboratories also lowered their voltage unit on 1 January 1969 [8], the size of the decrease being determined by the difference between V_{LAB} and V_{BIPM} obtained in the 1967 triennial international comparison of national units of voltage carried out under CCE auspices at the BIPM by transporting standard cells [7]. For example, on 1 January 1969 the NBS unit was reduced by 8.4 ppm since in 1967 V_{NBS}-V_{BIPM} was found to be -2.6 ppm.

Two other values of $2e/h$ are also in use: the Central Laboratory of the Electrical Industries (LCIE), France, employs [9]

$$(2e/h)_{\mathrm{LCIE}} \equiv 483594.64\ \mathrm{GHz/V_{LCIE}} \tag{6}$$

while the All-Union Scientific Research Institute of Metrology (or Mendeleyev Institute of Metrology, IMM), U.S.S.R., uses [10]

$$(2e/h)_{\mathrm{IMM}} \equiv 483596.176\ \mathrm{GHz/V_{IMM}} \quad . \tag{7}$$

The French and U.S.S.R. units are thus 2.52 and 5.70 ppm larger than the U.S. unit, respectively. The French value of $2e/h$ was chosen for the same reason as was the U.S. value, that is, to prevent a discontinuity in the French volt when converting from standard cells to the Josephson effect as the basis for V_{LCIE}. The U.S.S.R value was selected in the late 1970's to make V_{IMM} more consistent with the SI unit and stems from an IMM analysis of certain fundamental constant determinations (to be touched upon later).

2.2 Quantum Hall Effect

The quantum Hall effect (QHE) promises to do for resistance-unit definition and maintenance what the Josephson effect has done for voltage-unit definition and maintenance [11]. Like the Josephson effect the QHE is a low-temperature, solid-state physics phenomenon. However, the materials involved are semiconductors rather than superconductors. The QHE is characteristic of a two-dimensional electron gas (2DEG) realized, for example, in classic Hall-bar geometry, high-mobility semiconductor devices such as silicon MOSFETs and GaAs-$\mathrm{Al_xGa_{1-x}As}$ heterostructures when in an applied perpendicular magnetic field of order 10 T and cooled to a few kelvin. Under these conditions the 2DEG is completely quantized and there are regions in the curve of Hall voltage vs. gate voltage for a MOSFET, or Hall voltage vs. magnetic field for a heterostructure, where the Hall voltage remains constant as the gate voltage or magnetic field is varied. On these so-called Hall plateaus the Hall resistance $R_{\mathrm{H}}(\mathrm{i})$, defined as the ratio of the Hall voltage of the ith plateau $V_{\mathrm{H}}(\mathrm{i})$ to the current I through the device, $R_{\mathrm{H}}(\mathrm{i}) = V_{\mathrm{H}}(\mathrm{i})/I$, is quantized and given by $R_{\mathrm{H}}(\mathrm{i}) = h/(e^2\mathrm{i})$ with the quantum integer i equal to the plateau number. Numerically, $h/e^2 \approx 25812.8\ \Omega$ and hence the resistance of the readily obtainable $\mathrm{i}=4$ plateau is $\approx 6453.2\ \Omega$. A QHE device can thus be viewed as a resistor whose resistance depends only on the fundamental-constant ratio h/e^2. As such it can be used to define and maintain Ω_{LAB} to an accuracy limited only by the uncertainty with which the resistance of the device (when on a plateau) can be compared with the 1-Ω resistance of a standard resistor. Eventually this is expected to be in the range 0.01 to 0.1 ppm for all laboratories; 0.022 ppm is the smallest uncertainty reported to date [12]. In analogy with the standard cell and the Josephson effect, the standard resistor would serve only to store Ω_{LAB} between QHE measurements.

The defining equation for Ω_{LAB} based on the quantum Hall effect may be written as

$$(h/e^2)_{\mathrm{LAB}} \equiv 25812.8?\ \Omega_{\mathrm{LAB}} \quad , \tag{8}$$

where in analogy with eq (3) $(h/e^2)_{\mathrm{LAB}}$ is the specific value of h/e^2 adopted by the laboratory to define Ω_{LAB}. (In this case the question mark means that a specific value has yet to be adopted by any laboratory.) The combination of constants h/e^2 has been termed the quantized Hall resistance R_{H}. It is related to the inverse of the fine-structure constant α, the dimensionless coupling constant or fundamental expansion parameter of quantum electrodynamic theory (QED), by

$$h/e^2 \equiv R_{\mathrm{H}} = \mu_0 c \alpha^{-1}/2 \quad . \tag{9}$$

Here μ_0 is the magnetic permeability of vacuum and exactly equal to $4\pi \times 10^{-7}$ N/A^2. (Note that 1 N$=$1 m $\cdot$ kg $\cdot$ s^{-2} and that in the SI the ampere is related to the meter, kilogram, and second in such a way that μ_0 is an exact constant). The quantity c is the speed of light in vacuum and as a result of the recent redefinition of the meter [13] is an exact constant given by $c \equiv 299792458$ m $\cdot$ s^{-1}. Since both μ_0 and c are defined constants, if α^{-1} is known from some other experiment with a given uncertainty, R_{H} will be known with the same uncertainty.

All of the major national standards laboratories as well as the BIPM are currently putting into place the apparatus necessary to define and maintain their unit of resistance using the QHE. However, as of this writing no laboratory has officially converted to the QHE; most national units of resistance are still based on the generally time-dependent, mean resistance of a particular group of wire-wound resistors. For example, in the U.S. Ω_{NBS} is still defined in terms of the mean resistance of five specific Thomas one-ohm resistors and, as will be noted later, is decreasing relative to the SI unit by about 0.06 ppm per year [14,15]. Since the drift of the unit of resistance of a number of other countries and of the BIPM is comparable [15], in analogy with the present state of the various national units of voltage brought about by the Josephson effect, implementation of the QHE will at the very least lead to the various national units of resistance remaining constant relative to the SI unit and one another, and to their differences always being well known.

3. Absolute Realizations

While the Josephson and quantum Hall effects allow $\mathrm{V_{LAB}}$ and Ω_{LAB} to be maintained constant in time with an uncertainty between 0.01 and 0.1 ppm, thereby solving Problem 1 above, unless $2e/h$ and R_{H} are known in SI units to the same level of accuracy, the as-maintained and SI systems of electrical units will not be consistent and Problem 2 above will remain unsolved. In practice there are two general approaches to determining $2e/h$ and R_{H} in SI units. The first is to carry out experiments to realize *directly* the SI definitions of V, Ω, and A or equivalently, experiments which use electromagnetic theory in combination with the SI definitions; the second is to carry out experiments to determine various fundamental constants from which V, Ω, and A may be *indirectly* derived. As it will shortly be shown, the latter approach can yield uncertainties comparable with or smaller than those of the former.

3.1 Direct Determinations

The following is a brief summary of some of the ways the SI volt, ohm, and ampere are being directly realized at present [16].

Volt. By measuring the force between electrodes to which a voltage known in terms of $\mathrm{V_{LAB}}$ has been applied, and the capacitance between the electrodes (determined in SI units via a calculable cross capacitor as discussed below), the ratio $\mathrm{V_{LAB}/V}$ can be obtained. In practice, determining this ratio is what is meant by the terms "absolute realization of the volt" or "realization of the SI volt." Defining $(\mathrm{K_V})_{\mathrm{LAB}} \equiv \mathrm{V_{LAB}/V}$ and recognizing that $(2e/h)_{\mathrm{LAB}}$ is used to define $\mathrm{V_{LAB}}$, we may write

$$(\mathrm{K_V})_{\mathrm{LAB}} \equiv \mathrm{V_{LAB}/V} = (2e/h)_{\mathrm{LAB}}/(2e/h) \ . \tag{10}$$

A realization of the SI volt is thus equivalent to determining $2e/h$ in SI units [recall that $(2e/h)_{\mathrm{LAB}}$ is an adopted number with no uncertainty]. The smallest uncertainty reported to date for the direct realization of the SI volt is about 0.3 ppm [17], at least an order of magnitude larger than the uncertainty with which $\mathrm{V_{LAB}}$ may be maintained via the Josephson effect.

Ohm. The SI ohm may be realized using a so-called Thompson-Lampard calculable cross capacitor [16] which allows the capacitance of a special configuration of electrodes to be calculated (in SI units) to very high accuracy from a single length measurement and the permittivity of vacuum ϵ_0. (Since $\epsilon_0=1/\mu_0 c^2$ and μ_0 and c are exactly known constants, ϵ_0 is also exactly known.) The impedance of the calculable capacitor is compared with the resistance of the one-ohm standards which represent Ω_{LAB} using a complex series of bridges. Defining $(\mathrm{K}_\Omega)_{\mathrm{LAB}}\equiv\Omega_{\mathrm{LAB}}/\Omega$ and assuming $(R_{\mathrm{H}})_{\mathrm{LAB}}$ is used to define Ω_{LAB}, we may write

$$(\mathrm{K}_\Omega)_{\mathrm{LAB}}\equiv\Omega_{\mathrm{LAB}}/\Omega=R_{\mathrm{H}}/(R_{\mathrm{H}})_{\mathrm{LAB}}\ . \qquad (11)$$

A realization of the SI ohm is thus equivalent to determining R_{H} in SI units, which in turn is equivalent to determining the inverse fine-structure constant [see eq (9)]. The uncertainty of such an experiment is on the order of 0.03 to 0.1 ppm, comparable to the yearly stability of good resistance standards and the accuracy with which Ω_{LAB} may be currently maintained via R_{H}. However, because of the complexity of the experiment only one laboratory in the world has yet been able to maintain its unit of resistance consistently via the calculable capacitor. It would thus appear that the QHE will become the method of choice in most laboratories.

Ampere. By measuring the force between coils of known dimensions carrying a current known in terms of $\mathrm{A}_{\mathrm{LAB}}$, the ratio $\mathrm{A}_{\mathrm{LAB}}/\mathrm{A}$ can be determined. Defining $(\mathrm{K}_\mathrm{A})_{\mathrm{LAB}}\equiv\mathrm{A}_{\mathrm{LAB}}/\mathrm{A}$, we may write

$$(\mathrm{K}_\mathrm{A})_{\mathrm{LAB}}\equiv\mathrm{A}_{\mathrm{LAB}}/\mathrm{A}=(\mathrm{K}_\mathrm{V})_{\mathrm{LAB}}/(\mathrm{K}_\Omega)_{\mathrm{LAB}}\ . \qquad (12)$$

A realization of the SI ampere measures neither $2e/h$ or R_{H} but the product $(2e/h)R_{\mathrm{H}}$ [see eqs (10 and 11)], which is equivalent to measuring the elementary charge e in SI units. The smallest uncertainty claimed to date for such an experiment is 4 ppm [18], about two orders of magnitude larger than the uncertainty with which $\mathrm{A}_{\mathrm{LAB}}$ can be maintained via the Josephson and quantum Hall effects.

It should be noted from eq (12) that the determination of any pair of the three quantities $(\mathrm{K}_\mathrm{A})_{\mathrm{LAB}}$, $(\mathrm{K}_\mathrm{V})_{\mathrm{LAB}}$, and $(\mathrm{K}_\Omega)_{\mathrm{LAB}}$ is sufficient to yield a value for the third. Hence, accurate measurements of all three can provide a useful check of their consistency.

3.2 Indirect Determinations

As indicated above, $(\mathrm{K}_\mathrm{V})_{\mathrm{LAB}}$, $(\mathrm{K}_\Omega)_{\mathrm{LAB}}$, and $(\mathrm{K}_\mathrm{A})_{\mathrm{LAB}}$ may also be obtained from appropriate combinations of various fundamental physical constants. In addition to μ_0, c, $(2e/h)_{\mathrm{LAB}}$, and $(R_{\mathrm{H}})_{\mathrm{LAB}}$ discussed above, these include (with the smallest uncertainty currently achieved shown in parenthesis [15,19,20]), the Rydberg constant for infinite mass R_∞ (0.00055 ppm), the magnetic moment of the proton in $\mathrm{H_2O}$ in units of the Bohr magneton $\mu'_{\mathrm{p}}/\mu_{\mathrm{B}}$ (0.011 ppm), the molar mass of the proton M_{p} (0.012 ppm), the ratio of the proton mass to electron mass $m_{\mathrm{p}}/m_{\mathrm{e}}$ (0.020 ppm), the inverse fine-structure constant α^{-1} (0.038 ppm), the Faraday constant measured in laboratory electrical units F_{LAB} (1.3 ppm), the gyromagnetic ratio of the proton in $\mathrm{H_2O}$ measured by the low and high field methods in laboratory electrical units $\gamma'_{\mathrm{p}}(\mathrm{low})_{\mathrm{LAB}}$ and $\gamma'_{\mathrm{p}}(\mathrm{high})_{\mathrm{LAB}}$ (0.21 ppm and 1.0 ppm, respectively), and the Avogadro constant N_{A} (1.3 ppm).

It should be recognized that the electric-unit-dependent constants in the above group have not all been measured in the same national standards laboratory and thus in terms of the same set of national electrical units. It is possible, however, to re-express all such quantities in terms of a single set of laboratory units, for example, those of BIPM, with little loss in accuracy by using the known values of $(2e/h)_{\mathrm{LAB}}$ and the results of direct resistance-unit comparisons carried out by means of transportable resistance standards. [If the national laboratories carrying out the measurements had been using the quantum Hall effect to define and maintain their unit of resistance, the required resistance-unit differences could have been readily obtained from the known values of $(R_{\mathrm{H}})_{\mathrm{LAB}}$ adopted by the different national laboratories.]

As might be imagined, there are a number of different combinations of these constants which yield values of the three quantities $(\mathrm{K}_\mathrm{V})_{\mathrm{LAB}}$, $(\mathrm{K}_\Omega)_{\mathrm{LAB}}$, and $(\mathrm{K}_\mathrm{A})_{\mathrm{LAB}}$ [14,19,20]. For example, for the volt one has

$$(\mathrm{K}_\mathrm{V})^2_{\mathrm{BIPM}}=\frac{\mu_0 c^2 M_{\mathrm{p}}(2e/h)^2_{\mathrm{BIPM}}}{16R_\infty(m_{\mathrm{p}}/m_{\mathrm{e}})\alpha^{-1}N_{\mathrm{A}}}\ , \qquad (13)$$

where we have assumed all electric-unit-dependent quantities have been expressed in terms of the laboratory units of BIPM. Based on the uncertainties given above for the relevant constants entering eq (13), it yields an indirect value of $(\mathrm{K}_\mathrm{V})_{\mathrm{BIPM}}$ with an uncertainty of about 0.65 ppm, only about twice that of the most accurate direct SI volt realization reported to date [17]. [Equation (13) was used by the U.S.S.R. to derive the value of $(2e/h)_{\mathrm{IMM}}$ given in eq (7).]

For the ohm one may write

$$(\mathrm{K}_{\Omega})^{3}_{\mathrm{BIPM}}=\frac{\mu_0^2c^3(\mu_p'/\mu_B)(2e/h)_{\mathrm{BIPM}}}{16R_\infty(R_\mathrm{H})^2_{\mathrm{BIPM}}\gamma_p'(\mathrm{low})_{\mathrm{BIPM}}}\ , \qquad (14)$$

which yields an indirect value of $(\mathrm{K}_{\Omega})_{\mathrm{LAB}}$ with an uncertainty of about 0.07 ppm. This is comparable with the uncertainty of direct calculable capacitor determinations.

For the ampere one has

$$(\mathrm{K}_{\mathrm{A}})^{2}_{\mathrm{BIPM}}=\frac{M_p\gamma_p'(\mathrm{low})_{\mathrm{BIPM}}}{(m_p/m_e)(\mu_p'/\mu_B)\,F_{\mathrm{BIPM}}}\ , \qquad (15)$$

gives an indirect value of $(\mathrm{K}_{\mathrm{A}})_{\mathrm{BIPM}}$ with an uncertainty of about 0.7 ppm. This is significantly less than the uncertainty of present-day direct current balance determinations which is in the range 4 to 10 ppm [7,8,16,18,19], and only about twice as large as that obtained from the relatively new approach of equating electrical and mechanical work [21].

4. Prognosis

Based on all of the data currently available, including both direct and indirect realizations of the SI electrical units as outlined above, there is strong evidence (first pointed out nearly a decade ago [22]) that the value of the Josephson frequency-voltage ratio adopted by the CCE in 1972 is smaller than the SI value by about 8 ppm with an uncertainty of about 0.3 ppm [14,15,17,19,21]. This means that the laboratory unit of voltage maintained by the BIPM and all of the other national standards laboratories which use the 1972 CCE recommended value of $2e/h$ is smaller than the SI unit by this same amount. For France and the U.S.S.R. the corresponding figure is about 6.7 and 3.5 ppm, respectively. Since $(2e/h)_{\mathrm{CCE}}$ exceeds $(2e/h)_{\mathrm{NBS}}$ by 1.2 ppm, the SI volt exceeds the U.S. Legal Volt by about 9.2 ppm. Thus, to bring the U.S. unit into agreement with the SI unit would require that the U.S. unit be increased by this amount. The observant reader will notice that this would bring the U.S. unit essentially back to where it was (within 1 ppm) prior to its 8.4 ppm decrease on 1 January 1969.

In a similar manner, based on all of the data currently available [14,15,19], there is strong evidence that the BIPM unit of resistance is about 1.6 ppm smaller than the SI unit with an uncertainty of about 0.1 ppm and that the BIPM unit is decreasing relative to the SI unit at a rate of about 0.06 ppm per year. The U.S. unit of resistance is smaller than the SI unit by approximately the same amount and is decreasing at about the same rate as the BIPM unit. Most other national units of resistance also differ from the SI unit by less than 2 ppm and are drifting relative to the SI unit by less than 0.1 ppm per year.

Because of the relatively large differences between national voltage and resistance units and the SI, and the rapid development of the quantum Hall effect as a resistance standard, the CCE is considering adopting in the future 1) a new value, consistent with the SI, for the Josephson frequency-voltage ratio $2e/h$ to be used by *every* national standards laboratory which employs the Josephson effect to define and maintain its laboratory unit of voltage; and 2) a value for the quantized Hall resistance R_H, consistent with the SI, to be used by *every* national standards laboratory which employs the quantum Hall effect to define and maintain its laboratory unit of resistance.

5. Conclusion

If the results of new, more accurate experiments currently underway are consistent among themselves and reaffirm the results of the earlier experiments upon which the differences given above are based, then an increase in the U.S. Legal Volt of approximately 9 ppm and in the U.S. Legal Ohm of approximately 1.5 ppm could be expected sometime within the next five years, along with the implementation at NBS of the quantum Hall effect to define and maintain the U.S. unit of resistance. Similar changes would be made by other national standards laboratories as well as the BIPM. The end result would be that most major national standards laboratories would have in place two quantum phenomena, the Josephson and quantum Hall effects, to define and maintain their national electrical units in terms of invariant fundamental constants of nature to within an uncertainty of 0.01 to 0.1 ppm. Since all laboratories would use the same values for these constants and these values would be consistent with their SI values to within an uncertainty of 0.1 to 0.3 ppm, the practical electrical units for voltage, resistance, and current of most major industrialized countries would be equivalent to within an uncertainty of 0.01 to 0.1 ppm and consistent with their SI definitions to within an uncertainty of 0.1 to 0.3 ppm. This would clearly represent a major advance in ensuring the compatibility of electrical measurements made throughout the world and their consistency with the SI.

References

[1] *The International System of Units (SI)*, Goldman, D. T., and R. J. Bell, eds., Natl. Bur. Stand. (U.S.), Spec. Publ. 330 (U.S. Government Printing Office, Washington, DC, 1981).

[2] Gallop, J. C., Metrologia **18** 67 (1982).

[3] Field, B. F.; T. F. Finnegan and J. Toots, Metrologia **9** 155 (1973).

[4] Terrien, J., Metrologia **9** 40 (1973).

[5] Terrien, J., Metrologia **5** 68 (1969).

[6] Terrien, J., IEEE Trans. Instrum. Meas. **IM-15** 140 (1966).

[7] Taylor, B. N.; W. H. Parker and D. N. Langenberg, Rev. Mod. Phys. **41** 375 (1969).

[8] Cohen, E. R., and B. N. Taylor, J. Phys. Chem. Ref. Data **2** 663 (1973).

[9] Leclerc, G., Metrologia **14**, 171 (1978); Erratum, Metrologia **15** 116 (1979).

[10] Krzhimovskii, V. I.; Kh. A. Ainitdinov, S. I. Borovitskii, and A. S. Gokhner, Izmer. Tekh. **19** 31 (Feb. 1983). [English transl.: Meas. Tech. **26** 123 (1983).]

[11] Klitzing, v. K., and G. Ebert, Metrologia **21** 11 (1985).

[12] Delahaye, F.; D. Dominguez, F. Alexandre, J. P. Andre, J. P. Hirtz, and M. Razeghi, Metrologia **22** 103 (1986).

[13] Giacomo, P., Metrologia **20** 25 (1984).

[14] Taylor, B. N., J. Res. Natl. Bur. Stand. **90** 91 (1985).

[15] Cohen, E. R., and B. N. Taylor, to be published.

[16] Petley, B. W., in *Metrology and fundamental constants*, A. F. Milone, P. Giacomo, and S. Leschiutta, eds., (North Holland, Amsterdam, 1980), p. 358; *The fundamental physical constants and the frontier of measurement* (Adam Hilger, Bristol, 1985).

[17] Sloggett, G. J.; W. K. Clothier, M. F. Currey, D. J. Benjamin, and H. Bairnsfarther, IEEE Trans. Instrum. Meas. **IM-34** 187 (1985).

[18] Vigoureux, P., and N. Dupuy, National Physical Laboratory (U.K.) Report DES 59, January 1980.

[19] Taylor, B. N., IEEE Trans. Instrum. Meas. **IM-34** 155 (1985).

[20] Taylor, B. N., Metrologia **21** 37 (1985).

[21] Kibble, B. P.; R. C. Smith and I. A. Robinson, IEEE Trans. Instrum Meas. IM-32 141 (1983).

[22] Taylor, B. N.; Metrologia **12** 81 (1976).

Technical News Briefs

New Technical Developments

NEW WAY TO MEASURE CORROSION IN HIGHWAY BRIDGES

NBS has developed a new system for highway engineers to measure the corrosion rate of steel reinforcing bars in concrete. The system will provide engineers with a way to evaluate the effectiveness of various surface coatings and sealers applied to bridge decks to reduce internal corrosion. The technique, developed for the Federal Highway Administration, uses a portable, computerized system for making nondestructive spot measurements within a matter of minutes. It eliminates the need to bore holes in concrete to inspect steel reinforcing bars. The system consists primarily of a small computer, a data logger and two probes for sending and receiving electrical impulses. Measurements are made by placing the probes on a bridge deck to make contact with internal steel reinforcing bars. One of the probes is used to polarize the steel bars and the other is used to measure the change in voltage. The new system has wide potential for inspecting buildings, parking garages, and other reinforced concrete structures subject to corrosion.

For further information contact Edward Escalante, National Bureau of Standards, Gaithersburg, MD 20899.

ARSON DETECTION IS GOAL OF ANALYTICAL METHOD BEING DEVELOPED

Experiments in analytical chemistry have uncovered a technique that shows promise as a method of detecting arson. NBS scientists have found that the fire "accelerants" many arsonists use, such as gasoline and kerosene, produce specific by-products that become part of soot. Known as polycyclic aromatic hydrocarbons (PAHs), these products can be removed by solvent extraction from sooty deposits sampled at the scene of a fire. Gas chromatography is used to detect PAH presence. The technique has been successful in identifying PAHs both in soot from controlled laboratory fire tests and in samples taken from on-location fires started with accelerants. The Treasury Department's Bureau of Alcohol, Tobacco and Firearms has provided soot samples from training fires in abandoned residential buildings. While NBS researchers describe the PAH test as "a simple one that could be easily used as a forensic device," they emphasize that the method is only experimental at this point and that it cannot be applied to all arson situations. NBS plans to test the technique further and to produce a report aimed at forensic chemists.

For further information contact Stephen Chesler, National Bureau of Standards, Gaithersburg, MD 20899.

NBS IMPROVED PHASE ANGLE DEVICE DESCRIBED IN REPORT

The invention of a 50-kHz phase angle calibration standard by an NBS physicist received considerable attention when it was announced in 1985. Three commercial versions of the device are presently on the market. Now the inventor has authored a technical report [1] that gives a detailed description of the device and suggestions for its efficient operation. Calibrated phase angle equipment is needed for such applications as testing aircraft instruments, tracking satellites, and checking the functioning of electrical power lines. The NBS-developed device improves the speed of existing phase angle calibrators by 10 times or more. It works by creating two sinusoidal signals with an accurately known phase angle between them. Signals are generated using digital waveform synthesis and are programmable in amplitude (0 to 100 V) and in frequency (2 Hz to 50 kHz).

For more information contact Raymond Turgel, National Bureau of Standards, Gaithersburg, MD 20899.

Reference

[1] NBS 50 kHz Phase Angle Calibration Standard (TN 1220), Stock Number 003-003-02726-0, the Superintendent of Documents, U.S. Government Printing Office, Washington, DC 20402 (price $4, prepaid).

EXPLOSION INVESTIGATION UNCOVERS WIDE POTENTIAL HAZARD

NBS researchers' findings into a steel pressure vessel accident should concern the operators of hundreds of similar pieces of equipment all over the United States and the world [1]. The tank, at the Union Oil Company's Chicago refinery, apparently had been built properly, operated properly, and inspected at regular intervals. Nonetheless, it developed severe cracks and failed, with fatal results.

At the request of the U.S. Occupational Safety and Health Administration, and after an on-site inspection by NBS researchers, pieces of the destroyed tank were shipped to the Bureau's laboratories in Boulder, CO, for examination. There, exhaustive tests determined the composition and strength of the materials used, the condition of the tank before it failed, and the probable sequence of events leading to failure.

Chemical and mechanical testing showed that the materials used to build the tank met or exceeded specifications, and that the welds were stronger than the base metal.

Corrosion and hydrogen cracking tests performed on samples from the tank showed that the materials were susceptible to hydrogen pressure cracking in the sort of environment that existed in the tank.

Magnetic particle, ultrasonic, and metallurgical studies of the fracture surfaces and adjacent areas revealed that extensive cracking had occurred, particularly in the heat-affected zone near repair welds. These areas near welds were hardened by the repair welding and especially susceptible to hydrogen cracking. One of the cracks extended more than nine-tenths of the way through the inch-thick tank wall, leaving insufficient steel to contain the internal pressure. Once a leak penetrated at this crack, the crack continued to grow right around the tank, like unzipping a zipper. The final, near-instantaneous fracture was triggered by this crack because the toughness of the steel had been reduced by hydrogen embrittlement.

Reference

[1] Examination of a Pressure Vessel that Ruptured at the Chicago Refinery of the Union Oil Company on July 23, 1984 (NBSIR 86-3049), Stock Number PB 226594/AS, National Technical Information Service, Springfield, VA 22161 (price $22.95, prepaid).

COMPANIES, AGENCIES STUDY IMPROVED FLOW MEASUREMENTS

In an effort to reduce financial losses from inaccurate measurements, several industrial makers and users of meters that measure the multibillion-dollar flow of materials through pipes—commodities such as oil, natural gas, and chemicals—are working with NBS to examine ways of improving flow metering.

Because research programs needed to understand the complexities of fluid-flow phenomena are costly, several corporations have entered into cooperative agreements with NBS as cost-effective approaches to improving flow measurements. One such agreement, a consortium on meter "installation effects," is investigating the persistent problem of how to get satisfactory results from meters installed in "non-ideal" locations: too close to a pipe "elbow" or valve for instance.

Another consortium is focusing on the performance of vortex-shedding flowmeters, which determine flow rate by detecting the whirl-shaped vortexes produced by flow through the meter. The goal is to combine the measurement expertise and fluid research facilities at NBS with the industrial needs of the consortium members.

For further information contact George Mattingly, National Bureau of Standards, Gaithersburg, MD 20899.

NBS EXAMINES LITERATURE ON GASES FROM BURNING PLASTICS

Smoke and toxic gases, not burns, kill 80 percent of the people who die in fires. In a project partially sponsored by the Consumer Product Safety Commission, the NBS Center for Fire Research conducted an extensive literature review on the toxicity and chemistry of the gases produced when seven synthetic materials were exposed to high temperatures. More than 400 different gases were identified.

Except in a few cases involving additives, the literature shows that these seven plastics did not produce extremely or unusually toxic products when compared to those of other synthetic or natural materials. But NBS researchers note that these exceptions cause concern that other untested materials or future formulations may produce such toxic products. They also caution that toxicity is only one factor in determining the total harmful effects from a fire. Other factors to be considered include the quantity of material, its proximity to other combustibles, ventilation conditions, and fire protection systems. Separate reviews on each of the seven materials are cited in an NBS summary report of the literature reviews [1].

Reference

[1] A Summary of the NBS Literature Reviews on the Chemical Nature and Toxicity of the Pyrolysis and Combustion Products from Seven Plastics: Acrylonitrile-Butadiene-Styrenes (ABS), Nylon, Polyesters, Polystyrenes, Poly (Vinyl Chlorides) and Rigid Polyurethane Foams (NBSIR 85-3267), Stock Number PB 86-230679, National Technical Information Service, Springfield, VA 22161 (price $9.95, prepaid).

THREE DEVELOPMENTS IN SUPPORT OF COMPUTER COMPATIBILITY

Efforts toward realizing computer compatibility through Open Systems Interconnection (OSI) appear to be gathering momentum, if the following three developments are accurate indicators:

- As the world's largest user of computers, the Federal government is organizing itself to work with industry to meet the special computer compatibility needs of Federal agencies.

NBS hosted the new "Government OSI Users Committee," involving 15 Federal agencies, in its first meeting on September 9. The group addressed the Federal government's interest in emerging network standards for computer compatibility. The Office of Management and Budget is developing a policy which would require the Federal government to use products for computer-to-computer communication which implement Open Systems Interconnection (OSI) standards. OSI standards provide a set of rules, known as protocols, which enable information processing devices to communicate with one another in a network. These standards will make it possible to connect off-the-shelf computer products from different manufacturers through a variety of communications technologies. OSI development has extensive government and private sector support. Over the next several years, the committee will work with industry to accelerate the development of OSI-compatible products that meet the special needs of the Federal government.

For further information contact Robert Blanc, National Bureau of Standards, Gaithersburg, MD 20899.

- Twenty-five industry and government organizations have agreed to jointly develop OSINET, an experimental computer network for Open Systems Interconnection standards. To be coordinated by NBS, this network will help speed up the development and use of OSI in industry and government. It will enable cooperating organizations to build and verify test systems, conduct company- to-company testing, and carry out OSI-related research. Participants include: Amdahl, AT&T, Boeing Computer Services, Charles River Data Systems Defense Communications Agency, Digital Equipment Corporation, General Motors, Hewlett-Packard, Honeywell, IBM, ICL, Industrial Networking Inc., NBS, NCR Comten, Olivetti, OMNICOM, Protocom Devices, Retix, Sperry, System Development Corporation, Tandem Computers Inc., The Analytic Sciences Corporation, Department of Agriculture, Department of the Navy, and Wang Laboratories. These organizations plan to cooperate with other groups, such as the Corporation for Open Systems and the MAP/TOP Users Group, that are advancing the development and use of OSI standards.

For further information contact John Heafner, National Bureau of Standards, Gaithersburg, MD 20899.

- In another development related to Open Systems Interconnection, NBS is working with the Defense Communications Agency to build gateways between Department of Defense protocols and OSI protocols. The gateways will be used to maintain the agency's operations during conversion to OSI networks. A guest scientist from IBM is working with an NBS research team to develop automated techniques to test the gateways' computer network being developed cooperatively by 25 industry and government organizations, including NBS, IBM, and DCA.

For further information contact Stephen Nightingale, National Bureau of Standards, Gaithersburg, MD 20899.

REVISED FEDERAL STANDARD FOR COBOL ISSUED

A revised Federal Information Processing Standard (FIPS) for the programming language COBOL [1] went into effect October 1, 1986. A one-year transition period will give industry time to produce COBOL processors conforming to the standard. (FIPS are developed by NBS for use by the Federal Government.) The revised standard, which was approved by the Secretary of Commerce earlier this year, adopts an American National Standard (ANSI X3.23-1985) which reflects major changes and improvements in the COBOL specifications. The specifications are for use by industry as the reference authority in developing processors and by users who need to know the precise syntactic and semantic rules of the standard language. The FIPS also contains changes which recognize advances in programming technology and make the standard consistent with other Federal standards for languages.

Reference

[1] FIPS PUB 21-2, COBOL, National Technical Information Service (NTIS), Springfield, VA 22161; $42.

New Services From NBS

TELECOMMUNICATIONS LABS GET U.S., INTERNATIONAL RECOGNITION FOR TESTING SERVICES

Fourteen private sector laboratories that perform electromagnetic compatibility (EMC) and telecommunications equipment testing have been accredited under the National Voluntary Laboratory Accreditation Program (NVLAP) managed by NBS.

The laboratories were accredited for selected test methods under a new electromagnetics laboratory accreditation program (Journal of Research, Vol. 91, No. 2, p. 106). This LAP was established by NBS at the request of five commercial testing laboratories seeking international recognition for EMC accreditation. International recognition of U.S. laboratories and test methods has been a high priority of industry groups and manufacturers to aid them in exporting their products to foreign countries.

With NVLAP accreditation, the laboratories automatically receive international recognition for their testing services through NBS' agreements with the United Kingdom's National Measurement Accreditation Service, Australia's National Association of Testing Authorities, and New Zealand's Testing Laboratory Registration Council. Under these agreements, test data reports issued by an accredited laboratory in one system are recognized by the other national accreditation systems.

The laboratories accredited under the electromagnetic LAP are: Amador Corporation, AT&T Information Systems, Communication Certification Laboratory, Continental Testing Laboratories, D.L.S. Electronic Systems, Inc., Dash, Straus, and Goodhue, Inc., Elite Electronic Engineering Company, Emaco, Inc., GTE Evaluation and Support Department, MET Electrical Testing Company, Inc., Norand EMC Test Lab, Retlif, Inc. Testing Laboratories, R & B Enterprises, Underwriters Laboratories Inc. Under NVLAP procedures, laboratories can apply for accreditation in one or more of the recognized test methods that make up the electromagnetics LAP. The LAP provides recognition to accredited laboratories that are capable of performing specific test methods for conducted emissions, radiated emissions, and terminal equipment compatibility in accordance with Federal Communications Commission (FCC) standards.

Established in 1976, NVLAP is a voluntary system whereby organizations and individuals request NBS to establish a laboratory accreditation program. On an individual basis, laboratories seek accreditation for having the competence to use specific test methods.

"Competence" is determined by evaluating applicant laboratories to assure that they have the equipment, staff, and procedures necessary to perform recognized tests in accordance with nationally or internationally accepted standards or test methods.

NVLAP-accredited laboratories pay annual fees, go through on-site reassessment every 2 years, and participate in scheduled proficiency testing to maintain accredited status. The laboratories are listed in the NVLAP directory that is distributed worldwide.

Currently, approximately 200 laboratories are accredited in programs administered by NBS for thermal insulation, carpet, concrete, solid-fuel room heaters, acoustical testing services, personnel radiation dosimeters, commercial products (paint, paper, and mattresses), building seals and sealants, and electromagnetic compatibility and telecommunications equipment testing. Other LAPs have been proposed for asbestos abatement, construction testing services, electrical and safety testing, and metals testing.

For further information, contact: Manager, Laboratory Accreditation, A531 Administration Building, National Bureau of Standards, Gaithersburg, MD 20899; telephone: 301-921-3431.

New Standard Reference Materials*

NEW STANDARD REFERENCE MATERIALS WILL AID PCB ANALYSIS

Laboratories that use chromatographic instruments to analyze environmental samples such as air and water for the presence of polychlorinated biphenyls (PCBs) should find Standard Reference Material (SRM) 1585 useful. Developed for calibrating analytical equipment such as gas chromatographs, SRM 1585 contains certified concentra-

---

*SRMs can be ordered from the Office of Standard Reference Material, NBS, Gaithersburg, MD 20899, Telephone 301-921-2045.

trations of eight related chlorinated biphenyls. These were chosen because of their environmental interest. For example, three are indicative of Aroclors 1254 and 1260, which are PCB mixtures found in some transformer oils. SRM 1585, Chlorinated Biphenyls in 2,2,4-Trimethyl-pentane (Isooctane), contains five sealed vials, each with about 1.2 milliliters of solution. It is available for $161.

New Standard Reference Data

BASIC TABLES FOR CHEMICAL ANALYSIS

NBS has published a new set of handy reference tables of important data for use in analytical chemistry laboratories [1]. The tables include, in a single source, information not easily obtainable elsewhere about gas, liquid, and thin-layer chromatography, infrared and ultraviolet spectrophotometry, nuclear magnetic resonance and mass spectrometry, and "wet" chemical tests. Sections on hazardous materials and unit conversions also are included. Some typical tables are carrier gas properties, solvents for liquid chromatography, infrared optics materials and characteristics absorptions, natural abundance of important isotopes, mass fragmentation patterns, and flammability hazards of common solvents.

Reference

[1] Basic Tables for Chemical Analysis (TN 1096), Stock No. 003-003-02724-3, U.S. Government Printing Office, Washington, DC 20402 (price $11, prepaid).

☆U.S. GOVERNMENT PRINTING OFFICE: 1986-181-096:40011